12-5-2019

Extended Version of Simple Sagittal Running: Stability of a Quadrupedal Bound

Jeff Duperret
University of Pennsylvania, jdup@seas.upenn.edu

D. E. Koditschek
University of Pennsylvania

Extended Version of Simple Sagittal Running: Stability of a Quadrupedal Bound

Abstract

This paper develops a three degree-of-freedom sagittal-plane hybrid dynamical systems model of a bounding quadruped. Simple within-stance controls yield a closed form expression for a family of hybrid limit cycles that represent bounding behavior over a range of user-selected fore-aft speeds as a function of the model's kinematic and dynamical parameters. Controls acting on the hybrid transitions are structured so as to achieve a cascade composition of in-place bounding driving the fore-aft degree of freedom thereby decoupling the linearized dynamics of an approximation to the stride map. Careful selection of the feedback channels used to implement these controls affords infinitesimal deadbeat stability which is relatively robust against parameter mismatch. Experiments with a physical quadruped reasonably closely match the bounding behavior predicted by the hybrid limit cycle and its stable linearized approximation.

Disciplines

Electrical and Computer Engineering | Engineering | Systems Engineering

Extended Version of Simple Sagittal Running: Stability of a Quadrupedal Bound

Jeffrey M. Duperret, *Student Member, IEEE,* and Daniel E. Koditschek, *Life Fellow, IEEE*

Abstract—

This paper develops a three degree-of-freedom sagittal-plane hybrid dynamical systems model of a bounding quadruped. Simple within-stance controls yield a closed form expression for a family of hybrid limit cycles that represent bounding behavior over a range of user-selected fore-aft speeds as a function of the model's kinematic and dynamical parameters. Controls acting on the hybrid transitions are structured so as to achieve a cascade composition of in-place bounding driving the fore-aft degree of freedom thereby decoupling the linearized dynamics of an approximation to the stride map. Careful selection of the feedback channels used to implement these controls affords infinitesimal deadbeat stability which is relatively robust against parameter mismatch. Experiments with a physical quadruped reasonably closely match the bounding behavior predicted by the hybrid limit cycle and its stable linearized approximation.

*Index Terms—***Legged Robots, Simplified Models of Running, Hybrid Dynamical Systems**

This work is an extended version of [1], providing Appendices B-F.

I. INTRODUCTION

LEGGED robots exhibit increasingly successful steady-state [2], [3] and transitional [3]–[5] behaviors, yet they remain scarce in real-world applications. One challenge impeding their widespread adoption is the difficulty of developing parametrized families of controllers that work over identifiable ranges of body and environmental parameters. Today's most successful gait control methods for high degree of freedom legged machines generally appeal to numerical optimization [6]–[8], yielding increasingly impressive controls for specific mechanisms at specific operating conditions in specific environments. Achieving stable gait controllers with functional dependence on task and environment parameters that specify the operating characteristics of useful legged machines is fundamentally hard, owing to the non-integrability of their high dimensional nonlinear hybrid dynamics. Prior results of this nature are rare even for three degree-of-freedom mechanisms [9]–[11]. The authors are not aware of any complete stability result for three or higher degree-of-freedom models of quadrupedal locomotion (where the various appendages do not connect to the body at a common point in the simplified model).

This paper presents a parametrized family of controllers that stabilize a hybrid dynamical systems model of quadrupedal bounding arising from a simple three degree-of-freedom sagittal plane representation of a legged robot. The stability guarantees extend over a specified range of variations in body mass, length, and moment of inertia that dictate the achievable range of commanded forward running speeds and thereby, in turn, the full set of controller parameters. These formal results arise from key approximations and a controller structure that exploits them to afford a decomposition of the full model into the cascade of a two degree-of-freedom in-place bounding component forward-coupled to drive a one degree-of-freedom fore-aft component. This model and the resulting controller are simple in the sense that they encode ground-reaction force laws resulting in trivial continuous body dynamics and they achieve the family of asymptotically stable limit cycles representing the desired steady state gait using proportional control on the hybrid transitions. Nevertheless, the model is sufficiently faithful and the controller is sufficiently robust as to permit empirical implementation over many repeated trials (accumulating hundreds of body lengths) on a physical robot, Inu [12], displayed in Figure 1.
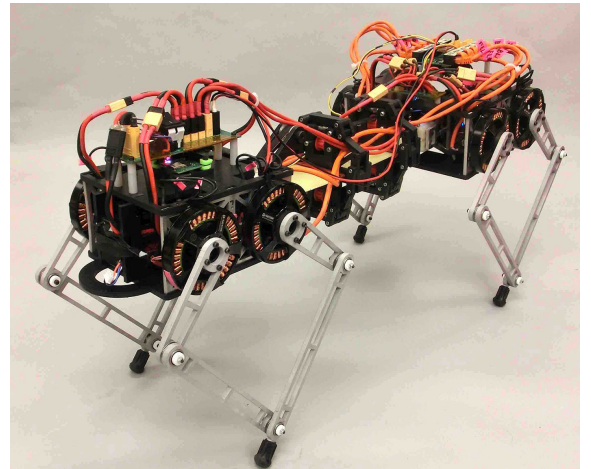
Fig. 1. The controller presented in this work is empirically demonstrated on the Inu robot [12]. Empirical bounding corresponding to the analytically predicted limit cycles derived in Proposition 1 using the simplified dynamics of Figure 4 implemented using the physical parameters listed in Table III is documented in Figures 9, 10.

A. Cascade Compositions

The use of simplified models for the control of legged running has a rich history of empirical [13]–[15] and analytical

[16]–[18] success. We are particularly interested in modular approaches that can offer an analytically tractable path to formal results, as they decouple the stability problem into a composition of lower-dimensional subproblems. For example, "parallel composition" – approximation in terms of modules operating simultaneously in isolation – was pioneered with great success empirically by Raibert [13], and has been formally redeveloped in recent years for bipedal [9], quadrupedal [19], and more general [20] legged systems. While empirically very effective, this recent formal analysis of legged parallel composition uses the framework of hybrid dynamical averaging [21] requiring not only that the neglected "crosstalk" between modules be sufficiently small but that potentially deleterious components (that cannot be averaged away) be identified and compensated by feedback.

In this paper, we introduce a cascade composition (1) to control quadrupedal bounding, which – in contrast to parallel compositions – allows for arbitrarily large feed-forward signals from one module to another cascaded module. From the analytical perspective, the cascade also achieves an eigenvalue separation property in the stride-map Jacobian that guarantees local stability of coupled modules so long as they are stable in isolation, providing a separation of concerns to the designer. Cascade compositions have long been used to reduce the complexity of adding dimensionality both in continuous-time systems [22], [23] and iterated maps [24]. However – to the best of our knowledge – their formal consideration for simplified models of dynamic quadrupedal locomotion has only been used to "extract" away fast actuator dynamics [25] or for similar situations with multiple timescales [26] that reduce to feed-forward cascades in Fenichel normal form [27].

We say an iterated map $P : \mathbb{R}^n \times \mathbb{R}^m \to \mathbb{R}^n \times \mathbb{R}^m$ is a *cascade composition* if it is of the form:

$$P(x, y) = \begin{pmatrix} P_1(x) \\ P_2(x, y) \end{pmatrix}, \tag{1}$$

where $x \in \mathbb{R}^n, y \in \mathbb{R}^m, P_1 : \mathbb{R}^n \to \mathbb{R}^n, P_2 : \mathbb{R}^n \times \mathbb{R}^m \to \mathbb{R}^m$. Such a system has the block-triangular Jacobian:

$$DP = \begin{pmatrix} D_x P_1 & 0 \\ D_x P_2 & D_y P_2 \end{pmatrix}, \tag{2}$$

in which the eigenvalues of DP consist of the eigenvalues of the smaller $(n \times n)$ matrix $D_x P_1$ and $(m \times m)$ matrix $D_y P_2$. The task of showing that the spectral radius of DP has modulus less than unity for a linearized stability analysis then reduces to establishing the same property individually for the smaller constituent matrices, $D_x P_1$ and $D_y P_2$, generally a much easier task.

B. Controlling on Hybrid Transitions

The long practiced tradition of achieving control through shaping a hybrid dynamical system's guards and resets (the hybrid transitions) has been used since the earliest days of empirically successful dynamical robots when Raibert used the fact that a robot leg's angle in flight could be freely set to affect touchdown conditions and thereby control forward running speed [13] (inspiring many similarly conceived subsequent speed controllers [17], [19], [28]). This insight was generalized by Seyfarth [29], initiating a "swing-leg retraction" literature (e.g. [30], [31]) that occasioned two fundamental observations that bear on our work. First, minimally sensed stabilization is not only achievable (demonstrated numerically [32] and analytically [33]) by control on hybrid transitions, but can afford deadbeat performance[1] as well with only a bit more sensing. Specifically, as shown numerically [35] and analytically [36], proper feed-forward servoing of sagittal leg angle in flight affords control over the apex height with no sensing required other than the detection of the apex and touchdown events, even when running over uneven terrain. Second, the implicit function theorem provides sufficient conditions for the existence of deadbeat control given a sufficiently expressive input vector using full state feedback [34]. Studies in humans [37] and birds [38]–[40] document some combination of feed-forward and feedback hybrid transition control strategies during biological running, further motivating their study for roboticists.

Previous results on hybrid transition control (particularly the deadbeat literature) are limited in several ways. The majority of results are limited to simulation and the recent preliminary experimental work in this area [41], [42] suggest performance is very sensitive to state estimation error or perhaps model parametric uncertainty, conceivably limiting the application of deadbeat results to robots in controlled environments such as motion capture feedback systems. Even methods requiring no sensing aside from the detection of apex suffer from the fact that the apex event is difficult to precisely detect in practice without motion capture data.

Noting that previous work controlling hybrid transitions in legged locomotion has been limited to varying the flight leg angle, we take inspiration from Blickhan's studies indicating that humans vary both their leg angle and leg length in flight to affect touchdown conditions [43], [44] and expand consideration of hybrid transition control to vary flight leg angle and length. We also allow our hybrid transition controller to affect liftoff conditions. In these ways, we more fully leverage the affordance inherently provided by making and breaking contact in sagittal running. Moreover, aiming for greater robustness and avoiding the need to detect the apex event, we forgo deadbeat control for a linearized version of it and also use a combination of feed-forward and feedback control -– only using feedback on states that can be accurately measured on-board the robot.

C. Outline

Section II introduces a simplified hybrid dynamical systems model (3) representing a bounding quadruped, with a rigid-bar body and massless legs that exert ground-reaction forces at the toes. Ground reaction force laws and hybrid transition behaviors are specified that make the dynamics a cascaded composition of two hybrid dynamical system modules. Simplifying assumptions (shown in Section III to be approximately valid) give these modules trivial dynamics. Section III formulates a stride map for a bounding gait,

---

[1]Here, deadbeat control refers to a strategy resulting in exact correction to perturbations in a finite (typically minimum) number of steps [34].

Symbol	Description
$\mathcal{H} := (\mathcal{J}, \mathcal{T}, \mathcal{D}, \mathcal{F}, \mathcal{G}, \mathcal{R})$	Hybrid system (3), (5), (6), (13), (17), (18)
F, D, R	Hybrid modes (4)
$D_i, G_{i,j}, R_{i,j}, F_i$	Mode domains (7), guards (17), (24), resets (19), (29) and vector fields (14)
t	Time
y, φ, τ	Mass-center height, body pitch, mode timer (10), Figure 2
x, x^f, x^r	Mass-center and front/rear toe horizontal positions (11), Figure 2
$\Delta x^f = x^f - x, \ \Delta x^r = x^r - x$	Front and rear horizontal leg-splay distance (11), (12), measured from the mass-center
$\boldsymbol{x}_i := (\boldsymbol{x}_i^{I\,T}, \boldsymbol{x}_i^{H\,T})^T$	State (9) in mode i, with in-place (10) and horizontal (11) components
$\boldsymbol{x}^I := (\boldsymbol{q}^I, \dot{\boldsymbol{q}}^I, \tau)^T, \quad \boldsymbol{q}^I := (y, \varphi)^T$	In-place state, configuration (10)
m, I, g, d	Physical model parameters (Figure 2)
$\Delta x^{\mathrm{Avg}}, a, l_0$	Pseudo-physical parameters related to control parameters (22), (23), (25), (also Figure 2)
$G_{i,j}^I$	In-place components of the guard set (24), (25)
$y^{fhip}(\boldsymbol{x}^I), y^{rhip}(\boldsymbol{x}^I), \dot{y}^{fhip}(\boldsymbol{x}^I), \dot{y}^{rhip}(\boldsymbol{x}^I)$	Front/rear hip heights and velocity maps (28)
$g_{TD}(\boldsymbol{x}_{\mathrm{F}}^I), g_{LO}(\boldsymbol{x}_{\mathrm{D}}^I)$	Guard "control" functions for touchdown, liftoff events (25), (57)
$\boldsymbol{k}^I = (\boldsymbol{k}^I{}_{\mathrm{F}}{}^T, \boldsymbol{k}^I{}_{\mathrm{D}}{}^T)^T$	In-place guard control weights (25)
$y^{fhip}{}_{i0}(\boldsymbol{x}^I), y^{rhip}{}_{i0}(\boldsymbol{x}^I)$	Front and rear initial hip height in mode i (58)
b, b^I, b^H	"Bounding" symmetry map (40), with in-place (26) and horizontal (32) components
$\mathcal{L}_f V(x) := \frac{\partial}{\partial x} V(x) \cdot f(x)$	Lie derivative (27) of scalar field V along vector field f at point x
$R_{i,j}^I, R_{i,j}^H$	In-place (30), horizontal (31) reset function components
$r_{\mathrm{F,D}}(\boldsymbol{x}_{\mathrm{F}}^H), r_{\mathrm{D,R}}(\boldsymbol{x}_{\mathrm{D}}^H)$	Reset "control" functions (31), (62)
$\boldsymbol{k}^H := (k_{\mathrm{F}}^H, k_{\mathrm{D},1}^H, k_{\mathrm{D},2}^H)^T \in \mathbb{R}^3$	Reset control weights (63)
Δx^{Nom}	Nominal touchdown leg splay for front leg (31)
$\bar{y}$	Mass-center constant-height approximation value (Approximation 1)
$u_y \in (\frac{g}{2}, g), \quad u_{xi}(\boldsymbol{x})$	Vertical (16), (20), (33), horizontal (16), (21) (mass-specific) force from each hip
$\phi_i^t(\boldsymbol{x}^I), \quad \hat{\phi}_i^t(\boldsymbol{x}^H)$	In-place (34), horizontal (35) mode-i flow
$\boldsymbol{c}_i$	(y, φ) simplified acceleration vector for mode i (34)
$C_{\mathrm{F}}, C_{\mathrm{D}}, C_{\mathrm{R}}$	Matrix components used in the description of $\hat{\phi}_i^t(\boldsymbol{x}^H)$ (35)
$\Phi_{i,j}, \Phi_{i,j}^I, \Phi_{i,j}^H$	Mode map (37) from mode i to j, with in-place, horizontal components (38)
$T_{i,j}^I(\boldsymbol{x}^I)$	Mode i time-to-impact map (39) with guard $G_{i,j}^I$
$\widetilde{D}_i := \widetilde{D}_i^I \times \widetilde{D}_i^H$	Reduced domain for stride map with horizontal, in-place components (41)
$\widetilde{\boldsymbol{x}} := (\widetilde{\boldsymbol{x}}^{I\,T}, \widetilde{\boldsymbol{x}}^{H\,T})^T$	Reduced (stride map) state with in-place and horizontal components (42)
$\Pi(\boldsymbol{x}), \Sigma(\widetilde{\boldsymbol{x}})$	Projection and lift maps (43)
$\Pi^I(\boldsymbol{x}^I), \Sigma^I(\widetilde{\boldsymbol{x}}^I), \Pi^H(\boldsymbol{x}^H), \Sigma^H(\widetilde{\boldsymbol{x}}^H)$	In-place, horizontal projection and lift maps (43)
S, H	Stride (44) and "flipped" half-stride (46) maps
$\widetilde{\bar{\boldsymbol{x}}} = (\widetilde{\bar{\boldsymbol{x}}}^{I\,T}, \widetilde{\bar{\boldsymbol{x}}}^{H\,T})^T \in \widetilde{D}_{\mathrm{F}}$	Fixed point of H (47)
$\bar{\Delta x}^f, \bar{\Delta x}^r$	Leg splay components of $\widetilde{\bar{\boldsymbol{x}}}^H$ (49)
$\bar{T}_{\mathrm{Stance}}, \delta \bar{x}_{\mathrm{Stance}}$	Total hip stance duration (53) and leg sweep distance (54) on the hybrid periodic orbit associated with $\widetilde{\bar{\boldsymbol{x}}}^H$
$\bar{\boldsymbol{x}} = \Sigma(\widetilde{\bar{\boldsymbol{x}}}) \in D_{\mathrm{F}}$	Lift of $\widetilde{\bar{\boldsymbol{x}}}$ (59)
$\bar{T}_{i,j}, \bar{\boldsymbol{x}}_{i0,j}^I$	Mode i's duration (51) and initial state (60) as it evolves into mode j under the hybrid execution from $\bar{\boldsymbol{x}}^I$
$V^I, \Lambda^I, A^I, \boldsymbol{d}^I, R^I, T^I$	Matrices/vectors used in Lemma 2 (77), (78)
$\widetilde{b}^I, D\widetilde{\Phi}_{i,j}^I$	Simplified factors of H's in-place component (72)
$\widetilde{\boldsymbol{k}}_{\mathrm{F}}^I, \widetilde{\boldsymbol{k}}_{\mathrm{D}}^I$	Change of variables for $\boldsymbol{k}^I{}_{\mathrm{F}}, \boldsymbol{k}^I{}_{\mathrm{D}}$ (73)
$A^H, \boldsymbol{d}^H, R^H := (\boldsymbol{d}^H, A^H \boldsymbol{d}^H)$	Matrices/vectors used in Lemma 3 (84)

TABLE I

MAIN SYMBOLS USED IN THIS WORK WITH REFERENCE TO THEIR EQUATIONS OF INTRODUCTION

and factors it into a more easily analyzable half-stride map. A fixed point representing a hybrid periodic orbit is found in Proposition 1, and its properties are examined. Section IV formulates control on the hybrid transitions to make the aforementioned periodic orbit an attracting limit cycle. Control weights are chosen in Proposition 2 so that the stride map representing the orbit is infinitesimally deadbeat. Section V details the empirical instantiation of the controlled model on the Inu robot. Experimental results indicate reasonably close correspondence to the theoretically predicted behavior of the simplified model. Section VI provides a brief discussion about the ideas in the paper, and Section VII provides concluding remarks. Proofs and lemmas are given in the appendices. A table of symbols is provided in Table I.

II. MODEL

This section introduces the simplified model shown in Figure 2 of a quadrupedal robot bounding in the sagittal-plane. The model consists of a rigid bar representing a robot body with massless legs protruding from the hips that are able to generate ground-reaction forces at the toes. This basic model has been used to describe sagittal quadrupeds since Raibert's work [13, p. 139], typically using torques and radial forces generated at the hips (equivalent to ours through a change of coordinates). It has been used more recently with commanded Cartesian ground-reaction forces to model both steady-state and transitional empirical behaviors [4], [14]. The model should approximately represent the sagittal dynamics of physical bounding robots with mass-center roughly halfway between their hips, as long as the leg inertia is sufficiently

less than that of the body so as to satisfy the massless leg approximation.

Section II-A gives the model's hybrid dynamical system description for a non-aerial bound (because of the actuator limits described in Section V-A) as depicted in Figure 3. Section II-B constrains the ground-reaction force laws (20), (21), and hybrid transitions (24), (29) to enact a cascade composition. Section II-C introduces dynamical simplifications in the form of Approximations 2, 1, and (33) that – together with the previous modeling choices – give the cascaded system the trivial dynamics depicted in Figure 4. These modeling and control choices yield simple closed form expressions for the flow on the hybrid modes (34), (35), that in turn allow a closed form expression for the targeted bounding limit cycles in Section III and a tractable stability analysis in Section IV.
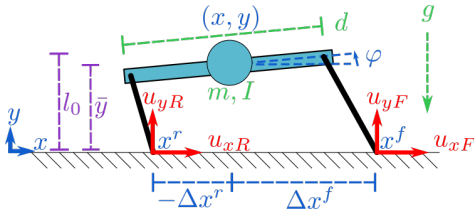
A. Hybrid Dynamical System Description

Fig. 2. The simplified massless-leg representation of a quadrupedal robot bounding in the sagittal-plane. The model's configuration is shown in blue and is given by the body's location in $SE(2)$ with mass-center position (x, y) and body-pitch φ, as well as the horizontal location of the front and rear toes encoded either by their toe positions x^i or splay-distance Δx^i from the mass-center, $i \in \{f, r\}$. The physical parameters shown in green are the body's mass m and moment-of-inertia I about its mass-center, the body length d, and gravity's acceleration g. Each leg in contact with the ground imparts a vertical (u_y) and horizontal (u_x) mass-specific ground-reaction force law at each toe shown in red. Purple values relate to control parameters. The value l_0 is a nominal vertical leg length at the touchdown and liftoff events (used as a control parameter in (25)). In Approximation 1 we introduce $\bar{y}$ as a representing the approximately-constant mass-center stance height under a suitable choice of ground-reaction force control laws.

Following the convention of [45], we define the hybrid system $\mathcal{H}$ representing the sagittal-plane massless-leg robot model depicted in Figures 2 and 3 as the tuple:

$$\mathcal{H} := (\mathcal{J}, \mathcal{T}, \mathcal{D}, \mathcal{F}, \mathcal{G}, \mathcal{R}). \tag{3}$$

The set:

$$\mathcal{J} := \{F, D, R\} \tag{4}$$

represents the hybrid modes corresponding to front single-support F, double-support D, and rear single-support R, respectively. No flight mode is given due to the actuator constraints of the Inu robot as explained in Section V-A, but a similar analysis is possible replacing the double support phase with a flight phase.

The allowed hybrid transitions are given by:

$$\mathcal{T} := \{(F, D), (D, R), (R, D), (D, F)\}. \tag{5}$$

The set of continuous domains is given by:

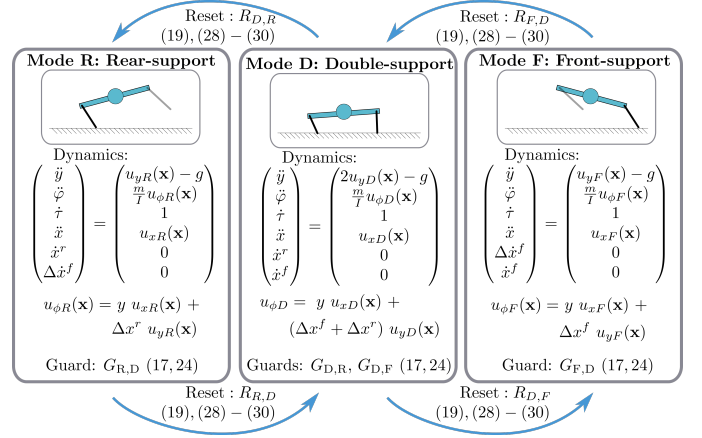$$\mathcal{D} := \bigsqcup_{i \in \mathcal{J}} D_i, \tag{6}$$

Fig. 3. The hybrid dynamical system (3) representing the model shown in Figure 2 with state $\boldsymbol{x}_i = (\boldsymbol{x}^{I\,T}, \boldsymbol{x}_i^{H\,T})^T$. The state component $\boldsymbol{x}^I$ (10) gives the state related to the mass center's vertical height and pitch states, as well as mode timers; while $\boldsymbol{x}_i^H$ (11) gives the mass center's horizontal position and velocity, as well as the horizontal toe positions. The guards $G_{i,j}$ and resets $R_{i,j}$ are introduced in (17) and (19), respectively, and further specified in (24)-(25) and (29)-(31) to decouple the hybrid transitions as shown in Figure 4. Approximation 1 and the choice of force laws (21), (33) decouple the continuous dynamics as shown in Figure 4. There is no flight phase due to actuator limitations when running at speed on the physical machine as described in Section V-A, however accounting for an aerial mode instead of double support would yield a system for which a similar control strategy as described in Section IV could be applied. Note that the horizontal toe locations indicated by Δx^i and x^i, $i \in \{f, r\}$ – unchanged by the continuous dynamics – are set by the resets as control inputs.

where – to aid with the decoupling introduced in Section II-B – we decompose each continuous domain into the product:

$$D_i := D_i^I \times D_i^H, \tag{7}$$

of "in-place" and "horizontal" respective state components that will form the basis for a cascaded composition (1), where:

$$D_i^I := T(\mathbb{R} \times \mathbb{S}) \times \mathbb{R}, \qquad D_i^H := T(\mathbb{R}) \times \mathbb{R}^2, \tag{8}$$

with state:

$$\boldsymbol{x}_i = \begin{pmatrix} \boldsymbol{x}_i^I \\ \boldsymbol{x}_i^H \end{pmatrix}, \tag{9}$$

where $\boldsymbol{x}_i^I$ represents the "in-place" state components relating to vertical and pitching motions, and $\boldsymbol{x}_i^H$ represents the "horizontal" state components relating to horizontal motions. We will drop mode subscripts when appropriate.

The in-place state $\boldsymbol{x}^I$ is given by:

$$\boldsymbol{x}^I := \begin{pmatrix} \boldsymbol{q}^I \\ \dot{\boldsymbol{q}}^I \\ \tau \end{pmatrix}, \ \boldsymbol{q}^I := \begin{pmatrix} y \\ \varphi \end{pmatrix}, \tag{10}$$

representing the configuration and velocity of the mass center's height y and body pitch φ as depicted in Figure 2, as well as the integrated mode duration τ – appended to the state so we can use mode duration as a state variable in the guard events (25), (57). Intuitively these components represent the state of the robot when it is bounding in-place.

The horizontal state $\boldsymbol{x}_i^H$ in mode $i \in \mathcal{J}$ is given by:

$$\boldsymbol{x}_F^H = \begin{pmatrix} x \\ \dot{x} \\ \Delta x^r \\ x^f \end{pmatrix}, \quad \boldsymbol{x}_D^H = \begin{pmatrix} x \\ \dot{x} \\ x^r \\ x^f \end{pmatrix}, \quad \boldsymbol{x}_R^H = \begin{pmatrix} x \\ \dot{x} \\ x^r \\ \Delta x^f \end{pmatrix}, \quad (11)$$

where – as depicted in Figure 2 – x and $\dot{x}$ respectively represent the mass center's horizontal position and velocity, x^f and x^r respectively represent the front and rear foot position, and Δx^f and Δx^r respectively represent the relative distance of the front and rear toe to the mass center according to:

$$\Delta x^f = x^f - x, \quad \Delta x^r = x^r - x. \quad (12)$$

The reason for switching between the Δx^i and x^i state representations is simply mathematical convenience as it allows us to represent the continuous evolution of the foot with a zero vector field in (14) (although the behavior on the hybrid resets is more complicated), where in stance a hip's toe position x^i does not move and in flight a hip's toe position relative to its mass center Δx^i does not change.

The continuous dynamics of the system are shown in Figure 3. To represent them as first-order vector fields, we define the hybrid vector field:

$$\mathcal{F} : \mathcal{D} \to T\mathcal{D} \quad (13)$$

that restricts to the vector fields $F_i := \mathcal{F}|_{D_i}$ for each $i \in \mathcal{J}$ such that:

$$F_F(\boldsymbol{x}) := \begin{pmatrix} \dot{\boldsymbol{q}}^I \\ u_{y_F}(\boldsymbol{x}) - g \\ \frac{m}{I} u_{\varphi_F}(\boldsymbol{x}) \\ 1 \\ \dot{x} \\ u_{x_F}(\boldsymbol{x}) \\ 0 \\ 0 \end{pmatrix}, \quad F_R(\boldsymbol{x}) := \begin{pmatrix} \dot{\boldsymbol{q}}^I \\ u_{y_R}(\boldsymbol{x}) - g \\ \frac{m}{I} u_{\varphi_R}(\boldsymbol{x}) \\ 1 \\ \dot{x} \\ u_{x_R}(\boldsymbol{x}) \\ 0 \\ 0 \end{pmatrix},$$

$$(14)$$

$$F_D(\boldsymbol{x}) := \begin{pmatrix} \dot{\boldsymbol{q}}^I \\ u_{y_D}(\boldsymbol{x}) - g \\ \frac{m}{I} u_{\varphi_D}(\boldsymbol{x}) \\ 1 \\ \dot{x} \\ u_{x_D}(\boldsymbol{x}) \\ 0 \\ 0 \end{pmatrix},$$

where:

$$u_{\varphi_F}(\boldsymbol{x}) = y\, u_{x_F}(\boldsymbol{x}) + \Delta x^f\, u_{y_F}(\boldsymbol{x}), \quad (15)$$
$$u_{\varphi_R}(\boldsymbol{x}) = y\, u_{x_R}(\boldsymbol{x}) + \Delta x^r\, u_{y_R}(\boldsymbol{x}),$$
$$u_{\varphi_D}(\boldsymbol{x}) = y\, u_{x_D}(\boldsymbol{x}) + (\Delta x^f + \Delta x^r)\, u_{y_D}(\boldsymbol{x}).$$

In Section II-C, $u_{y_i}(\boldsymbol{x})$ and $u_{\varphi_i}(\boldsymbol{x})$ will be set to be constant throughout each of the stance modes. Until then, we use the more general functional form to illustrate in Section II-B that we can achieve a cascaded composition without requiring constant values.

For simplicity, we identify $\bar{y}$ with the value of fixed point's height component of (15) via the following approximation.

This, along with (the to be introduced) Approximation 2 and (33), will allow an explicit representation of a relevant hybrid periodic orbit derived in Section III:

Approximation 1. *In the pitching acceleration components* (15), *we take the stance height terms y to be the constant* $\bar{y} \in \mathbb{R}^+$.

Approximation 1 has the effect of replacing y with $\bar{y}$ in the horizontal force law (21). This assumption is approximately valid in the experiments of Section V as shown by the nearly-constant height in Figures 9 and 10. Further implications of this assumption are discussed in Section III-C.

The set of physical parameters is the body length d, gravity's acceleration g, the body mass m, and moment of inertia I (also we later introduce Δx^{Avg} (22), a (23), and l_0 (25) as pseudo-physical parameters chosen by the user for the controller that are strongly influenced by the physical parameters), and the vertical and horizontal (mass-specific) force laws are respectively:

$$u_{y_i} : D_i \to (\frac{g}{2}, g), \quad (16)$$
$$u_{x_i} : D_i \to \mathbb{R},$$

which we later set in (21), (33). The interval bounds on the codomain of $u_{y_i}(\cdot)$ is artificially imposed both to take into account the actuator constraints of Section V-A and to give the range of vertical forces over which the hybrid periodic orbit result described in Proposition 1 holds. Note that $u_{x_D}(\boldsymbol{x})$ is the sum of the double-support force components from each leg, how this force burden is distributed to the legs is an implementation detail (e.g., adjusted in case of reduced traction detected at one or another toe). The experiments of Section V used an even distribution.

The collection of guards is:

$$\mathcal{G} := \sqcup_{(i,j) \in \mathcal{T}} G_{i,j}, \quad (17)$$

where $G_{i,j} \subset D_i$ for each $(i,j) \in \mathcal{T}$. We assume that the robot's hip is able to retract its legs in stance to force a flight event and similarly protract its legs in flight to influence the timing of a stance event, according to intersection with a guard set. The guards are considered part of the controller and are further specified in (24), (25) and in Section IV-A.

Finally, the hybrid reset map is given by:

$$\mathcal{R} : \mathcal{G} \to \mathcal{D}, \quad (18)$$

which restricts to:

$$R_{i,j} := \mathcal{R}|_{G_{i,j}} \quad (19)$$
$$R_{i,j} : G_{i,j} \to D_j,$$

for each $(i,j) \in \mathcal{T}$. The resets – considered part of the controller and specified in (29) and Section IV-B – move the horizontal state of the toes instantaneously in flight (taking advantage of the assumption of massless legs) and reset the mode timer component τ to zero. To avoid physically unrealistic situations, we require that the resets give all other states continuous motion across hybrid transitions as these states have associated mass.

B. Cascaded Composition

We impose a cascaded composition (Section I-A) with the following choice of force laws and hybrid transitions. We first decouple the horizontal state from the in-place continuous dynamics by choice of horizontal and vertical force laws, giving the in-place acceleration components $c_i(\cdot)$ the form $c_i(x) = c_i(x^I) \ \forall i \in \mathcal{J}$. To do so, we specify the vertical force law to be only a function of in-place state:

$$u_{y_i}(\boldsymbol{x}) = u_{y_i}(\boldsymbol{x}^I), \quad \forall i \in \mathcal{J} \tag{20}$$

(which will be set to the constant the constant $u_{y_i}(\boldsymbol{x}^I) = u_y$ in Section II-C), and let the horizontal force law be given by[2]:

$$u_{x\mathrm{F}}(\boldsymbol{x}) = \frac{u_y(\boldsymbol{x}^I)}{\bar{y}}(\quad \Delta x^{\mathrm{Avg}} - \Delta x^f), \tag{21}$$

$$u_{x\mathrm{D}}(\boldsymbol{x}) = -\frac{u_{y\mathrm{D}}(\boldsymbol{x}^I)}{\bar{y}}(\quad \Delta x^f + \Delta x^r),$$

$$u_{x\mathrm{R}}(\boldsymbol{x}) = \frac{u_{y\mathrm{R}}(\boldsymbol{x}^I)}{\bar{y}}(-\Delta x^{\mathrm{Avg}} - \Delta x^r),$$

which makes the pitch dynamics act as if the only torque on the body were from a vertically applied $u_{y_i}(\boldsymbol{x}^I)$ associated with a leg splay of:

$$\Delta x^{\mathrm{Avg}} \in \mathbb{R}. \tag{22}$$

We choose to set Δx^{Avg} to equal $\frac{d}{2}$, representing pitch dynamics that mimic the toes being directly below the hips – a choice that maximizes the platform's achievable running speed as discussed in Section III-E. In principle any Δx^{Avg} could be chosen, and so for generality we don't fix Δx^{Avg} in our mathematical results. The resulting pitch dynamics from the force law (21) are:

$$\ddot{\varphi}_{\mathrm{F}} = \frac{2u_{y\mathrm{F}}(\boldsymbol{x}^I)}{da}, \quad \ddot{\varphi}_{\mathrm{D}} = 0, \quad \ddot{\varphi}_{\mathrm{R}} = -\frac{2u_{y\mathrm{R}}(\boldsymbol{x}^I)}{da}$$

(which in Section II-C become the constants $\ddot{\varphi}_{\mathrm{F}} = \frac{2u_y}{da}$, $\ddot{\varphi}_{\mathrm{D}} = 0$, $\ddot{\varphi}_{\mathrm{R}} = -\frac{2u_y}{da}$ with the choice $u_{y_i}(\boldsymbol{x}^I) = u_y$), where:

$$a := \frac{I}{m\frac{d}{2}\Delta x^{\mathrm{Avg}}} \tag{23}$$

is a dimensionless generalized Murphy number [13, p. 193] induced by the leg splay Δx^{Avg} and body parameters [3].

We next decouple the horizontal state from the in-place hybrid transitions. To do so, we first let only the in-place state components determine the guard intersections:

$$G_{i,j} := \{\boldsymbol{x} \in D_i \mid \boldsymbol{x}^I \in G_{i,j}^I\}. \tag{24}$$

[2]The smallest value of y is physically bounded by the kinematics to be far from zero so the quotient in (21) would never create a problem.

[3]We define our generalized Murphy number as $a := \frac{I}{m\frac{d}{2}\Delta x^{\mathrm{Avg}}}$, where I is the body's moment of inertia, d is the body length, and m is the body mass. When the leg splay distance Δx^{Avg} goes to $\frac{d}{2}$, then our definition agrees with Raibert's presentation of the Murphy number, which he represented by the symbol j. "Murphy found that when $j < 1$ the attitude of the body can be passively stabilized in a bounding gait. When $j > 1$, stabilization is not so easily obtained" [13, p. 193]. We use a generalized version of Murphy's result because we feel that accounting for a toe not being directly under the hips when bounding in-place is important, as the user may want to use an arbitrary leg splay. See Figure 7 for a visual depiction of the Murphy number as it relates to this paper's simplified model.

If instead we allowed the horizontal state to enter into the form of the guards, then the horizontal flow could influence the mode transitions via the time-to-guard-impact map and thereby affect the the in-place state components, violating the feedforward dependence we are constructing.

Specifically, we define the mode guard set $G_{i,j}^I$ as when a hip's height $y^{j_{hip}} : D^I \to \mathbb{R}$, $j \in \{f, r\}$ is moving in the correct direction for a mode change and is equal to some value $l_0 \in \mathbb{R}^+$ plus the value of a control function $g(\boldsymbol{x}^I) : D^I \to \mathbb{R}$ as given by:

$$G_{\mathrm{F,D}}^I := \{\boldsymbol{x}^I \in D^I{}_{\mathrm{F}} \mid y^{r_{hip}}(\boldsymbol{x}^I) = l_0 + g_{TD}(\boldsymbol{x}^I) \tag{25}$$
$$\wedge \ \dot{y}^{r_{hip}}(\boldsymbol{x}^I) < 0\},$$
$$G_{\mathrm{D,R}}^I := \{\boldsymbol{x}^I \in D^I{}_{\mathrm{D}} \mid y^{f_{hip}}(\boldsymbol{x}^I) = l_0 + g_{LO}(\boldsymbol{x}^I)$$
$$\wedge \ \dot{y}^{f_{hip}}(\boldsymbol{x}^I) > 0\},$$
$$G_{\mathrm{R,D}}^I := \{\boldsymbol{x}^I \in D^I{}_{\mathrm{R}} \mid b^I(\boldsymbol{x}^I) \in G_{\mathrm{F,D}}^I\},$$
$$G_{\mathrm{D,F}}^I := \{\boldsymbol{x}^I \in D^I{}_{\mathrm{D}} \mid b^I(\boldsymbol{x}^I) \in G_{\mathrm{D,R}}^I\},$$

where the guard $G_{\mathrm{F,D}}^I$ represents the rear leg's touchdown event that initiates double support, $G_{\mathrm{D,R}}^I$ represents the front leg's liftoff event that initiates rear stance, $G_{\mathrm{R,D}}^I$ represents the front leg's touchdown event that initiates double-support, and $G_{\mathrm{D,F}}^I$ represents the rear leg's liftoff event that initiates front stance.

In (25), the function $b^I : D^I \to D^I$ is an involutory symmetry map intended to enforce a symmetric bound:

$$b^I(\boldsymbol{x}^I) := (y, -\varphi, \dot{y}, -\dot{\varphi}, \tau)^T, \tag{26}$$

and the functions g_{LO}, g_{TD} represent the control functions used to modify the touchdown or liftoff hip height from the nominal value of l_0 as a function of state so as to achieve the desired gait. The control functions are chosen in (57) of Section IV-A, but for now we require that they go to zero when the state lies on the desired gait and that:

$$\mathcal{L}_{F_{\mathrm{F}}^I} \, g_{TD} \geq 0, \quad \mathcal{L}_{F_{\mathrm{D}}^I} \, g_{LO} \leq 0, \tag{27}$$

so that the hip-height at which touchdown occurs is never decreasing in time during flight and the hip-height at which liftoff occurs is never increasing in time during stance – conditions that will be used in the proof of Proposition 1 to guarantee the existence of a specific hybrid periodic orbit. Here F_{F}^I and F_{D}^I represent the in-place components of the vector field (14) in modes F and D, respectively. The value l_0 represents the leg length at touchdown and liftoff on the hybrid limit cycle and should be chosen to be sufficiently far from the workspace singularity as to have room to implement g_{LO}, g_{TD} to stabilize the gait.

Approximation 2. *We use a small-angle approximation on the robot pitch for purposes of checking guard intersections.*

Thus, in the representation of the guards in (25), we take the hip heights to be:

$$y^{r_{hip}}(\boldsymbol{x}^I) := y - \frac{d}{2}\varphi, \qquad y^{f_{hip}}(\boldsymbol{x}^I) := y + \frac{d}{2}\varphi, \tag{28}$$

$$\dot{y}^{r_{hip}}(\boldsymbol{x}^I) := \dot{y} - \frac{d}{2}\dot{\varphi}, \qquad \dot{y}^{f_{hip}}(\boldsymbol{x}^I) := \dot{y} + \frac{d}{2}\dot{\varphi}.$$

We expect this to be reasonably valid at lower levels of pitching such as those observed in the experiments of Section V, but expect its validity will deteriorate if limiting behavior with high pitch is commanded.

Finally, we give the resets $R_{i,j}$ the cascaded form (1):

$$R_{i,j}(\boldsymbol{x}^I, \boldsymbol{x}^H) = \begin{pmatrix} R_{i,j}^I(\boldsymbol{x}^I) \\ R_{i,j}^H(\boldsymbol{x}^I, \boldsymbol{x}^H) \end{pmatrix}. \tag{29}$$

There is relatively little choice in how to reset the state components since they are largely physically determined, however we are free to reset the mode timers τ as they are non-physical and to reset the horizontal toe positions in flight.

Specifically, we define the in-place resets as:

$$R_{i,j}^I : G_{i,j}^I \to D_j^I \tag{30}$$
$$(\boldsymbol{q}^I \dot{\boldsymbol{q}}^I, \tau) \mapsto (\boldsymbol{q}^I \dot{\boldsymbol{q}}^I, 0)$$

for each $(i,j) \in \mathcal{T}^I$, where $R_{i,j}^I \equiv R^I$ simply zeros the timer component of the state. The horizontal resets represent the affordance to stabilize the horizontal components of the model for a bounding gait, in the same manner as the guards for the in-place state components. In placing the foot horizontally ahead or behind of a nominal touchdown configuration according to some control function, they function much like Raibert's neutral point controller [13]. They are defined as:

$$R_{\mathrm{F,D}}^H : \begin{pmatrix} x \\ \dot{x} \\ \Delta x^r \\ x^f \end{pmatrix} \mapsto \begin{pmatrix} x \\ \dot{x} \\ x + \Delta x^r + r_{\mathrm{F,D}}(\boldsymbol{x}_{\mathrm{F}}^H) \\ x^f \end{pmatrix}, \tag{31}$$
$$R_{\mathrm{R,D}}^H(\boldsymbol{x}_{\mathrm{R}}^H) = b^H \circ R_{\mathrm{F,D}}^H \circ b^H(\boldsymbol{x}_{\mathrm{R}}^H),$$
$$R_{\mathrm{D,R}}^H : \begin{pmatrix} x \\ \dot{x} \\ x^r \\ x^f \end{pmatrix} \mapsto \begin{pmatrix} x \\ \dot{x} \\ x^r \\ \Delta x^{\mathrm{Nom}} + r_{\mathrm{D,R}}(\boldsymbol{x}_{\mathrm{D}}^H) \end{pmatrix},$$
$$R_{\mathrm{D,F}}^H(\boldsymbol{x}_{\mathrm{D}}^H) = b^H \circ R_{\mathrm{D,R}}^H \circ b^H(\boldsymbol{x}_{\mathrm{D}}^H),$$

where:

$$b^H : \mathbb{R}^4 \to \mathbb{R}^4 \tag{32}$$
$$: \begin{pmatrix} x_1 \\ x_2 \\ x_3 \\ x_4 \end{pmatrix} \mapsto \begin{pmatrix} x_1 \\ x_2 \\ x_4 - 2\Delta x^{\mathrm{Avg}} \\ x_3 + 2\Delta x^{\mathrm{Avg}} \end{pmatrix}$$

is an involutory symmetry map intended to enforce a symmetric bound. The control functions $r_{\mathrm{F,D}}(\boldsymbol{x}_{\mathrm{F}}^H), r_{\mathrm{D,R}}(\boldsymbol{x}_{\mathrm{D}}^H)$ (chosen in (62) of Section IV-B) modify the horizontal foot placement in flight prior to touchdown, and – like g_{LO}, g_{TD} – we require that they go to zero when the state lies on the desired gait. The constant value $\Delta x^{\mathrm{Nom}} \in \mathbb{R}$ (chosen in (50) of Section III-C) represents a nominal touchdown leg splay magnitude.

Having removed all influence of the horizontal state from the in-place hybrid dynamics, we have endowed a feed-forward structure in which the in-place state alone determines the in-place hybrid execution and which feeds forward into the horizontal dynamics, making any suitably chosen Poincaré map for the system have the cascaded architecture (1).

C. Dynamical Simplification

To further simplify the dynamics, we choose the (mass-specific) vertical force component generated at each foot to be the constant u_y:

$$u_{y_i}(\boldsymbol{x}^I) = u_y \quad \forall i \in \mathcal{J}, \tag{33}$$

giving the in-place state components a mode-i flow $\phi_i^t(\boldsymbol{x}^I)$ of the form:

$$\phi_i^t(\boldsymbol{x}^I) = \begin{pmatrix} I & tI & 0 \\ 0 & I & 0 \\ 0 & 0 & 1 \end{pmatrix} \boldsymbol{x}^I + \begin{pmatrix} \frac{t^2}{2}\boldsymbol{c}_i \\ t\boldsymbol{c}_i \\ t \end{pmatrix}, \tag{34}$$

$$\boldsymbol{c}_{\mathrm{F}} = \begin{pmatrix} u_y - g \\ \frac{2u_y}{da} \end{pmatrix}, \quad \boldsymbol{c}_{\mathrm{D}} = \begin{pmatrix} 2u_y - g \\ 0 \end{pmatrix}, \quad \boldsymbol{c}_{\mathrm{R}} = \begin{pmatrix} u_y - g \\ -\frac{2u_y}{da} \end{pmatrix}.$$

Approximations 1, 2 and (33) result in the simplified cascaded dynamics depicted in Figure 4. In particular, the choice of a constant vertical force gives rise to affine horizontal continuous dynamics with mass-center forwards acceleration given by:

$$\text{Mode F:} \quad \ddot{x} = \frac{u_y}{\bar{y}} \left(\Delta x^{\mathrm{Avg}} - \Delta x^f \right),$$

$$\text{Mode D:} \quad \ddot{x} = -\frac{u_y}{\bar{y}} \left(\Delta x^f + \Delta x^r \right),$$

$$\text{Mode R:} \quad \ddot{x} = \frac{u_y}{\bar{y}} \left(-\Delta x^{\mathrm{Avg}} - \Delta x^r \right),$$

and the corresponding mode-i horizontal-component flow $\hat{\phi}_i^t(\boldsymbol{x}_i^H)$ of the form:

$$\hat{\phi}_{\mathrm{F}}^t(\boldsymbol{x}_{\mathrm{F}}^H) = \tag{35}$$
$$\begin{pmatrix} e^{C_{\mathrm{F}}t}\begin{pmatrix} x \\ \dot{x} \end{pmatrix} + \left(e^{C_{\mathrm{F}}t} - I \right) C_{\mathrm{F}}^{-1} \begin{pmatrix} 0 \\ \frac{u_y}{\bar{y}}\left(\Delta x^{\mathrm{Avg}} - x^f \right) \end{pmatrix} \\ \Delta x^r \\ x^f \end{pmatrix},$$

$$\hat{\phi}_{\mathrm{D}}^t(\boldsymbol{x}_{\mathrm{D}}^H) = $$
$$\begin{pmatrix} e^{C_{\mathrm{D}}t}\begin{pmatrix} x \\ \dot{x} \end{pmatrix} + \left(e^{C_{\mathrm{D}}t} - I \right) C_{\mathrm{D}}^{-1} \begin{pmatrix} 0 \\ -\frac{u_y}{\bar{y}}\left(x^r + x^f \right) \end{pmatrix} \\ x^r \\ x^f \end{pmatrix},$$

$$\hat{\phi}_{\mathrm{R}}^t(\boldsymbol{x}_{\mathrm{R}}^H) = $$
$$\begin{pmatrix} e^{C_{\mathrm{R}}t}\begin{pmatrix} x \\ \dot{x} \end{pmatrix} + \left(e^{C_{\mathrm{R}}t} - I \right) C_{\mathrm{R}}^{-1} \begin{pmatrix} 0 \\ \frac{u_y}{\bar{y}}\left(-\Delta x^{\mathrm{Avg}} - x^r \right) \end{pmatrix} \\ x^r \\ \Delta x^f \end{pmatrix},$$

where:

$$C_{\mathrm{F}} = \begin{pmatrix} 0 & 1 \\ \frac{u_y}{\bar{y}} & 0 \end{pmatrix} \quad C_{\mathrm{D}} = \begin{pmatrix} 0 & 1 \\ \frac{2u_y}{\bar{y}} & 0 \end{pmatrix} \quad C_{\mathrm{R}} = \begin{pmatrix} 0 & 1 \\ \frac{u_y}{\bar{y}} & 0 \end{pmatrix}. \tag{36}$$

III. HYBRID PERIODIC ORBIT

The explicit flow representation (34), (35) – combined with guards (25) and resets (31) – yields expressions for the mode maps (37) (derived from the implicit function expressing time to the guard), which are composed in Sections III-A and III-B to form a stride map for the model. We take advantage of
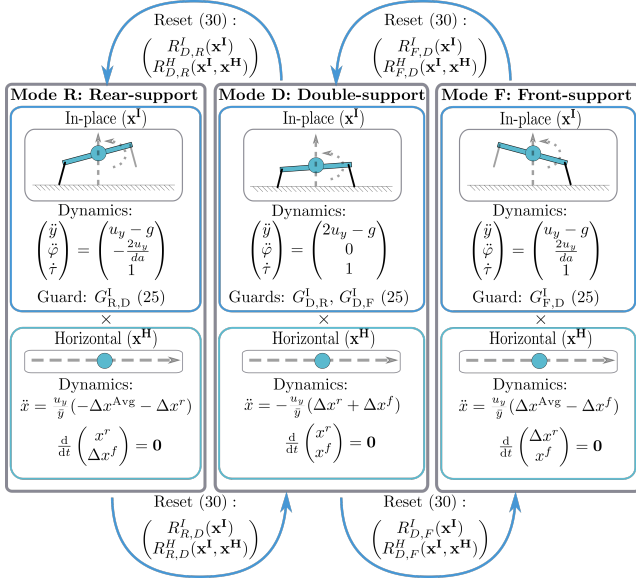
Fig. 4. Cascaded hybrid dynamics achieved through the choice of force laws and hybrid guards and resets. The choice of force laws (20), (21) decouple the continuous dynamics of the hybrid system (3) into the cross product of "in-place" and "horizontal" vector fields representing the behavior of the "in-place" vertical and pitching states $\boldsymbol{x}^I$ as well as the "horizontal" fore-aft mass-center and toe position states $\boldsymbol{x}^H$. The isolated continuous dynamics – along with the hybrid guards being purely dependent on the in-place states (24) and the hybrid reset maps having cascaded form (29) – endows a feed-forward relationship between the in-place states and horizontal states in which a linearized stability analysis of a hybrid periodic orbit's Poincaré map Jacobian has the separation of eigenvalues property indicated by (2), allowing for a more tractable analysis. A stable limit cycle is achieved by controlling on the hybrid guards and the resets via (25), (30), and (31). In the vertical states, this is accomplished on the guards by vertically retracting the leg in stance to transition to flight and similarly by protracting the leg in flight to affect the onset of stance. In the horizontal states, this is accomplished on the resets by placing the toe position horizontally in flight in a similar fashion to Raibert's neutral point algorithm [13].

symmetry to derive a simpler half-stride Poincaré map, and in Section III-C express a closed-form fixed point (Proposition 1) representing a hybrid periodic orbit. With the form of the hybrid periodic orbit in mind, Section III-D revisits the validity of Approximation 1 (assuming a constant mass-center height in the pitch dynamics), Section III-E discusses a forward-running speed limit associated with the kinematic limitations of a physical machine, and Section III-F discusses the actuator cost to enforce the cascaded decoupling of Section II-B.

A. Choice of Poincaré Section

We now introduce a symmetry that expresses the dynamics of the mode F and its transition into the mode D as a mirror image of mode R and its corresponding transition to D. By restricting attention to only symmetric bounds, this observation affords a factorization of the resulting Poincaré map modeling a stride cycle as comprising a pair of successive half-strides. These considerations in turn motivate our choice of a Poincaré section (with coordinates denoted by a $\sim$ superscript) at the image of the guards under the hybrid reset map of the paired half-strides corresponding to the event of the timer for one being reset to initiate the timer of the next.

Each hybrid mode has an associated map taking a starting state to its value along the forward flow intersecting a guard. For convenience we pre-compose this with the appropriate reset map, so that the hybrid mode-reset composition – which we refer to as the *mode map* and denote by $\Phi_{i,j}$ – maps a starting state in mode i to the reset of where the forward flow intersects the guard $G_{i,j}$. Specifically:

$$\Phi_{i,j} : \begin{pmatrix} U_{i,j}^I \\ D_i^H \end{pmatrix} \subset D_i \to D_j, \ (i,j) \in \mathcal{T}, \qquad (37)$$

$$\begin{pmatrix} \boldsymbol{x}^I \\ \boldsymbol{x}^H \end{pmatrix} \mapsto \begin{pmatrix} R^I \circ \phi_i^{T_{i,j}^I(\boldsymbol{x}^I)}(\boldsymbol{x}^I) \\ R_i^H \circ \hat{\phi}_i^{T_{i,j}^I(\boldsymbol{x}^I)}(\boldsymbol{x}^H) \end{pmatrix},$$

(recalling the forms of the resets R^I (30), R_i^H (31), the in-place flow ϕ_i (34), and the horizontal flow $\hat{\phi}_i$ (35)) where we denote the separate components of $\Phi_{i,j}$ as:

$$\Phi_{i,j}(\boldsymbol{x}^I, \boldsymbol{x}^H) = \begin{pmatrix} \Phi_{i,j}^I(\boldsymbol{x}^I) \\ \Phi_{i,j}^H(\boldsymbol{x}^I, \boldsymbol{x}^H) \end{pmatrix}, \qquad (38)$$

and where:

$$T_{i,j}^I : U_{i,j}^I \to \mathbb{R}^+ \qquad (39)$$
$$\boldsymbol{x}^I \mapsto \min\{t \in \mathbb{R}^+ | \phi_i^t(\boldsymbol{x}^I) \in G_{i,j}^I\}$$

denotes the implicit time-to-impact map of the flow with the guard. Here $U_{i,j}^I$ represents the largest subset of D_i^I over which $T_{i,j}^I(\cdot)$ is defined and over which the forward flow does not first intersect another guard. We show in the proof of Proposition 1 the existence of points $\bar{\boldsymbol{x}}_{\text{F0,D}}^I \in U_{\text{F,D}}^I$, $\bar{\boldsymbol{x}}_{\text{D0,R}}^I \in U_{\text{D,R}}^I$, $b^I(\bar{\boldsymbol{x}}_{\text{F0,D}}^I) \in U_{\text{R,D}}^I$, and $b^I(\bar{\boldsymbol{x}}_{\text{D0,R}}^I) \in U_{\text{D,F}}^I$, hence the sets $U_{i,j}^I$ are non-empty.

Define the involutory "bounding" symmetry map:

$$b : \quad D \to \quad D \qquad (40)$$
$$\begin{pmatrix} \boldsymbol{x}^I \\ \boldsymbol{x}^H \end{pmatrix} \mapsto \begin{pmatrix} b^I(\boldsymbol{x}^I) \\ b^H(\boldsymbol{x}^H) \end{pmatrix},$$

where b^I is given by (26) and b^H is given by (32). The map b induces a flow conjugacy between F_{F} and F_{R}, as well on flows in F_{D}. This, together with the guard symmetry (25) and reset symmetry (31), results in b inducing a topological conjugacy between $\Phi_{\text{F,D}}$ and $\Phi_{\text{R,D}}$, as well as between $\Phi_{\text{D,R}}$ and $\Phi_{\text{D,F}}$.

Define the reduced domains $\widetilde{D}_i$ to equal the domain D_i without mode-timer τ or forward position x components, so as to be of use in defining a stride map whose Poincaré section has the property $\tau = 0$ and does not contain a x component to permit stride map fixed points at speed. Specifically, let:

$$\widetilde{D}_i := \widetilde{D}_i^I \times \widetilde{D}_i^H, \quad i \in \mathcal{J}, \qquad (41)$$
$$\widetilde{D}_i^I := T(\mathbb{R} \times \mathbb{S}), \quad \widetilde{D}_i^H := \mathbb{R}^3$$

(where we sometimes drop the mode subscripts when appropriate), and the reduced state $\widetilde{\boldsymbol{x}} \in \widetilde{D}$ as:

$$\widetilde{\boldsymbol{x}} := \begin{pmatrix} \widetilde{\boldsymbol{x}}^I \\ \widetilde{\boldsymbol{x}}^H \end{pmatrix}, \quad \widetilde{\boldsymbol{x}}^I \in \widetilde{D}^I, \quad \widetilde{\boldsymbol{x}}^H \in \widetilde{D}^H. \qquad (42)$$

Specifically, passage between $\widetilde{D}$ and D occurs according to the projection $\Pi : D \to \widetilde{D}$ and lift $\Sigma : \widetilde{D} \to D$ maps:

$$\Pi(\boldsymbol{x}) \quad := \begin{pmatrix} \Pi^I(\boldsymbol{x}^I) \\ \Pi^H(\boldsymbol{x}^H) \end{pmatrix}, \tag{43}$$

$$\Pi^I(\boldsymbol{x}^I) := \begin{pmatrix} \boldsymbol{q}^I \\ \dot{\boldsymbol{q}}^I \end{pmatrix}, \quad \Pi^H : \begin{pmatrix} x_1 \\ x_2 \\ x_3 \\ x_4 \end{pmatrix} \mapsto \begin{pmatrix} x_2 \\ x_3 \\ x_4 - x_1 \end{pmatrix},$$

$$\Sigma(\boldsymbol{x}) \quad := \begin{pmatrix} \Sigma^I(\widetilde{\boldsymbol{x}}^I) \\ \Sigma^H(\widetilde{\boldsymbol{x}}^H) \end{pmatrix},$$

$$\Sigma^I(\widetilde{\boldsymbol{x}}^I) := \begin{pmatrix} \boldsymbol{q}^I \\ \dot{\boldsymbol{q}}^I \\ 0 \end{pmatrix}, \quad \Sigma^H : \begin{pmatrix} x_1 \\ x_2 \\ x_3 \end{pmatrix} \mapsto \begin{pmatrix} 0 \\ x_1 \\ x_2 \\ x_3 \end{pmatrix}.$$

B. Stride map

We are interested in the asymptotic behavior of a bounding gait with a periodic hybrid mode sequence $(F, D, R, D, ...)$. To this end, define the stride map S:

$$S : \begin{pmatrix} \widetilde{V}^I \\ \widetilde{D}^H \end{pmatrix} \subset \widetilde{D} \to \widetilde{D}, \tag{44}$$

$$\widetilde{\boldsymbol{x}} \mapsto \Pi \circ \Phi_{D,F} \circ \Phi_{R,D} \circ \Phi_{D,R} \circ \Phi_{F,D} \circ \Sigma,$$

local to some fixed point in the interior of the domain, where $\widetilde{V}^I \subset \Pi^I(U_{F,D}^I)$ is the largest subset of $\Pi^I(U_F^I)$ over which S^I is defined. We show in the proof of Proposition 1 the existence of such a fixed point of S^I, so $\widetilde{V}^I$ is not empty.

To simplify the analysis, we use the fact that the stride map factors according to:

$$\begin{aligned} S =& \Pi \circ \Phi_{D,F} \circ \Phi_{R,D} \circ \Phi_{D,R} \circ \Phi_{F,D} \circ \Sigma \tag{45} \\ =& \Pi \circ (b^H \circ \Phi_{D,R} \circ b^H) \circ (b^H \circ \Phi_{F,D} \circ b^H) \circ \\ & \quad \Phi_{D,R} \circ \Phi_{F,D} \circ \Sigma \\ =& \Pi \circ b^H \circ \Phi_{D,R} \circ \Phi_{F,D} \circ b^H \circ \Phi_{D,R} \circ \Phi_{F,D} \circ \Sigma \\ =& \Pi \circ b^H \circ \Phi_{D,R} \circ \Phi_{F,D} \circ (\Sigma \circ \Pi) \circ b^H \circ \\ & \quad \Phi_{D,R} \circ \Phi_{F,D} \circ \Sigma \\ =& (\Pi \circ b^H \circ \Phi_{D,R} \circ \Phi_{F,D} \circ \Sigma) \circ \\ & \quad (\Pi \circ b^H \circ \Phi_{D,R} \circ \Phi_{F,D} \circ \Sigma) \\ =& H^2, \end{aligned}$$

where $H : \begin{pmatrix} \widetilde{V}^I \\ \widetilde{D}^H \end{pmatrix} \to \widetilde{D}$ such that:

$$H := \Pi \circ b \circ \Phi_{D,R} \circ \Phi_{F,D} \circ \Sigma \tag{46}$$

represents a "flipped" (by b) half-stride of the stride map.

C. Stride Map Fixed Point

A stable fixed point of H is a stable fixed point of S, so we reduce our attention to the asymptotic behavior of H which is simpler. We note that we are interested in a symmetric bound so any fixed points of S that we are discarding by virtue of not being fixed points of H via the symmetry b are not symmetric.

Proposition 1. *The maps H and S have a fixed point at:*

$$\widetilde{\widetilde{\boldsymbol{x}}} := \begin{pmatrix} \widetilde{\widetilde{\boldsymbol{x}}}^I \\ \widetilde{\widetilde{\boldsymbol{x}}}^H \end{pmatrix}, \quad \widetilde{\widetilde{\boldsymbol{x}}}^I := \begin{pmatrix} \bar{y} \\ \bar{\varphi} \\ \dot{\bar{y}} \\ \dot{\bar{\varphi}} \end{pmatrix}, \quad \widetilde{\widetilde{\boldsymbol{x}}}^H := \begin{pmatrix} \dot{\bar{x}} \\ \bar{\Delta x^r} \\ \bar{\Delta x^f} \end{pmatrix}, \tag{47}$$

where:

$$\begin{pmatrix} \bar{y} \\ \bar{\varphi} \\ \dot{\bar{y}} \\ \dot{\bar{\varphi}} \end{pmatrix} = \begin{pmatrix} l_0 - \frac{u_y(g-u_y)}{4a(2u_y-g)} \bar{T}_{F,D}^2 \\ -\frac{u_y(g-u_y)}{2ad(2u_y-g)} \bar{T}_{F,D}^2 \\ \frac{g-u_y}{2} \bar{T}_{F,D} \\ -\frac{u_y}{ad} \bar{T}_{F,D} \end{pmatrix}, \tag{48}$$

and:

$$\bar{\Delta x^f} = \frac{\begin{pmatrix} 0 & 1 \end{pmatrix} \left(e^{C_F \bar{T}_{F,D}} - I \right) \begin{pmatrix} \Delta x^{Avg} \\ \dot{\bar{x}} \end{pmatrix}}{\begin{pmatrix} 0 & 1 \end{pmatrix} \left(e^{C_F \bar{T}_{F,D}} - I \right) \begin{pmatrix} 1 \\ 0 \end{pmatrix}}, \tag{49}$$

$$\begin{aligned} \bar{\Delta x^r} =& \bar{\Delta x^f} - 2\Delta x^{Avg} + \begin{pmatrix} 1 & 0 \end{pmatrix} \left(e^{C_D \bar{T}_{D,R}} + I \right)^{-1} \\ & \left(e^{C_D \bar{T}_{D,R}} - I \right) \left(e^{C_F \bar{T}_{F,D}} + I \right) \begin{pmatrix} \Delta x^{Avg} - \bar{\Delta x^f} \\ \dot{\bar{x}} \end{pmatrix}, \end{aligned}$$

where (recall (36)) $C_F = \begin{pmatrix} 0 & 1 \\ \frac{u_y}{\bar{y}} & 0 \end{pmatrix}$ and $C_D = \begin{pmatrix} 0 & 1 \\ \frac{2u_y}{\bar{y}} & 0 \end{pmatrix}$.

The fixed point $\widetilde{\widetilde{\boldsymbol{x}}}^H$ is parametrized by the physical parameters of the system, the duration $\bar{T}_{F,D} \in \mathbb{R}^+$ of the periodic orbit's evolution in mode F (equal to its duration in mode R), and the forward speed component $\dot{\bar{x}}$ of the fixed point. The term Δx^{Nom} in (31) is given by:

$$\Delta x^{\text{Nom}} = \bar{\Delta x^r} + 2\Delta x^{Avg}, \tag{50}$$

and the terms $\bar{\Delta x^r}_D$, $\bar{\Delta x^f}_D$ – defined in (49) and used in (62) – have the property that:

$$\bar{\Delta x^r}_D = \bar{\Delta x^f} - 2\Delta x^{Avg},$$
$$\bar{\Delta x^f}_D = -\bar{\Delta x^r}.$$

Additionally, the duration $\bar{T}_{D,R} = \bar{T}_{D,F}$ of the periodic orbit's evolution in mode D is equal to:

$$\bar{T}_{D,R} = \bar{T}_{F,D} \frac{g - u_y}{2u_y - g}. \tag{51}$$

Proof. See Appendix C. $\square$

The form of the fixed point does not give much insight into the nature of the resulting orbit and how parameter choices (particularly u_y and $\bar{T}_{F,D}$) affect it. As such, we give the minimum and maximum state variable values along the orbit associated with $\widetilde{\widetilde{\boldsymbol{x}}}$ in Table II. Recall that $u_y \in (\frac{g}{2}, g)$ (16) and $\bar{T}_{F,D} \in \mathbb{R}^+$, where the interval constraint on u_y guarantees a physically realistic double support phase on the hybrid periodic orbit to capture the actuator constraints of Section V-A. Additionally, the mass center height varies by a value of:

$$\frac{\bar{T}_{F,D}^2}{8} \frac{g - u_y}{2u_y - g} u_y \tag{52}$$

along the orbit.

The "user-specified" terms in the form of the hybrid periodic orbit (the terms not determined by the physical robot

State	Min value along orbit	Max value along orbit
y	$l_0 + \frac{1}{8}\bar{T}_{\mathrm{F,D}}^2 \frac{g-u_y}{2u_y-g}(\zeta-u_y)$	$l_0 + \frac{1}{8}\bar{T}_{\mathrm{F,D}}^2 \frac{g-u_y}{2u_y-g}\zeta$
	$\zeta = 2u_y(1-a^{-1}) - g$	
φ	$-\frac{gu_y\bar{T}_{\mathrm{F,D}}^2}{4ad(2u_y-g)},$	$\frac{gu_y\bar{T}_{\mathrm{F,D}}^2}{4ad(2u_y-g)}$
$\dot{y}$	$-\frac{g-u_y}{2}\bar{T}_{\mathrm{F,D}},$	$\frac{g-u_y}{2}\bar{T}_{\mathrm{F,D}}$
$\dot{\varphi}$	$-\frac{u_y}{ad}\bar{T}_{\mathrm{F,D}},$	$\frac{u_y}{ad}\bar{T}_{\mathrm{F,D}}$
$|\dot{x}|$	$\sqrt{\dot{\bar{x}}^2 - \xi},$	$|\dot{x}|$
	$\xi = \frac{u_y}{\bar{y}}\cdot\max\left\{(\Delta x^{\mathrm{Avg}} - \bar{\Delta x}^f)^2,\ \frac{1}{2}(\Delta x^{\mathrm{Nom}} - \bar{\Delta x}^f)^2\right\}$	
Δx^r	$-\Delta x^{\mathrm{Nom}},$	$-(2\Delta x^{\mathrm{Avg}} - \Delta x^{\mathrm{Nom}})$
Δx^f	$2\Delta x^{\mathrm{Avg}} - \Delta x^{\mathrm{Nom}},$	Δx^{Nom}

TABLE II
MINIMUM AND MAXIMUM STATE VALUES ALONG THE HYBRID PERIODIC ORBIT

Minimum and maximum state values along the hybrid periodic orbit associated with the fixed point $\tilde{\bar{x}}$ (defined in Proposition 1) of H (46) as determined by the parameters and "user-specified" selection of $u_y \in (\frac{g}{2}, g)$ (16), $\bar{T}_{\mathrm{F,D}} \in \mathbb{R}^+$, and $\dot{\bar{x}} \in \mathbb{R}$. In practice $\dot{\bar{x}}$ is not truly a free variable, as a speed limit (approximated by (55)) exists by virtue of a machine's inherently limited leg workspace constraining the maximum achievable leg sweep distance. Both legs sweep a distance of $\delta\bar{x}_{\mathrm{Stance}} = |2(\Delta x^{\mathrm{Nom}} - \Delta x^{\mathrm{Avg}})|$ during their stance phases, a complicated expression (due to the form of Δx^{Nom} (50)) for which an approximation is proposed in (54). Figure 5 shows the hybrid periodic orbit trajectory when using the parameters of Table III, illustrating where in the mode sequence the minima and maxima occur.

parameters) are u_y, $\bar{T}_{\mathrm{F,D}}$, and $\dot{\bar{x}}$. The (mass-specific) applied vertical force at the toe u_y can be thought of as analogous to a spring constant: increasing u_y decreases vertical height and pitch oscillations[4], as well as total hip stance time (by decreasing the double-support time $\bar{T}_{\mathrm{D,R}}$ (51)), where the total hip's stance time $\bar{T}_{\mathrm{Stance}}$ is equal to:

$$\bar{T}_{\mathrm{Stance}} := \bar{T}_{\mathrm{F,D}} + 2\bar{T}_{\mathrm{D,R}} = \bar{T}_{\mathrm{F,D}}\left(\frac{g}{2u_y-g}\right). \quad (53)$$

The value of $\bar{T}_{\mathrm{F,D}}$ directly sets the single-support stance duration (equal to a hip's flight duration) and can be thought of as the dominant determiner of a hip's total stance time $\bar{T}_{\mathrm{Stance}}$ in cases with shorter double support $\bar{T}_{\mathrm{D,R}}$[5]. Larger values of $\bar{T}_{\mathrm{F,D}}$ increase vertical height and pitch oscillations. Smaller values of $\bar{T}_{\mathrm{F,D}}$ leaves less time for the leg to reset its position in flight, and sufficiently small values will be prohibitive for the actuators. The value of $\dot{\bar{x}}$ sets the desired speed at mode transitions.

[4]The reason that increasing the stance force u_y decreases height y and pitch φ variations of the orbit is because total stance time (53) is reduced by an increase in u_y, giving the system configuration less time to change in stance. While the variations in y and φ decrease with increasing u_y, total energy of the orbit increases.

[5]Our regime of operation involves a short double support time $\bar{T}_{\mathrm{D,R}}$, however the double support time would be longer for very low vertical forces approaching just barely supporting the weight of the robot. In this case a change of variables to total support time might be more insightful.
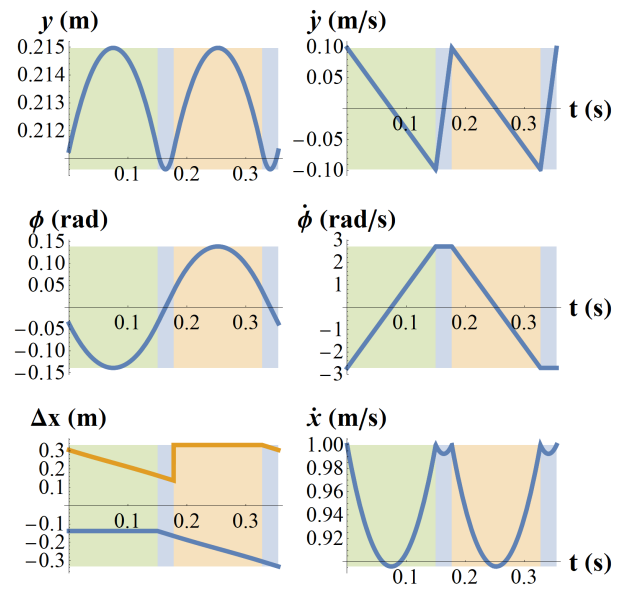

Fig. 5. Traces of the hybrid periodic orbit over a full stride using the parameters of Table III at a commanded speed of 1 m/s. The background color indicates the mode (4). Green is F, blue is D, and yellow is R. In the Δx graph, the blue trace gives Δx^r while the orange trace gives Δx^f (12). Notice that deviations in body height y and forward speed $\dot{x}$ are quite small, indicating a valid Approximation 1 as discussed in Section III-D and a small value of ξ from Table II.

D. Constant Stance Height Approximation

With an explicit representation for the hybrid periodic orbit's mass-center height variation (52) in hand, we revisit Approximation 1's usage of a constant stance height in the pitching acceleration components of the dynamics (15). Approximation 1 will hold on the hybrid periodic orbit for height variation values of (52) that are small compared to the height of the robot.

For Inu using the experimental parameters of $u_y = 8.5$ m/s^2 and $\bar{T}_{\mathrm{F,D}} = 0.15$ seconds as indicated in Table III, the height variation of the mass-center along the desired limit cycle is equal to a deviation of 4 mm, thus the height is only expected to change 1% from its nominal value of 0.21 meters during the periodic orbit, which begins to approach the noise floor on our sensors and is thus more than sufficient for a constant approximation assumption. This is illustrated in the experimental traces of Inu running in Figures 9 and 10, where the mass-center height is approximately constant both in the experimental data and in the desired limit cycle.

More generally, the validity of this approximation is strongly dependent on the duration of the hip's stance but – for the following reasons – we expect it to hold for a large class of machines. In terms of the duration of the hip's stance (equal to 205 ms on Inu with the parameters of Table III), the mass-center's height deviation is equal to:

$$\frac{1}{8}\frac{\bar{T}_{\mathrm{Stance}}^2}{g^2}u_y(g-u_y)(2u_y-g),$$

which is maximized by u_y when $u_y = \frac{g}{6}(3+\sqrt{3}) \approx 0.79g$, resulting in a mass-center height deviation of $\frac{g\bar{T}_{\mathrm{Stance}}^2}{48\sqrt{3}}$. Stance durations of approximately 300 ms or less – where 300 ms

is a relatively long stance duration for robots of Inu's mass scale – result in mass-center height deviations of 1 cm or less – a small value compared to Inu's nominal mass-center height 0.21 meters while running. In biology, the duration of stance has a strong scale dependence: it generally increases with body mass and animals up to the size of horses have been documented having stance times of 300 ms or less [46][6]. If the same results were to hold on robots, even when using our antagonistic value of u_y we would expect that larger robots would satisfy Approximation 1 and that smaller robots (with much shorter stance times) would have an even smaller height deviation for their size[7]. Of course, one could design a robot with an artificially long stance duration to break the validity of Approximation 1 but this would result in a severely speed-limited robot as discussed in Section III-E.

E. Speed Limit

The inherently limited workspace of a leg's kinematic linkage induces a speed limit to running [47]. In our case, the leg linkage workspace must accommodate the maximum and minimum values of the leg splays Δx^r and Δx^f in Table II to physically instantiate the periodic orbit associated with the fixed point $\widetilde{x}$. This results in a horizontal leg-sweep distance of $\delta \bar{x}_{\text{Stance}} = |2(\Delta x^{\text{Nom}} - \Delta x^{\text{Avg}})|$, where recall Δx^{Nom} is speed dependent (50). The sweep distance has a complicated form in terms of the model parameters as Δx^{Nom} involves the complicated expression $\Delta \bar{x}^r$ (49), however we can understand the dominant terms using a simple approximation.

Approximate the average forward speed in stance by $\dot{\bar{x}}$, which is valid given a small value of the term ξ in Table II relative to $\dot{\bar{x}}^2$ (this applies to Inu as indicated by the small speed deviations in both the hybrid periodic orbit in Figure 5 and the robot's instantiation of those orbits in Figures 9, 10). Then the mass center's (and thus the hip's) horizontal sweep distance in stance $\delta \bar{x}_{\text{Stance}}$ is:

$$\delta \bar{x}_{\text{Stance}} \approx \dot{\bar{x}}(\bar{T}_{\text{F,D}} + 2\bar{T}_{\text{D,R}}) \qquad (54)$$
$$= \dot{\bar{x}}\bar{T}_{\text{F,D}} \left(\frac{g}{2u_y - g} \right)$$
$$\overset{(53)}{=} \dot{\bar{x}}\bar{T}_{\text{Stance}}.$$

A robot with a horizontal leg-stroke distance that is kinematically limited to $\delta x^{\text{Max}}_{\text{Stance}}$ and with a stance time $\bar{T}_{\text{Stance}}$ (limited from below by a value of u_y achievable by the actuators) would physically be able to instantiate an orbit with a maximum running speed magnitude $\dot{\bar{x}}^{\text{Max}}$ of:

$$\dot{\bar{x}}^{\text{Max}} \approx \frac{\delta x^{\text{Max}}_{\text{Stance}}}{\bar{T}_{\text{Stance}}} = \delta x^{\text{Max}}_{\text{Stance}} \frac{2u_y - g}{g\bar{T}_{\text{F,D}}}, \qquad (55)$$

a value of 1.6 m/s for Inu as explained in Section V-A.

We now revisit our decision in Section II-B to set Δx^{Avg} to equal $\frac{d}{2}$ so as to maximize forward running speed. The horizontal interval that the legs sweep when operating on the periodic orbit is centered at a distance of Δx^{Avg} from the mass center as calculated from Table II. Coarsely assume that the leg linkage workspace permits an interval of horizontal reach centered at the hip. The horizontal leg-sweep interval must be contained in the leg workspace interval for a physically realizable gait. The maximum speed that can be physically realized occurs when the horizontal leg-sweep interval and leg workspace interval are identical, which requires that they be centered at the same point, which requires Δx^{Avg} equal $\frac{d}{2}$.

F. Cost of Enforcing a Cascade

Proposition 1 allows us to revisit the cost of enforcing the cascade composition of Section II-B with the horizontal force law (21) along the hybrid periodic orbit. Very often in robotics, a disadvantage of canceling the natural system dynamics with control is that it requires significant actuation affordance. However – as we argue below – at lower speeds the horizontal forces needed to achieve this dynamic decoupling are quite small; they are only a fraction of the applied constant vertical force.

We quantify this by considering the maximum horizontal leg force magnitude encountered during a stride on the periodic orbit. This maximum value is obtained when the horizontal length from the toe to the mass-center is furthest from Δx^{Avg} (21). When operating on the hybrid periodic orbit, recall that the leg sweeps an interval of length $\delta \bar{x}_{\text{Stance}}$ centered at a distance Δx^{Avg} from the mass center (Section III-E), thus reaching out a maximum distance of $\frac{1}{2}\delta \bar{x}_{\text{Stance}}$ from the centered distance of Δx^{Avg} and giving the horizontal force the maximum stance magnitude[8]:

$$|u_{x\,\text{Max}}| = \frac{1}{2}|\delta \bar{x}_{\text{Stance}}|\frac{u_y}{\bar{y}}.$$

Putting this in terms of forward running speed using the approximation (54) gives:

$$|u_{x\,\text{Max}}| \approx \frac{1}{2}|\dot{\bar{x}}|\bar{T}_{\text{Stance}}\frac{u_y}{\bar{y}}. \qquad (56)$$

This force would be briefly equal to the applied specific vertical force u_y in stance at an average stance speed of $\dot{\bar{x}} = \frac{2\bar{y}}{\bar{T}_{\text{Stance}}}$. Using a duration of hip-stance of $\bar{T}_{\text{Stance}} = 0.2$ seconds and an average mass-center stance height of 0.21 meters (Inu's experimental parameters derived from Table III) results in a speed of 2.1 m/s where the maximum horizontal and vertical forces are briefly equal. Inu is kinematically limited to a running speed of approximately 1.6 m/s, so the platform cannot approach the high-cost-of-cascade-enforcement regime. On a quadruped not kinematically limited, higher speeds than $\dot{\bar{x}} = \frac{2\bar{y}}{\bar{T}_{\text{Stance}}}$ require that the toes reach sufficiently in front of or behind the hips to the point of causing the horizontal cascade-enforcement force to briefly eclipse the vertical at the

---

[6]In the study, ground contact time was found to be generally proportional to $M^{0.19 \pm 0.06}$ for animals with body mass M.

[7]One would also need to reconsider the use of this approximation when using a much more energetic gait that has a flight phase, but of course this would assume a difference hybrid mode sequence than is considered in this work.

[8]The given maximum horizontal force is really a conservative upper bound, as it corresponds to the double-support mode and a sensible user would not program both the front and rear legs to generate opposing internal forces of this magnitude, rather they could achieve the same total horizontal force on the body with much smaller horizontal toe forces to decrease internal forces. The user's choice of front/rear force distribution in double support is elaborated on near the end of Section II-A

beginning and end of stance. In these cases we can consider the cascade enforcement to be "expensive" for the actuators. A shorter stance duration (53) would mitigate this cost, achieving this through reducing $\bar{T}_{\mathrm{F,D}}$ would increase the actuator cost of resetting the leg's position in flight, and achieving this through increasing u_y would also tax the actuators.

The approximate cost of enforcing the cascade is linear in speed (56), going to zero when bounding in-place. Thus at low speeds and small horizontal forces we believe that the natural dynamics are themselves "almost" a feedforward cascade of the in-place module with the horizontal bead-on-a-wire dynamics, and that our choice of a horizontal force law represents only a slight "nudge" to the dynamics so as to complete this decoupling (Figure 4) and provide us with a tractable stability analysis.

IV. CONTROLLER

Control of the system to achieve a symmetric bound occurs on the hybrid guards and resets. Recall from Section II-B that cascading the dynamics naturally places the in-place control gains in the guards and the horizontal control gains in the resets. A summary of our control strategy is as follows.

The in-place controllers perform feedback on the mode timers and hip heights, as time and kinematic configuration are the most accurately measured aspects of the state as discussed in Section VI-A. Instead of controlling on the continuous value of the hip heights, we only control on their value at the start of the mode. This has the practical benefit of providing hip-height measurements for the controller even when the hip is in flight (having measured its value at liftoff), as well as the algebraic benefit of simplifying the stability calculations in Section IV-C as the hip-height values being controlled on don't change over the course of a mode. The fact that six easily measurable quantities exist per half-stride (two modes, each with one timer and two hip-height measurements) results in six control gains. Four of the gains are used to place the four poles of the stride map corresponding to the four in-place components (recall that the presence of the timer coordinate in the dynamics gives four in-place Poincaré map components, not three), and the remaining two gains are used to optimize for other performance criteria.

The reset controllers perform feedback on the system's forward speed and the two toe positions. This gives three gains (rather than six, as the controllers can only set the horizontal toe position in flight and not in stance) to place the three poles of the stride map corresponding to the three horizontal components (recall that one component corresponds to forward speed and the other two correspond to the horizontal toe locations). In principle the horizontal controller could be chosen to take in additional inputs and thereby allow the user to optimize for other performance criteria, for example the in-place mode timers and hip heights, however we found that performance was reasonable without needing to introduce additional feedback paths.

Section IV-A specifies the controller on the guards, which stabilizes the in-place state components. Section IV-B specifies the controller on the resets, which stabilizes the horizontal state components. Section IV-C presents the central stability result of the paper. Specifically, we present a choice of control weights that makes the Poincaré map Jacobian evaluated at the fixed point nilpotent (Proposition 2), making the closed-loop dynamics infinitesimally deadbeat.

A. Hybrid Guard Control

Recall that hybrid guards intersections (24), (25) require the appropriate hip height equal some nominal value l_0 plus some (to-be-specified) state-dependent guard control function $g_{LO}, g_{TD} : D^I \to \mathbb{R}$. Recall from above, we choose to use guard controllers that are functions of the mode timers and hip-heights – giving six control gains as shown below in (57) – as mode time and kinematic configuration (hip height) are the most accurately measured aspects of the in-place state by our robot as discussed in Section VI-A. Specifically, we use guard control functions of the following form:

$$g_{TD}(\boldsymbol{x}^I) := {\boldsymbol{k}^I}_{\mathrm{F}}^T \begin{pmatrix} y^{r_{hip}}{}_{\mathrm{F0}}(\boldsymbol{x}^I) - y^{r_{hip}}(\bar{\boldsymbol{x}}^I_{\mathrm{F0,D}}) \\ y^{f_{hip}}{}_{\mathrm{F0}}(\boldsymbol{x}^I) - y^{f_{hip}}(\bar{\boldsymbol{x}}^I_{\mathrm{F0,D}}) \\ \tau - \bar{T}_{\mathrm{F,D}} \end{pmatrix}, \quad (57)$$

$$g_{LO}(\boldsymbol{x}^I) := {\boldsymbol{k}^I}_{\mathrm{D}}^T \begin{pmatrix} y^{r_{hip}}{}_{\mathrm{D0}}(\boldsymbol{x}^I) - y^{r_{hip}}(\bar{\boldsymbol{x}}^I_{\mathrm{D0,R}}) \\ y^{f_{hip}}{}_{\mathrm{D0}}(\boldsymbol{x}^I) - y^{f_{hip}}(\bar{\boldsymbol{x}}^I_{\mathrm{D0,R}}) \\ \tau - \bar{T}_{\mathrm{D,R}} \end{pmatrix},$$

where the vectors $\boldsymbol{k}^I_{\mathrm{F}}, \boldsymbol{k}^I_{\mathrm{D}} \in \mathbb{R}^3$ represent control weights, $y^{f_{hip}}, y^{r_{hip}} : D^I \to \mathbb{R}$ give the front and rear hip heights (28), and the functions $y^{r_{hip}}{}_{i0}, y^{f_{hip}}{}_{i0} : D^I_i \to \mathbb{R}, i \in \mathcal{J}^I$ give the mode's initial hip heights (according to the hip heights that occurred when $\tau = 0$) via:

$$\begin{aligned} y^{r_{hip}}{}_{i0}(\boldsymbol{x}^I) &:= y^{r_{hip}} \circ \phi_i^{-\tau}(\boldsymbol{x}^I), \\ y^{f_{hip}}{}_{i0}(\boldsymbol{x}^I) &:= y^{f_{hip}} \circ \phi_i^{-\tau}(\boldsymbol{x}^I). \end{aligned} \quad (58)$$

The values of $\bar{\boldsymbol{x}}^I_{i0,j}$ in (57) are set as follows and represent "target" states for the controller to track, we choose them so that the control functions vanish by design along the hybrid orbit associated with a privileged fixed point of H. Denote the lift (43) of the stride map fixed point $\widetilde{\boldsymbol{x}}$ in Proposition 1 from $\widetilde{D}$ to D_{F} by:

$$\bar{\boldsymbol{x}} = \begin{pmatrix} \bar{\boldsymbol{x}}^I \\ \bar{\boldsymbol{x}}^H \end{pmatrix} := \Sigma(\widetilde{\boldsymbol{x}}), \quad (59)$$

and set $\bar{\boldsymbol{x}}^I_{i0,j}$ in (57) to equal the in-place component of the state of the hybrid execution initialized at $\bar{\boldsymbol{x}}$ as it periodically enters mode i before entering mode j according to:

$$\bar{\boldsymbol{x}}^I_{\mathrm{F0,D}} := \bar{\boldsymbol{x}}^I, \quad \bar{\boldsymbol{x}}^I_{\mathrm{D0,R}} := \Phi^I_{\mathrm{F,D}}(\bar{\boldsymbol{x}}^I). \quad (60)$$

Finally, let $\bar{T}_{\mathrm{F,D}}$ and $\bar{T}_{\mathrm{D,R}}$ in (57) agree with the durations of the hybrid trajectory in modes F and D, respectively.

Let $k^I{}_{\mathrm{F}i}$ and $k^I{}_{\mathrm{D}i}$ denote the i'th components of control parameter vectors $\boldsymbol{k}^I_{\mathrm{F}}$ and $\boldsymbol{k}^I_{\mathrm{D}}$, respectively. We impose the requirement that:

$$k^I{}_{\mathrm{F3}} \geq 0, \quad k^I{}_{\mathrm{D3}} \leq 0, \quad (61)$$

so that the hip-height necessary for touchdown is not decreasing in time and the hip-height necessary for liftoff is not increasing in time, satisfying (27).

Intuitively, the guard control functions (57) act as proportional controllers and modify the nominal touchdown or liftoff hip heights according to a weighted sum of errors between scalar-valued functions of the state and constant "target" values. These scalar-valued functions consist of the hip height values at the start of the mode execution (calculated by backflowing the state until the component τ coincides with 0 and examining the hip heights at that time instance, and physically implemented by measuring the state variables at the start of the mode) and the current mode duration according to τ. The "target" states were chosen to force the control functions to zero at the hybrid transitions along the privileged periodic orbit of Proposition 1, by setting them to equal the state along the orbit when the evolution initially enters mode i as it evolves to mode j. The control weights $\boldsymbol{k}^I{}_{\mathrm{F}}, \boldsymbol{k}^I{}_{\mathrm{D}}$ will be chosen in Section IV-C and Appendix A to make the periodic hybrid trajectory associated with $\widetilde{\widetilde{\boldsymbol{x}}}$ a stable hybrid limit cycle.

B. Hybrid Reset Control

Recall that the in-place components of the hybrid resets simply zero the mode timer variable τ, while the horizontal components of the reset place the foot horizontally in flight from a nominal value according to control functions $r_{\mathrm{F,D}}, r_{\mathrm{D,R}} : D^H \to \mathbb{R}$ (31). We choose reset control functions of the following form:

$$r_{\mathrm{F,D}}(\boldsymbol{x}_{\mathrm{F}}^H) := k_{\mathrm{F}}^H \left(\dot{x} - \dot{\bar{x}} \right), \tag{62}$$

$$r_{\mathrm{D,R}}(\boldsymbol{x}_{\mathrm{D}}^H) := \begin{pmatrix} k_{\mathrm{D},1}^H, & k_{\mathrm{D},2}^H \end{pmatrix} \begin{pmatrix} \Delta x^r - \Delta \bar{x}^r{}_{\mathrm{D}} \\ \Delta x^f - \Delta \bar{x}^f{}_{\mathrm{D}} \end{pmatrix},$$

where:

$$\boldsymbol{k}^H := \begin{pmatrix} k_{\mathrm{F}}^H & k_{\mathrm{D},1}^H & k_{\mathrm{D},2}^H \end{pmatrix}^T \in \mathbb{R}^3, \tag{63}$$

are control weight constants that will be chosen to stabilize the horizontal components of the gait in Section IV-C and Appendix A. The values of $\dot{\bar{x}}, \Delta \bar{x}^r{}_{\mathrm{D}}, \Delta \bar{x}^f{}_{\mathrm{D}} \in \mathbb{R}$ are equal to the values in Proposition 1 so that the control functions vanish along the privileged fixed point of the stride map (on the periodic orbit's intersection with $G_{\mathrm{D,R}}$, $\Delta \bar{x}^r{}_{\mathrm{D}}$ equals $(x^r - x)$ and $\Delta \bar{x}^f{}_{\mathrm{D}}$ equals $(x^f - x)$).

Intuitively, the reset control functions (62) act as proportional controllers – much like the guard control functions – to correctly place the foot horizontally in flight so as to control the horizontal state components. Note that the reset $R_{\mathrm{F,D}}^H$ takes place at the touchdown event, at which time the toe cannot move horizontally without undesirable slipping. Thus, in the physical implementation of $R_{\mathrm{F,D}}^H$ one should apply the control function $r_{\mathrm{F,D}}(\boldsymbol{x}_{\mathrm{F}}^H)$ continuously in flight (as in [36]) so that when touchdown does occur the toe is in the correct position to satisfy $R_{\mathrm{F,D}}^H$.

C. Controller Stability Analysis

In the half-stride map H (46), the horizontal states have no influence on the in-place components of H, giving the map the cascade form:

$$H(\widetilde{\boldsymbol{x}}) = \begin{pmatrix} H^I(\widetilde{\boldsymbol{x}}^I) \\ H^H(\widetilde{\boldsymbol{x}}^I, \widetilde{\boldsymbol{x}}^H) \end{pmatrix}, \tag{64}$$

and endowing a block-diagonal Jacobian (2) whose structure we will now take advantage of. The Jacobian of H is given by:

$$DH = D\Pi \cdot Db \cdot D\Phi_{\mathrm{D,R}} \cdot D\Phi_{\mathrm{F,D}} \cdot D\Sigma, \tag{65}$$

where:

$$D\Pi = \begin{pmatrix} D\Pi^I & 0 \\ 0 & D\Pi^H \end{pmatrix}, \quad Db = \begin{pmatrix} Db^I & 0 \\ 0 & Db^H \end{pmatrix},$$

$$D\Sigma = \begin{pmatrix} D\Sigma^I & 0 \\ 0 & D\Sigma^H \end{pmatrix},$$

with in-place components:

$$D\Pi^I = \begin{pmatrix} I & 0 & 0 \\ 0 & I & 0 \end{pmatrix}, \quad Db^I = \begin{pmatrix} 1 & 0 & 0 & 0 & 0 \\ 0 & -1 & 0 & 0 & 0 \\ 0 & 0 & 1 & 0 & 0 \\ 0 & 0 & 0 & -1 & 0 \\ 0 & 0 & 0 & 0 & 1 \end{pmatrix}, \tag{66}$$

$$D\Sigma^I = \begin{pmatrix} I & 0 \\ 0 & I \\ 0 & 0 \end{pmatrix},$$

and horizontal components:

$$D\Pi^H = \begin{pmatrix} 0 & 1 & 0 & 0 \\ 0 & 0 & 1 & 0 \\ -1 & 0 & 0 & 1 \end{pmatrix}, \quad Db^H = \begin{pmatrix} 1 & 0 & 0 & 0 \\ 0 & 1 & 0 & 0 \\ 0 & 0 & 0 & 1 \\ 0 & 0 & 1 & 0 \end{pmatrix},$$

$$D\Sigma^H = \begin{pmatrix} 0 & 0 & 0 \\ 1 & 0 & 0 \\ 0 & 1 & 0 \\ 0 & 0 & 1 \end{pmatrix}.$$

The mode-map Jacobians have the form:

$$D\Phi_{i,j}\Big|_{\boldsymbol{x}} = \begin{pmatrix} D_{\boldsymbol{x}^I}\Phi_{i,j}^I & 0 \\ D_{\boldsymbol{x}^I}\Phi_{i,j}^H & D_{\boldsymbol{x}^H}\Phi_{i,j}^H \end{pmatrix}\Big|_{\boldsymbol{x}},$$

where $D_{\boldsymbol{x}^I}\Phi_{i,j}^I \equiv D\Phi_{i,j}^I$ is given by (recalling the structure of the flow (34) and reset (30)):

$$D\Phi_{i,j}^I = \begin{pmatrix} I & T_{i,j}(\boldsymbol{x}^I{}_i)I & 0 \\ 0 & I & 0 \\ 0 & 0 & 0 \end{pmatrix} + \begin{pmatrix} \dot{\boldsymbol{q}} + \boldsymbol{c}_i T_{i,j}(\boldsymbol{x}_i^I) \\ \boldsymbol{c}_i \\ 0 \end{pmatrix} \frac{\partial T_{i,j}}{\partial \boldsymbol{x}^I}, \tag{67}$$

and where $\Phi_{i,j}^H(\boldsymbol{x}) = R_{i,j}^H \circ \hat{\phi}_i^{T_{i,j}^I(\boldsymbol{x}^I)}(\boldsymbol{x}^H)$ (37), with resets $R_{i,j}^H$ (31), (62), and horizontal flow $\hat{\phi}_i^t$ (35). Note that all the factors of DH are lower block-triangular.

The half-stride map Jacobian $DH\big|_{\widetilde{\boldsymbol{x}}}$ has the form:

$$DH\big|_{\widetilde{\boldsymbol{x}}} = \begin{pmatrix} D_{\widetilde{\boldsymbol{x}}^I}H^I & 0 \\ D_{\widetilde{\boldsymbol{x}}^I}H^H & D_{\widetilde{\boldsymbol{x}}^H}H^H \end{pmatrix}\Big|_{\widetilde{\boldsymbol{x}}}, \tag{68}$$

indicating the eigenvalue separation property discussed in Sections I-A. Four of the eigenvalues are determined from $D_{\widetilde{\boldsymbol{x}}^I}H^I\big|_{\widetilde{\boldsymbol{x}}} \equiv DH^I\big|_{\widetilde{\boldsymbol{x}}^I}$, given by:

$$DH^I\big|_{\widetilde{\boldsymbol{x}}^I} = D\Pi^I \cdot Db^I \cdot D\Phi_{\mathrm{D,R}}^I\big|_{\Phi_{\mathrm{F,D}}^I(\bar{\boldsymbol{x}}^I)} \cdot D\Phi_{\mathrm{F,D}}^I\big|_{\bar{\boldsymbol{x}}^I} \cdot D\Sigma^I, \tag{69}$$

where $\Phi_{\mathrm{F,D}}^{I}(\bar{\boldsymbol{x}}^{I})$ simplifies to $\begin{pmatrix} \bar{y}, & \bar{\varphi}, & -\dot{\bar{y}}, & -\dot{\bar{\varphi}}, & 0 \end{pmatrix}^{T}$. The remaining three eigenvalues are from $D_{\widetilde{\boldsymbol{x}}^{H}}H^{H}\big|_{\widetilde{\boldsymbol{x}}} \equiv D_{\widetilde{\boldsymbol{x}}^{H}}H^{H}\big|_{\widetilde{\boldsymbol{x}}^{I}}$, which has the form:

$$D_{\widetilde{\boldsymbol{x}}^{H}}H^{H}\big|_{\widetilde{\boldsymbol{x}}^{I}} = D\Pi^{H} \cdot Db^{H} \cdot D_{\boldsymbol{x}^{H}}R_{\mathrm{D,R}}^{H} \cdot D_{\boldsymbol{x}^{H}}\hat{\phi}_{\mathrm{D}}^{\bar{T}_{\mathrm{D,R}}} \cdot$$
$$D_{\boldsymbol{x}^{H}}R_{\mathrm{F,D}}^{H} \cdot D_{\boldsymbol{x}^{H}}\hat{\phi}_{\mathrm{F}}^{\bar{T}_{\mathrm{F,D}}} \cdot D\Sigma^{H}, \quad (70)$$

where:

$$D_{\boldsymbol{x}^{H}}\hat{\phi}_{\mathrm{F}}^{\bar{T}_{\mathrm{F,D}}} = \begin{pmatrix} e^{C_{\mathrm{F}}\bar{T}_{\mathrm{F,D}}} & (e^{C_{\mathrm{F}}\bar{T}_{\mathrm{F,D}}} - I)\begin{pmatrix} 0 & -1 \\ 0 & 0 \end{pmatrix} \\ 0 & I \end{pmatrix},$$

$$D_{\boldsymbol{x}^{H}}\hat{\phi}_{\mathrm{D}}^{\bar{T}_{\mathrm{D,R}}} = \begin{pmatrix} e^{C_{\mathrm{D}}\bar{T}_{\mathrm{D,R}}} & \frac{1}{2}(e^{C_{\mathrm{D}}\bar{T}_{\mathrm{D,R}}} - I)\begin{pmatrix} -1 & -1 \\ 0 & 0 \end{pmatrix} \\ 0 & I \end{pmatrix},$$

$$D_{\boldsymbol{x}^{H}}R_{\mathrm{F,D}}^{H} = \begin{pmatrix} I & 0 \\ \begin{pmatrix} 1 & k_{\mathrm{F}}^{H} \\ 0 & 0 \end{pmatrix} & I \end{pmatrix},$$

$$D_{\boldsymbol{x}^{H}}R_{\mathrm{D,R}}^{H} = \begin{pmatrix} I & 0 \\ \begin{pmatrix} 0 & 0 \\ -(k_{\mathrm{D,1}}^{H} + k_{\mathrm{D,2}}^{H}) & 0 \end{pmatrix} & \begin{pmatrix} 1 & 0 \\ k_{\mathrm{D,1}}^{H} & k_{\mathrm{D,2}}^{H} \end{pmatrix} \end{pmatrix},$$

and C_{F} and C_{D} are given in (36).

We can further simplify the Jacobian block $DH^{I}\big|_{\widetilde{\boldsymbol{x}}^{I}}$. By multiplying the values of Π^{I}, Σ^{I} through, (69) simplifies to:

$$DH^{I}\big|_{\widetilde{\boldsymbol{x}}^{I}} = D\widetilde{b}^{I} \cdot D\widetilde{\Phi}_{\mathrm{D,R}}^{I}\big|_{\Phi_{\mathrm{F,D}}^{I}(\bar{\boldsymbol{x}}^{I})} \cdot D\widetilde{\Phi}_{\mathrm{F,D}}^{I}\big|_{\bar{\boldsymbol{x}}^{I}}, \quad (71)$$

where:

$$D\widetilde{\Phi}_{i,j}^{I} = \begin{pmatrix} I & T_{i,j}(\boldsymbol{x}^{I}{}_{i})I \\ 0 & I \end{pmatrix} + \begin{pmatrix} \dot{\boldsymbol{q}} + \boldsymbol{c}_{i}T_{i,j}(\boldsymbol{x}_{i}^{I}) \\ \boldsymbol{c}_{i} \end{pmatrix} \frac{\partial T_{i,j}}{\partial \widetilde{\boldsymbol{x}}^{I}}, \quad (72)$$

$$D\widetilde{b}^{I} = \begin{pmatrix} 1 & 0 & 0 & 0 \\ 0 & -1 & 0 & 0 \\ 0 & 0 & 1 & 0 \\ 0 & 0 & 0 & -1 \end{pmatrix},$$

and – as specified in (71) – the points of evaluation for the terms $\frac{\partial T_{i,j}}{\partial \widetilde{\boldsymbol{x}}^{I}}$ all have in common that $\tau = 0$. The form of $\frac{\partial T_{i,j}}{\partial \widetilde{\boldsymbol{x}}^{I}}$ is given in Lemma 1.

We now have explicit expressions for all terms in the iterated map Jacobian DH (65) and can begin analysis of the map's local stability at $\widetilde{\boldsymbol{x}}$. It remains to choose weights $\boldsymbol{k}^{I}{}_{\mathrm{F}}, \boldsymbol{k}^{I}{}_{\mathrm{D}}$ in the hybrid guards (25), (57) and weights $\boldsymbol{k}^{H}$ (63) in the hybrid resets (31), (62) such that the spectral radius of $DH\big|_{\widetilde{\boldsymbol{x}}}$ (68) is less than unity.

Given the unwieldy form of the Jury stability criteria for fourth-order polynomials we instead opt to obtain an *infinitesimally deadbeat solution*, by which we mean that all the eigenvalues of the Jacobian of the iterated map evaluated at the fixed point are equal to zero.

Proposition 2. *For any operating point $\widetilde{\widetilde{\boldsymbol{x}}}$ (47), there exists a choice of gains $\boldsymbol{k}^{I}{}_{\mathrm{F}}$, $\boldsymbol{k}^{I}{}_{\mathrm{D}}$ (57), and $\boldsymbol{k}^{H}$ (63) that – conjectured on the conditions (82) – make the associated Poincaré map Jacobian $DH\big|_{\widetilde{\widetilde{\boldsymbol{x}}}}$ (68) nilpotent, endowing the operating point with infinitesimal deadbeat stability.*

Proof. The $D_{\widetilde{\boldsymbol{x}}^{I}}H^{I}$ component of $DH\big|_{\widetilde{\boldsymbol{x}}}$ in (68) is made nilpotent through the choice of gains $\boldsymbol{k}^{I}{}_{\mathrm{F}}$ and $\boldsymbol{k}^{I}{}_{\mathrm{D}}$ given in Lemma 2 (via the change of coordinates (74)), assuming the invertibility of the matrix (79) which we conjecture to be generically invertible[9]. The $D_{\widetilde{\boldsymbol{x}}^{H}}H^{H}$ component of $DH\big|_{\widetilde{\boldsymbol{x}}}$ is made nilpotent through the choice of gains $\boldsymbol{k}^{H}$ given in Lemma 3.

The eigenvalues of the block-triangular $DH\big|_{\widetilde{\boldsymbol{x}}}$ are given by the union of the eigenvalues of the diagonal blocks $D_{\widetilde{\boldsymbol{x}}^{I}}H^{I}$ and $D_{\widetilde{\boldsymbol{x}}^{H}}H^{H}$. These diagonal blocks are nilpotent, and so $DH\big|_{\widetilde{\boldsymbol{x}}}$ is nilpotent. $\qquad\square$

The procedure for choosing gains for infinitesimal deadbeat stability is algorithmic in the sense that the gain choices for $\boldsymbol{k}^{H}$ and $\boldsymbol{k}^{I}{}_{\mathrm{F}}$ are explicitly given by equations (80) (via the change of coordinates (74)) and (83), respectively; and equation (76) constrains $\boldsymbol{k}^{I}{}_{\mathrm{D}}$ to a hypersurface (a hyperplane constraint in the coordinates of (73)).

There still exists some freedom in choosing the control parameters as only a hypersurface constraint on the three-dimensional $\boldsymbol{k}^{I}{}_{\mathrm{D}}$ is required for infinitesimal deadbeat stability (nine control gains were used to place seven poles). We chose the remaining control parameters according to the procedure given in Appendix B. We found that selecting control parameters $\boldsymbol{k}^{I}{}_{\mathrm{D}}$ with parametric robustness and transients in mind was important; naively selecting values during the experiments resulted in poor performance. The numerical values chosen are shown in Table III.
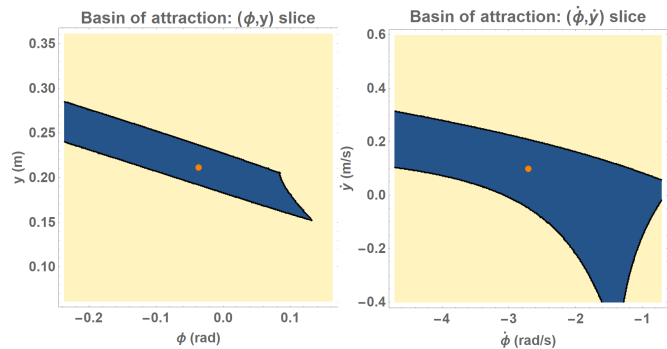
Fig. 6. Two slices of the numerically-computed basin of attraction when the hybrid mode sequence is enforced, using parameters given in Table III (left - in the (φ, y) plane, right - in the $(\dot{\varphi}, \dot{y})$ plane). The blue region indicates the basin, and the center orange dot corresponds with the fixed point $\bar{\boldsymbol{x}}^{I}$ of the map H^{I}. The enforcement of the hybrid mode sequence is a very conservative assumption for real-world implementation, as the ability to move through transient hybrid mode sequences is an inherent affordance of legs that provides robustness and motivates their use on machines.

Slices of the numerically-derived basin of attraction for the in-place components of the control scheme are depicted in Figure 6, using parameters given in Table III and enforcing the desired hybrid mode sequence. An enforced hybrid mode sequence is a conservative assumption compared to physical implementation on our robot where transient hybrid mode sequences are perfectly acceptable, and so we suspect that the

[9]We numerically verified invertibility of (79) when using the values from Table III.

actual basin of attraction without enforcing the hybrid mode sequence is larger.

Fig. 7. Robustness of deadbeat solution to perturbations in the parameters u_y and the unitless a, as indicated by the value of the spectral radius of the Jacobian of H^I when the true parameter values are varied from the parameter values used by the controller, evaluated at the fixed point that results from this parameter pert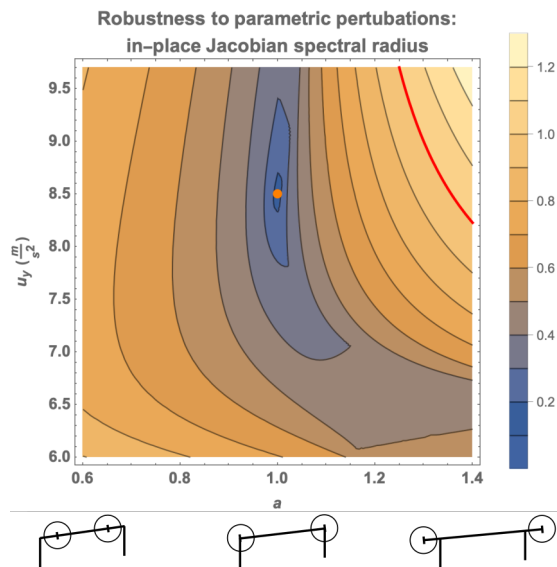urbation. This analysis uses the numerical parameter values given in Table III. To give the reader an intuition on the range of a displayed, below the graph are cartoon representations of the robot for a generalized Murphy value a of 0.6, 1.0, and 1.4, assuming all the robot mass is equally distributed at two point masses along the robot. The controller becomes unstable when the spectral radius exceeds unity, indicated by the red line. The parameters a and u_y are the two parameters which are difficult to measure on the physical robot. The large distance from the unperturbed case (indicated by the orange dot) to the onset of destabilizing perturbations (indicated by the red line) suggests a large degree of robustness to uncertainty in these parameters.

The robustness of the in-place components of the control scheme to parametric uncertainty is indicated in Figure 7. While we can measure the majority of the physical parameters of the robot quite well, we have a difficult time accurately measuring the body's moment of inertia which is folded into the generalized Murphy number a, as well as the stance specific vertical force u_y. Here, we show the spectral radius of the Jacobian of H^I when the "true" parameter values are varied from the parameter values used by the controller, evaluated at the fixed point that results from this parameter perturbation. The results of Figure 7 show that the controller will only destabilize when our error in estimating these two parameters is very large.

The basin of attraction for the horizontal components of the controller is global, as the iterated dynamics H^H are affine in $\widetilde{x}^H$. Of course, because H^H is also a function of $\widetilde{x}^I$, convergence in $\widetilde{x}^H$ is only guaranteed by our local stability analysis once $\widetilde{x}^I$ approaches its limiting value. We can think of the dynamics of the combined system H as containing an attracting invariant sub-manifold given by $\widetilde{x}^I = \widetilde{\widetilde{x}}^I$, on which the dynamics globally attract to $\widetilde{x}^H = \widetilde{\widetilde{x}}^H$.

We see from Figure 8 that the horizontal control scheme has a reasonable degree of robustness to parametric variation. Unlike the in-place control scheme, the horizontal does not have

any free control parameters to optimize performance metrics other than for achieving infinitesimal deadbeat stability. Thus this control scheme is hostage to whatever transients emerges as a result of the deadbeat control law Lemma 3, although we didn't observe large transients in the experiments of Section V. If we had, we could increase the number of state variables and control coefficients appearing in the input of the control functions (62) – for example, by introducing in-place state components – and then perform an optimization similar to the in-place control scheme to limit transients, however this would come at the cost of added feedback paths along which noise and the negative effects of measurement uncertainty would grow.
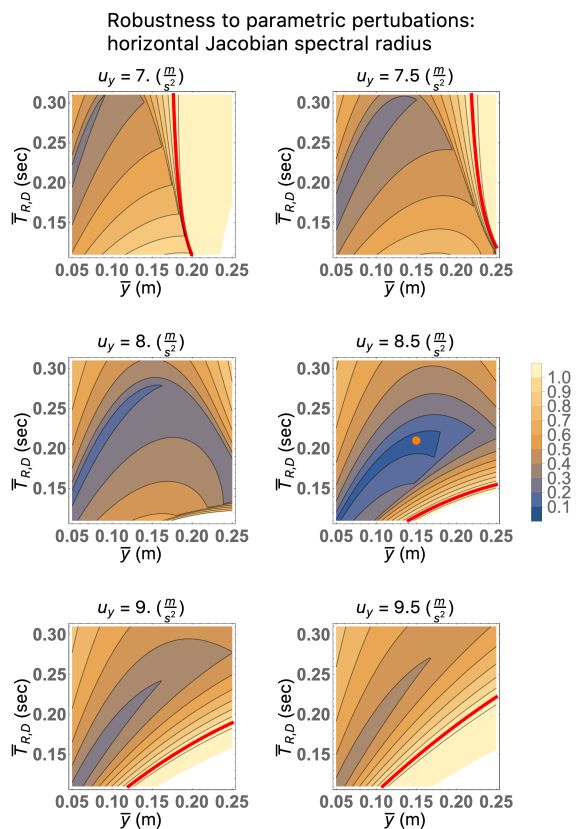
Fig. 8. Slices of the Jacobian spectral radius of H^H evaluated at the appropriate fixed point with parametric perturbations in the parameters $\bar{y}$, $T_{\mathrm{F,D}}$, and u_y – the only parameters entering into the Jacobian. This analysis uses numerical parameter values given in Table III as the unperturbed values. Here the control is being done using the unperturbed parameters, showing the robustness of the control scheme to parametric uncertainty. The distance from the orange dot in the lower-left plot (representing the unperturbed parameter values) to the red line (indicating slices of the edge of stability) demonstrates that the controller can withstand sizable perturbations in parameter space before going unstable.

V. EMPIRICAL DEMONSTRATION OF CONTROLLER

This section documents the implementation of the controller of Section IV on the Inu robot. Section V-A describes the experimental setup and Section V-B gives the experimental results.

A. Setup

We demonstrate the controller of Section IV implemented on the Inu robot [12], a direct-drive quadruped that has an articulated spine (held rigid in these experiments). While the experiments of this paper do not utilize Inu's flexible spine, we hope in future work to cascade another module (that encapsulates an added degree of freedom representing a bendable back) to the modeling composition and thus chose this robotic platform for continuity with future work.

The robot's lack of gearing in the legs necessitates operating the actuators far from their operating point of maximum power (although the lack of gearing provides benefits such as proprioceptive ground contact detection [48], [49]), which manifests itself in actuator saturation preventing the platform from achieving an aerial phase when running at faster speeds. We decided to forgo an aerial phase at slower speeds as well – hence the choice of hybrid modes (4) – to demonstrate consistent behavior across all feasible running speeds, and chose commanded vertically applied force and mode durations (u_y and $\bar{T}_{\mathrm{F,D}}$ in Table III) according to what the actuators could achieve at higher speeds.

Inu's parametric correspondence with the simplified model is given in Table III. While most of the simplified model parameters are easily measurable to a high degree of accuracy, calculating the robot's moment of inertia about its mass center (and hence its generalized Murphy number a) and the mass-specific vertically applied force u_y are more difficult. Our lab does not have the equipment to accurately measure these two parameters, however Figure 7 indicates a wide basin of stability to combined perturbations of these parameters and so we do not expect to see instability arise from our lack of good measurement capability.

Numerical parameters		
Physical and pseudo-physical parameters	d	$0.47m$
	l_0	$0.22m$
	a	1
	Δx^{Avg}	$\frac{d}{2}$
	$\bar{y}$	$0.21m$
	g	$9.81\frac{m}{s^2}$
Fixed-point parameters	u_y	$8.5\frac{m}{s^2}$
	$\bar{T}_{\mathrm{F,D}}$	$0.15s$
	$\dot{\tilde{x}}$	Varies by experiment
Control weights	$\boldsymbol{k}^I{}_{\mathrm{F}}$	$(0.5443,\ -0.0815,\ 0.2990)^T$
	$\boldsymbol{k}^I{}_{\mathrm{D}}$	$(0.4267,\ 0,\ -0.3139)^T$
	$\boldsymbol{k}^H$	$(0.2065, -0.1262, 0)^T$

TABLE III
PARAMETER VALUES USED IN EXPERIMENTS

Numerical reduced-order model and control parameters used in the experiments as well as in the calculations of Figures 5, 6, 7, and 8.

The robot is kinematically limited to a horizontal leg stroke distance of 32 cm when using a nominal touchdown height of 22 cm. Since the hip's stance time along the limit cycle (54) is equal to 20 ms, we have (as discussed in Section III-E) that the forward running speed is theoretically limited to approximately 1.6 m/s.

Inu executed a bounding run at several speeds to demonstrate the viability of the controller on physical hardware, using only its onboard MPU-6000 IMU[10] and motor encoders for sensing. A Vicon motion capture system[11] was used to log experimental kinematic data of Inu's mass-center and body-pitch trajectories and compare them with the predicted periodic orbits of the reduced-order model. The raw (unfiltered) trajectory data from motion capture is provided. In an effort to demonstrate the behavior of the in-place dynamics $H^I(\widetilde{\boldsymbol{x}}^I)$ (64) in isolation, we first ran the robot without implementing the horizontal reset speed controller – instead using a simple PD loop to dampen out horizontal movement. In a second set of experiments, we used the full controller to test the behavior at speeds up to the theoretical limit.

B. Results
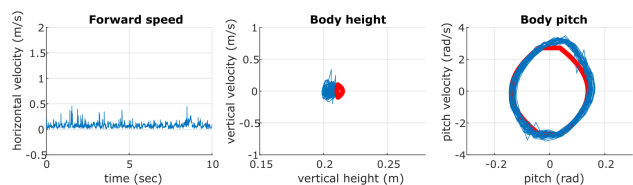
Fig. 9. The in-place component of the controller implemented on the Inu robot shows a good correspondence between the actual (blue) and analytically predicted (red) behavior of the robot over approximately 30 strides (10 seconds) of motion capture data. Here the horizontal toe position is maintained through the use of a simple PD controller with relatively high-magnitude derivative term to dampen out fore-aft oscillations.

The results of the experiments are summarized in Figures 9 and 10. The in-place controller was run on Inu over the course of approximately 30 strides as shown in Figure 9, demonstrating a good empirical correspondence between the robot and the predicted orbit of the in-place controller. The full controller's implementation in Figure 10 shows a reasonable agreement with the desired limit cycle at lower speeds, although the addition of the forward speed controller introduces more noise into the orbits as compared with the in-place controller. The predicted behavior was reliably repeatable over dozens of trials at many horizontal speed set points, $\dot{\tilde{x}}$, in the range allowed by (55). At higher speeds, we see the orbit of the pitch degree of freedom inconsistently sag during negative pitch values corresponding to when the front is in stance. This is due to the motors of the front body segment saturating when running at speed, the front is slightly inertially disadvantaged compared to the rear due to the battery weight being carried by the front. Inu can still run without falling when approaching the speed limit imposed by Inu's kinematics, however the legs are commanded to lift off prematurely when they near their kinematic singularity as shown in Figure 11 which results in inconsistent trajectories.

Inu is able to run up to its theoretical kinematic running speed of 1.6 m/s, but Figure 11 demonstrates that Inu is at the limit of it's available workspace at this speed. The robot wasn't

Fig. 10. Depicted are the actual (blue) and desired (red) orbits and trajectories under motion capture using the full controller of Section IV on the Inu robot over various running speeds up to Inu's kinematic speed limit (as discussed in Sections III-E and V-A). We see a reasonable agreement with the desired limit cycle at lower speeds (top), although the addition of the forw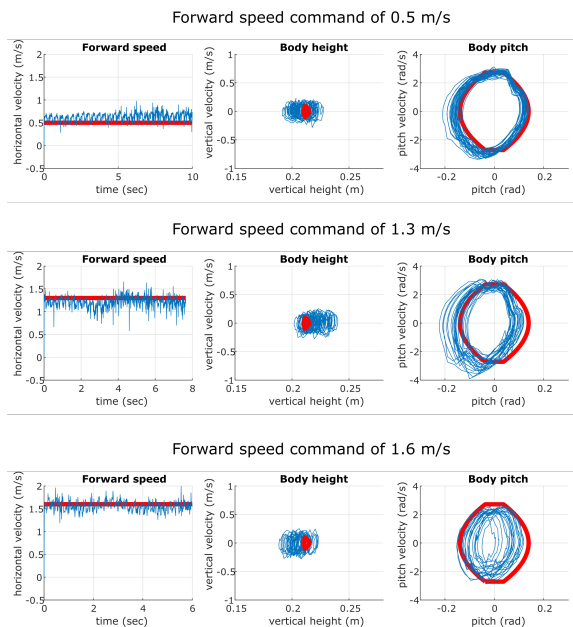ard speed controller introduces more noise into the orbits as compared with the isolated in-place controller shown in Figure 9. At higher speeds (middle) we see the orbit of the pitch degree of freedom inconsistently sag during negative pitch values corresponding to when the front is in stance. This is due to the motors of the front body segment saturating when running at speed, the front is slightly inertially disadvantaged compared to the rear due to the battery weight being carried by the front. Approaching the speed limit imposed by Inu's kinematics (bottom), Inu can still run without falling, however the legs are commanded to lift off prematurely when they near their kinematic singularity as shown in Figure 11 which results in inconsistent trajectories. The lower time durations of the faster experiments are the result of the robot running faster through the motion capture area.

able to exceed speeds higher than this, and commanding it to do so resulted in the legs hitting their kinematic singularity earlier in stance. This resulted in the robot stumbling, the onset of which lowered the running speed substantially. To run faster, either longer legs would be needed to increase the workspace (which would require greater motor torques via the increased lever arm) or a shorter stance duration would be required through increasing the applied vertical stance force. Both are precluded by Inu's inherently torque-limited actuation. In future work we will investigate the addition of a spine morphology to provide this added workspace without detracting from the hips torque generation affordance.

VI. DISCUSSION

A. Infinitesimally deadbeat nature of our result

Our stability result is not one that is deadbeat, but rather infinitesimally deadbeat by achieving a nilpotent stride map Jacobian at the fixed point. As such, local convergence to the fixed point is not in a finite number of steps but rather super-exponential due to the vanishing of linear terms in the Taylor approximation of the k-th iterate of the stride map at the fixed point for some $k \in \mathbb{N}$. We believe that finite step convergence
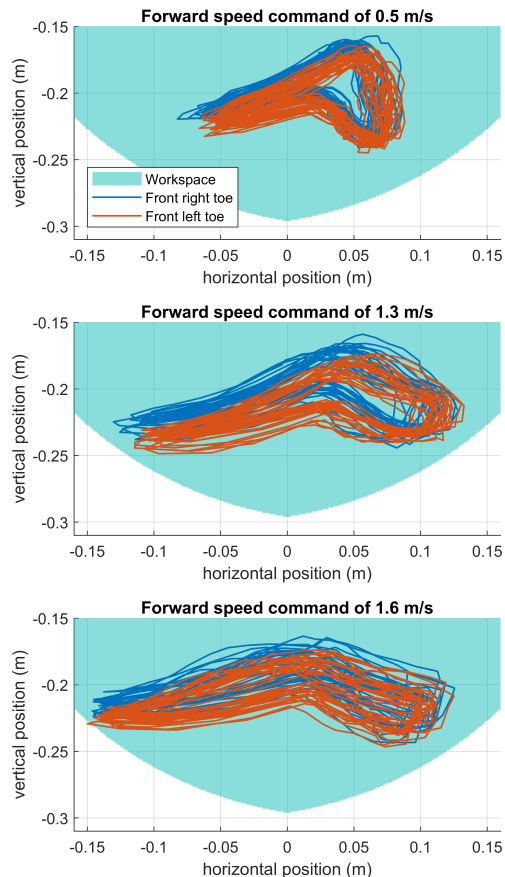
Fig. 11. Toe kinematic trajectories for the front legs in the local hip frame show that at running speeds of 1.6 m/s, the leg linkage is going close to singularity. This represents a constraint on maximum running speed, as the leg runs out of workspace to sweep the leg backwards in stance. Faster running with the control strategy of Section II could be achieved by either using longer legs to increase the workspace or by achieving shorter stance durations through increasing the applied vertical stance force. In future work we will investigate the addition of a spine morphology to provide this added workspace without detracting from the hip's torque generation affordance.

often comes with the price of an increased control burden that – as suggested by the current general lack of deadbeat results "in the wild" without utilizing motion capture – is poorly conditioned to state/parameter uncertainty.

Specifically, a k-step deadbeat control law requires the cancellation of all nonlinear terms in the Taylor series of a system's k-times composed Poincaré map local to the fixed point. Regarding state uncertainty, the canceling of the combined effect of these nonlinear terms can be worse-conditioned to errors in state measurement than only canceling the linear terms (sometimes much worse). We avoided the possibility of this ill-conditioning by both choosing not to cancel the nonlinear terms and by designing feedback paths in our control law to only use states that we felt we can accurately measure: time, kinematic configurations, and forward speed (which changes relatively slowly) – thus eschewing the common method of detecting a hip's apex event in flight as it is typically backed out of the hip's vertical liftoff velocity, which we have difficulty measuring in stance due to its quickly changing nature. We are wary of using these feedback paths for deadbeat

stability as state measurement error inherent to operation in the physical world is still present in states that we can "accurately" measure, and an ill-conditioned canceling of dynamics can still magnify their adverse effects to result in a controller with poor empirical performance. Regarding parametric uncertainty, deadbeat control amounts to inverse dynamics and it is known that cancellation of inertial terms can lead to poor parametric robustness. Rather, the empirical performance depicted in Figures 9, 10 demonstrates a reasonable degree of robustness to state measurement error inherent to operation in the physical world and Figures 7, 8 indicate a reasonable degree of parametric robustness.

B. Controlling on the hybrid transitions

In controlling on the guards and resets, we are utilizing a natural affordance provided by the use of legs. The control affordance provided by hybrid transitions is important because it is in some sense independent of actuator power constraints: on one hand, we achieve arbitrarily good pole placement with only modest control gains (Table III); while on the other, our specification of desired hybrid periodic orbit (Proposition 1, Section III-C) depends strongly on actuator performance but is almost entirely devoid of controller specification (Section IV). As we attempt to make more precise below, we believe that controlling on the hybrid transitions frees scarce actuator power resources from the task of shaping the continuous dynamics into the proper "funnel" [50] required for stability, allowing their application to go instead to accessing dynamical regimes of higher energy operation. Settings rich in hybrid interactions are ripe for this style of control, and as such the intrinsic necessity of making and breaking contact that accompanies legged robots is an opportunity for exploiting the natural hybrid nature of the dynamics to achieve stability.

The costs inherent to our control formulation are twofold. First, the actuator cost is equal to the enforcement of the (piecewise) Hamiltonian dynamics through generating conservative potential field force laws at the toes. In the vertical this is a constant force (20), in the horizontal the force is affine with respect to leg horizontal toe position (21). Due to the simple and transparent nature of these force laws (constant and affine), a user can easily evaluate if they are prohibitively costly at any point in the workspace and – as long as transients in state are not bad – shouldn't expect that operation near the hybrid periodic orbit would be suddenly costly for the actuators. The fact that the Inu robot used in the experiments is inherently force-limited (Section V-A) yet can tolerate using the force laws even as perturbations are corrected suggest the cost associated with it are not prohibitive.

Second, our hybrid transition control scheme consists of displacing the toe from some nominal location using proportional control. Practically, the toes can only tolerate so much displacement from the controllers (legs being limited in workspace, or perhaps needing to avoid a corner of the workspace with unfavorable actuator performance) which we relate to the tolerable state-error as follows. If one puts interval constraints on the values that a control function g_{TD}, g_{LO}, $r_{F,D}$, or $r_{D,R}$ (57), (62) may take, this is equivalent to being

able to – on the hybrid transitions – tolerate perturbations from the periodic orbit that satisfy two halfspace constraints (whose hyperplanes are parallel and offset). For example, specifying that $r_{D,R} \in (\delta r_{\mathrm{MIN}}, \delta r_{\mathrm{MAX}})$ in (62) is equivalent to the requirement that:

$$\delta r_{\mathrm{MIN}} < \boldsymbol{k}_{\mathrm{D}}^{H\,T} \begin{pmatrix} \Delta x^r - \bar{\Delta x}^r{}_{\mathrm{D}} \\ \Delta x^f - \bar{\Delta x}^f{}_{\mathrm{D}} \end{pmatrix} < \delta r_{\mathrm{MAX}},$$

allowing the user to quantify the state-errors tolerable by the leg mechanisms.

C. Cascade compositions as attracting invariant submanifolds

Stable fixed points of cascaded iterated maps necessarily have an attracting invariant submanifold. Let D_1 and D_2 be (respectively) n and m-dimensional differentiable manifolds, and suppose the iterated map $P : D_1 \times D_2 \to D_1 \times D_2$ has the form:

$$P(x, y) = \begin{pmatrix} P_1(x) \\ P_2(x, y) \end{pmatrix},$$

and stable fixed point $(\bar{x}, \bar{y})$. Then $\bar{x} \times D_2$ is an invariant submanifold, and is attracting due to $\bar{x}$ being attracting in P_1. In our system, the attracting invariant submanifold is given by the horizontal dynamics along the in-place limit cycle. It is interesting to note that in the language of templates and anchors [51], traditionally the dynamics on the attracting invariant submanifold – called the template dynamics – drive the hybrid transitions, while in our case it is the dynamics that collapse to the attracting invariant submanifold – called the anchor dynamics – that do so.

VII. CONCLUSION

This paper considered the problem of stabilizing a three mechanical degree-of-freedom simplified model of quadrupedal bounding in the sagittal plane. By using the continuous stance forces to effect simple continuous dynamics and a cascade dynamical decoupling giving a useful eigenvalue separation condition in the stride map Jacobian, we analytically showed local stability by controlling on the guards and resets to obtain an "infinitesimal" deadbeat result. The model, while simple, well-approximates physical robot experiments implementing the running controller. Aside from the contribution of the running controller, we hope this paper motivates further progress in analytical stability results of three degree-of-freedom (and higher) legged locomotion models – a currently underdeveloped literature that has the potential to greatly enhance the empirical performance of legged machines.

APPENDIX A
CONTROLLER STABILITY LEMMAS

This Appendix contains results related to the choice of control gains in Proposition 2 guaranteeing infinitesimal deadbeat stability of the half-stride map H (46) at the operating point (47). Lemma 1 gives the explicit form of the time-to-impact map Jacobians $\frac{\partial T_{\mathrm{F,D}}}{\partial \widetilde{\boldsymbol{x}}^I}\Big|_{\tau=0}$ and $\frac{\partial T_{\mathrm{D,R}}}{\partial \widetilde{\boldsymbol{x}}^I}\Big|_{\tau=0}$. The control weight change-of-coordinates (73) is given to assist in expressing the

deadbeat gain expressions, which are presented in Lemmas 2 and 3 below.

Lemma 1. *The relevant Jacobians of the time-to-guard-impact functions in* (72) *are given by:*

$$\frac{\partial T_{F,D}}{\partial \widetilde{\boldsymbol{x}}^I}\bigg|_{\tau=0} = \frac{1}{k_{F,3}^I - s_F}\begin{pmatrix} 1 - k_{F,1}^I - k_{F,2}^I \\ (-1 + k_{F,1}^I - k_{F,2}^I)\frac{d}{2} \\ \bar{T}_{F,D} \\ -\frac{d}{2}\bar{T}_{F,D} \end{pmatrix}^T,$$

$$s_F = \dot{y} - \frac{d}{2}\dot{\varphi} + \left((1 - a^{-1})u_y - g\right)\bar{T}_{F,D},$$

$$\frac{\partial T_{D,R}}{\partial \widetilde{\boldsymbol{x}}^I}\bigg|_{\tau=0} = \frac{1}{k_{D,3}^I - s_D}\begin{pmatrix} 1 - k_{D,1}^I - k_{D,2}^I \\ (1 + k_{D,1}^I - k_{D,2}^I)\frac{d}{2} \\ \bar{T}_{D,R} \\ \frac{d}{2}\bar{T}_{D,R} \end{pmatrix}^T,$$

$$s_D = \dot{y} + \frac{d}{2}\dot{\varphi} + (2u_y - g)\bar{T}_{D,R}.$$

Proof. See Appendix D. □

We introduce the following coordinate change to simplify the form of the time-to-guard-impact Jacobians above. Let:

$$\widetilde{\boldsymbol{k}}_F^I = \begin{pmatrix} \widetilde{k}_{F,1}^I \\ \widetilde{k}_{F,2}^I \\ \widetilde{k}_{F,3}^I \end{pmatrix} = \frac{1}{k_{F,3}^I - s_F}\begin{pmatrix} 1 - k_{F,1}^I - k_{F,2}^I \\ (-1 + k_{F,1}^I - k_{F,2}^I)\frac{d}{2} \\ \bar{T}_{F,D} \end{pmatrix},$$

$$\tag{73}$$

$$\widetilde{\boldsymbol{k}}_D^I = \begin{pmatrix} \widetilde{k}_{D,1}^I \\ \widetilde{k}_{D,2}^I \\ \widetilde{k}_{D,3}^I \end{pmatrix} = \frac{1}{k_{D,3}^I - s_D}\begin{pmatrix} 1 - k_{D,1}^I - k_{D,2}^I \\ (1 + k_{D,1}^I - k_{D,2}^I)\frac{d}{2} \\ \bar{T}_{D,R} \end{pmatrix},$$

such that:

$$\frac{\partial T_{F,D}}{\partial \widetilde{\boldsymbol{x}}^I}\bigg|_{\tau=0} = \widetilde{\boldsymbol{k}}_F^{I\,T}M_F^I, \quad M_F^I = \begin{pmatrix} 1 & 0 & 0 & 0 \\ 0 & 1 & 0 & 0 \\ 0 & 0 & 1 & -\frac{d}{2} \end{pmatrix},$$

$$\frac{\partial T_{D,R}}{\partial \widetilde{\boldsymbol{x}}^I}\bigg|_{\tau=0} = \widetilde{\boldsymbol{k}}_D^{I\,T}M_D^I, \quad M_D^I = \begin{pmatrix} 1 & 0 & 0 & 0 \\ 0 & 1 & 0 & 0 \\ 0 & 0 & 1 & \frac{d}{2} \end{pmatrix}.$$

This transformation is invertible via:

$$\boldsymbol{k}_F^I = \frac{\bar{T}_{F,D}}{d\,\widetilde{k}_{F,3}^I}\begin{pmatrix} -\frac{d}{2} & 1 & 0 \\ -\frac{d}{2} & -1 & 0 \\ 0 & 0 & 0 \end{pmatrix}\widetilde{\boldsymbol{k}}_F^I + \begin{pmatrix} 1 \\ 0 \\ s_F + \frac{\bar{T}_{F,D}}{\widetilde{k}_{F,3}^I} \end{pmatrix}, \tag{74}$$

$$\boldsymbol{k}_D^I = \frac{\bar{T}_{D,R}}{d\,\widetilde{k}_{D,3}^I}\begin{pmatrix} -\frac{d}{2} & 1 & 0 \\ -\frac{d}{2} & -1 & 0 \\ 0 & 0 & 0 \end{pmatrix}\widetilde{\boldsymbol{k}}_D^I + \begin{pmatrix} 0 \\ 1 \\ s_D + \frac{\bar{T}_{D,R}}{\widetilde{k}_{D,3}^I} \end{pmatrix},$$

where:

$$\widetilde{k}_{F,3}^I \neq 0, \quad \widetilde{k}_{D,3}^I \neq 0. \tag{75}$$

Lemma 2. *The following choice of $\widetilde{\boldsymbol{k}}_F^I$ and $\widetilde{\boldsymbol{k}}_D^I$ make $DH^I\big|_{\widetilde{\widetilde{\boldsymbol{x}}}^I}$ nilpotent assuming the conditions given in* (82) *can be satisfied. Choose $\widetilde{\boldsymbol{k}}_D^I$ such that:*

$$\widetilde{\boldsymbol{k}}_D^{I\,T}\begin{pmatrix} -\dot{y} \\ -\dot{\varphi} \\ 2u_y - g \end{pmatrix} = -1, \tag{76}$$

which zeros one eigenvalue of $D\widetilde{\Phi}_{D,R}^I\big|_{\Phi_{F,D}^I(\bar{\boldsymbol{x}}^I)}$ and hence of $DH^I\big|_{\widetilde{\widetilde{\boldsymbol{x}}}^I}$. Denote the resulting Jordan decomposition of $D\widetilde{\Phi}_{D,R}^I\big|_{\Phi_{F,D}^I(\bar{\boldsymbol{x}}^I)}$ by:

$$D\widetilde{\Phi}_{D,R}^I\big|_{\Phi_{F,D}^I(\bar{\boldsymbol{x}}^I)} = V^I\Lambda^I V^{I-1}, \tag{77}$$

where the zero eigenvalue is placed in the upper-left element of Λ^I and the explicit form of V^I and Λ^I is given in (94) *of Appendix E. Let:*

$$A^I = T^I\Lambda^I V^{I-1}\begin{pmatrix} I & I\bar{T}_{F,D} \\ 0 & I \end{pmatrix}D\widetilde{b}^I V^I T^{I\,T}, \tag{78}$$

$$\boldsymbol{d}^I = T^I\Lambda^I V^{I-1}\begin{pmatrix} -\dot{y} \\ -\dot{\varphi} \\ u_y - g \\ -\frac{2u_y}{da} \end{pmatrix},$$

$$T^I = \begin{pmatrix} 0 & 1 & 0 & 0 \\ 0 & 0 & 1 & 0 \\ 0 & 0 & 0 & 1 \end{pmatrix},$$

and:

$$R^I = \begin{pmatrix} \boldsymbol{d}^I & A^I\boldsymbol{d}^I & A^{I\,2}\boldsymbol{d}^I \end{pmatrix}. \tag{79}$$

Then choose:

$$\widetilde{\boldsymbol{k}}_F^I = -\begin{pmatrix} 0 & 0 & 1 \end{pmatrix}R^{I-1}A^{I\,3}\left(M_F^I D\widetilde{b}^I V^I T^{I\,T}\right)^{-1}. \tag{80}$$

Along with the hyperplane constraint (76), *we require that the choice of $\widetilde{\boldsymbol{k}}_D^I$ satisfy:*

$$\widetilde{k}_{D,1}^I \neq 0, -\frac{1}{2\dot{y}}, \quad \widetilde{k}_{D,2}^I \neq \frac{d}{2}\widetilde{k}_{D,1}^I, \quad \widetilde{k}_{D,3}^I \neq 0, \tag{81}$$

$$\widetilde{\boldsymbol{k}}_D^{I\,T}\begin{pmatrix} \dot{y} \\ -\dot{\varphi} \\ 2u_y - g \end{pmatrix} \neq -1,$$

$$\det(R^I) \neq 0,$$

$$\widetilde{k}_{F,3}^I \neq 0, \text{ (dependent on } \widetilde{\boldsymbol{k}}_D^I \text{ via (80)),}$$

according to (75), (80), (95), (97) *and to guarantee the invertibility of R^I* (96). *We leave as a conjecture that the constraints:*

$$\det(R^I) \neq 0, \quad \widetilde{k}_{F,3}^I \neq 0 \tag{82}$$

from (81) *don't produce an empty set of feasible choices for $\widetilde{\boldsymbol{k}}_D^I$.*

Proof. See Appendix E. □

We numerically verified (81) when using the values from Table III.

Lemma 3. *The following choice of $\boldsymbol{k}^H = (k_F^H, k_{D,1}^H, k_{D,2}^H)^T$ makes $D_{\widetilde{\boldsymbol{x}}^H} H^H|_{\widetilde{\boldsymbol{x}}^I}$ nilpotent. Let:*

$$\begin{pmatrix} k_F^H \\ k_{D,1}^H \end{pmatrix} = \begin{pmatrix} \cosh\left(\bar{T}_{F,D}\sqrt{\frac{u_y}{\bar{y}}}\right) & 0 \\ -\sqrt{\frac{u_y}{\bar{y}}}\sinh\left(\bar{T}_{F,D}\sqrt{\frac{u_y}{\bar{y}}}\right) & 1 \end{pmatrix}^{-1} \tag{83}$$
$$\left\{ \begin{pmatrix} \tilde{k}_F^H \\ \tilde{k}_{D,1}^H \end{pmatrix} - \begin{pmatrix} \sqrt{\frac{\bar{y}}{u_y}}\sinh\left(\bar{T}_{F,D}\sqrt{\frac{u_y}{\bar{y}}}\right) \\ 1 - \cosh\left(\bar{T}_{F,D}\sqrt{\frac{u_y}{\bar{y}}}\right) \end{pmatrix} \right\},$$
$$k_{D,2}^H = 0,$$

where:

$$\begin{pmatrix} \tilde{k}_F^H \\ \tilde{k}_{D,1}^H \end{pmatrix} = -\left(R^{H^{-1}} A^{H^2} \right)^T \begin{pmatrix} 0 \\ 1 \end{pmatrix},$$

and:

$$R^H = \begin{pmatrix} \boldsymbol{d}^H & A^H \boldsymbol{d}^H \end{pmatrix}, \tag{84}$$
$$A^H = \begin{pmatrix} 0 & 1 \\ -1 & 0 \end{pmatrix} e^{C_D \bar{T}_{D,R}} \left\{ e^{C_F \bar{T}_{F,D}} \begin{pmatrix} 0 & -1 \\ 1 & 0 \end{pmatrix} + \begin{pmatrix} 0 & \frac{1}{2} \\ 0 & 0 \end{pmatrix} \right\}$$
$$- \begin{pmatrix} 0 & 0 \\ 0 & \frac{1}{2} \end{pmatrix},$$
$$\boldsymbol{d}^H = \begin{pmatrix} 0 & 1 \\ -1 & 0 \end{pmatrix} e^{C_D \bar{T}_{D,R}} \begin{pmatrix} -\frac{1}{2} \\ 0 \end{pmatrix} + \begin{pmatrix} 0 \\ \frac{1}{2} \end{pmatrix}.$$

Proof. See Appendix F. ☐

APPENDIX B
CONTROL GAIN SELECTION PROCEDURE

The choice of control gains (76), (80), (83) that grants the system infinitesimal deadbeat stability fully constrains $\boldsymbol{k}^H$ and $\boldsymbol{k}^I_F$, and constrains $\boldsymbol{k}^I_D$ to a hypersurface. We chose where to place $\boldsymbol{k}^I_D$ on this hypersurface as follows.

We chose to fix $k_{D,3}^I$ as a function of $k_{D,1}^I$ and $k_{D,2}^I$ via (76), explicitly:

$$k_{D,3}^I = \frac{-1 + \dot{\bar{y}} k_{D,1}^I + \dot{\bar{\varphi}} k_{D,2}^I}{2u_y - g}.$$

We then chose to set the value of $k_{D,2}^I$ to zero, severing a feedback path in (57) that corresponds to the hip's usage of its own vertical height measurement in determining liftoff height. Setting $k_{D,2}^I$ to zero was observed in the experiment to improve performance, likely this feedback path made the controller very sensitive to the sagging of the front body segment due to actuator saturation when running at faster speeds (depicted in Figure 10).

We chose $k_{D,1}^I$ using the following constrained optimization problem in an effort to reduce transients and control gain magnitudes, and to increase parametric robustness:

$$\min_{k_{D,1}^I} \ c_1 \|\boldsymbol{k}^I\|^2 + c_2 \left\| DH^I|_{\widetilde{\boldsymbol{x}}^I} \right\|_F^2 + c_3 \left\| \frac{\partial}{\partial \widehat{\boldsymbol{k}^I}} \boldsymbol{p}(\widehat{\boldsymbol{k}^I}) \right\|_F^2$$
$$\text{s.t.} \quad k_{D,2}^I = 0$$
$$k_{D,3}^I = \frac{-1 + \dot{\bar{y}} k_{D,1}^I + \dot{\bar{\varphi}} k_{D,2}^I}{2u_y - g}$$
$$\boldsymbol{k}^I = \begin{pmatrix} \boldsymbol{k}^I_F \\ \boldsymbol{k}^I_D \end{pmatrix}$$
$$\widehat{\boldsymbol{k}^I} = \begin{pmatrix} \boldsymbol{k}^{I^T} & g & d & a & l_0 & u_y & \bar{T}_{F,D} \end{pmatrix}^T,$$

additionally subject to the constraints (76), (80), (83) granting infinitesimal deadbeat stability, and where $\boldsymbol{p}(\boldsymbol{k}^I)$ equals the coefficient vector for the characteristic polynomial of $DH^I|_{\widetilde{\boldsymbol{x}}^I}$. The terms associated with c_1 are intended to keep the control inputs relatively small, the terms associated with c_2 are intended to reduce transients, and the terms associated with c_3 are intended to increase robustness to parametric uncertainty and measurement errors in applying control. We used $c_1 = 500$, $c_2 = 1.1$, $c_3 = 1.5$ and numerically verified that the resulting control weights satisfied (81). The numerical values chosen are shown in Table III.

APPENDIX C
FIXED POINT CALCULATIONS

The following proof of Proposition 1 is given in two parts. The first derives the form of the fixed point $\widetilde{\boldsymbol{x}}^I$ for the map $H^I(\cdot)$. The second derives the form of the fixed point $\widetilde{\boldsymbol{x}}^H$ for the map $H^H(\widetilde{\boldsymbol{x}}^I, \cdot) \equiv H^H|_{\widetilde{\boldsymbol{x}}^I}(\cdot)$.

Proof of Proposition 1, part 1

Proof. Consider the in-place component of the "flipped" half-stride map (46) given by:

$$H^I = \Pi^I \circ b^I \circ \Phi^I_{D,R} \circ \Phi^I_{F,D} \circ \Sigma^I.$$

Recall that the maps Π^I (43), b^I (26), and Σ^I (43), in H^I are simple linear maps while the mode maps $\Phi^I_{i,j}$ (38) in H^I have the form $\Phi^I_{i,j}(\boldsymbol{x}^I) = R^I \circ \phi_i^{T^I_{i,j}(\boldsymbol{x}^I)}(\boldsymbol{x}^I)$, where $\phi_i^t(\boldsymbol{x}^I)$ is the continuous flow (34), $R^I : (\boldsymbol{q}^I, \dot{\boldsymbol{q}}^I, \tau) \mapsto (\boldsymbol{q}^I, \dot{\boldsymbol{q}}^I, 0)$, and $T^I_{i,j}$ (39) is the implicit time-to-guard-impact map given by $T^I_{i,j}(\boldsymbol{x}^I) = \min\{t \in \mathbb{R}^+ | \phi_i^t(\boldsymbol{x}^I) \in G^I_{i,j}\}$.

We wish to show that:

$$\widetilde{\boldsymbol{x}}^I = \begin{pmatrix} l_0 - \frac{a^{-1}u_y(g-u_y)}{4(2u_y-g)}\bar{T}_{F,D}^2 \\ -\frac{a^{-1}u_y(g-u_y)}{2d(2u_y-g)}\bar{T}_{F,D}^2 \\ \frac{g-u_y}{2}\bar{T}_{F,D} \\ -\frac{a^{-1}u_y}{d}\bar{T}_{F,D} \end{pmatrix}$$

is a fixed point of H^I and additionally that the hybrid execution from this fixed point spends a duration in mode D equal to:

$$\bar{T}_{D,R} = \bar{T}_{F,D}\frac{g-u_y}{2u_y-g}.$$

One could simply solve $H^I(\widetilde{\boldsymbol{x}}^I) = \widetilde{\boldsymbol{x}}^I$ algebraically to obtain this result, however this entails explicitly expressing the time-to-impact maps which have a complicated form involving roots of quadratic equations. Instead, it is much cleaner to first take the duration constants $\bar{T}_{F,D}$ and $\bar{T}_{D,R}$ as surrogates for the time-to-guard-impact maps and algebraically solve for the fixed point, then secondly verify that the resulting $\bar{T}_{F,D}$ and $\bar{T}_{D,R}$ agree with the values of time-to-guard-impact maps.

We first solve the equations:

$$\widetilde{\boldsymbol{x}}^I = \Pi^I \circ b^I \circ R^I \circ \phi_D^{\bar{T}_{D,R}} \circ R^I \circ \phi_F^{\bar{T}_{F,D}} \circ \Sigma^I(\widetilde{\boldsymbol{x}}^I), \tag{85}$$
$$l_0 = y^{rhip} \circ \phi_F^{\bar{T}_{F,D}} \circ \Sigma^I(\widetilde{\boldsymbol{x}}^I),$$

which have the expanded form:

$$\begin{pmatrix} \bar{\boldsymbol{q}}^I \\ \dot{\bar{\boldsymbol{q}}}^I \end{pmatrix} = \begin{pmatrix} \tilde{I} & 0 \\ 0 & \tilde{I} \end{pmatrix} \Bigg\{ \begin{pmatrix} \frac{\bar{T}_{\mathrm{D,R}}^2}{2}\boldsymbol{c}_{\mathrm{D}} \\ \bar{T}_{\mathrm{D,R}}\boldsymbol{c}_{\mathrm{D}} \end{pmatrix} + \begin{pmatrix} I & \bar{T}_{\mathrm{D,R}}I \\ 0 & I \end{pmatrix}$$

$$\left[\begin{pmatrix} I & \bar{T}_{\mathrm{F,D}}I \\ 0 & I \end{pmatrix} \begin{pmatrix} \bar{\boldsymbol{q}}^I \\ \dot{\bar{\boldsymbol{q}}}^I \end{pmatrix} + \begin{pmatrix} \frac{\bar{T}_{\mathrm{F,D}}^2}{2}\boldsymbol{c}_{\mathrm{F}} \\ \bar{T}_{\mathrm{F,D}}\boldsymbol{c}_{\mathrm{F}} \end{pmatrix} \right] \Bigg\}, \qquad (86)$$

$$l_0 = \begin{pmatrix} 1 \\ -\frac{d}{2} \end{pmatrix}^T \left(\bar{\boldsymbol{q}}^I + \bar{T}_{\mathrm{F,D}}\dot{\bar{\boldsymbol{q}}}^I + \frac{\bar{T}_{\mathrm{F,D}}^2}{2}\boldsymbol{c}_{\mathrm{F}} \right),$$

for state $\tilde{\bar{\boldsymbol{x}}}^I = \begin{pmatrix} \bar{\boldsymbol{q}}^I \\ \dot{\bar{\boldsymbol{q}}}^I \end{pmatrix} \in \widetilde{D}_{\mathrm{F}}^I$ and $\bar{T}_{\mathrm{D,R}} \in \mathbb{R}^+$. Here $\tilde{I} = \begin{pmatrix} 1 & 0 \\ 0 & -1 \end{pmatrix}$ and both (85) and (86) represents the requirement that – starting from $\Sigma^I(\tilde{\bar{\boldsymbol{x}}}^I)$ – the flow in F at time $\bar{T}_{\mathrm{F,D}}$ satisfies the first predicate of the definition of $G_{\mathrm{F,D}}^I$ (25). Solving these equations yields:

$$\tilde{\bar{\boldsymbol{x}}}^I = \begin{pmatrix} l_0 - \frac{a^{-1}u_y(g-u_y)}{4(2u_y-g)}\bar{T}_{\mathrm{F,D}}^2 \\ -\frac{a^{-1}u_y(g-u_y)}{2d(2u_y-g)}\bar{T}_{\mathrm{F,D}}^2 \\ \frac{g-u_y}{2}\bar{T}_{\mathrm{F,D}} \\ -\frac{a^{-1}u_y}{d}\bar{T}_{\mathrm{F,D}} \end{pmatrix},$$

$$\bar{T}_{\mathrm{D,R}} = \bar{T}_{\mathrm{F,D}}\frac{g-u_y}{2u_y-g},$$

where we will require that:

$$\bar{T}_{\mathrm{D,R}} \in \mathbb{R}^+, \qquad (87)$$

so as to satisfy the domain requirement in (39). Notice that $\frac{g-u_y}{2u_y-g} > 0$ in the expression for $\bar{T}_{\mathrm{D,R}}$ as $g \in \mathbb{R}^+$ and $u_y \in (\frac{g}{2}, g)$ as specified in (16).

The fact that the above computation, which involves the roots of quadratic equations, has a clean solution is due to the highly symmetric nature of the hybrid trajectory associated with the fixed point. Specifically, the configuration variables along this trajectory in each mode – in the case where they undergo a nonzero acceleration – end where they begin, so that the quadratic formula associated with solving the event time simplifies to a simple rational function. For example, the form of (86) is simplified by the fact that $(1, -\frac{d}{2})\bar{\boldsymbol{q}}^I = l_0$, which reduces (86) to:

$$\bar{T}_{\mathrm{F,D}}\begin{pmatrix} 1 \\ -\frac{d}{2} \end{pmatrix}^T \dot{\bar{\boldsymbol{q}}}^I + \frac{\bar{T}_{\mathrm{F,D}}^2}{2}\begin{pmatrix} 1 \\ -\frac{d}{2} \end{pmatrix}^T \boldsymbol{c}_{\mathrm{F}} = 0,$$

which then, because $\bar{T}_{\mathrm{F,D}} > 0$, further reduces to:

$$\begin{pmatrix} 1 \\ -\frac{d}{2} \end{pmatrix}^T \dot{\bar{\boldsymbol{q}}}^I + \frac{\bar{T}_{\mathrm{F,D}}}{2}\begin{pmatrix} 1 \\ -\frac{d}{2} \end{pmatrix}^T \boldsymbol{c}_{\mathrm{F}} = 0,$$

which does not possess any quadratic terms.

It remains to show that that the mode duration constants $\bar{T}_{\mathrm{F,D}}$ and $\bar{T}_{\mathrm{D,R}}$ agree with the value of time-to-guard-impact maps, specifically that:

$$\bar{T}_{\mathrm{F,D}} = T_{\mathrm{F,D}}^I \Big|_{\Sigma^I(\tilde{\bar{\boldsymbol{x}}}^I)}$$

$$= \min\{t \in \mathbb{R}^+ | \phi_{\mathrm{F}}^t \circ \Sigma^I(\tilde{\bar{\boldsymbol{x}}}^I) \in G_{\mathrm{F,D}}^I\},$$

$$\bar{T}_{\mathrm{D,R}} = T_{\mathrm{D,R}}^I \Big|_{\Phi_{\mathrm{F,D}}^I \circ \Sigma^I(\tilde{\bar{\boldsymbol{x}}}^I)}$$

$$= \min\{t \in \mathbb{R}^+ | \phi_{\mathrm{D}}^t \circ \Phi_{\mathrm{F,D}}^I \circ \Sigma^I(\tilde{\bar{\boldsymbol{x}}}^I) \in G_{\mathrm{D,R}}^I\},$$

where the relevant guards (25) are:

$$G_{\mathrm{F,D}}^I := \{\boldsymbol{x}^I \in D^I{}_{\mathrm{F}} \mid y^{r_{hip}}(\boldsymbol{x}^I) = l_0 + g_{TD}(\boldsymbol{x}^I)$$
$$\wedge \ \dot{y}^{r_{hip}}(\boldsymbol{x}^I) < 0\},$$

$$G_{\mathrm{D,R}}^I := \{\boldsymbol{x}^I \in D^I{}_{\mathrm{D}} \mid y^{f_{hip}}(\boldsymbol{x}^I) = l_0 + g_{LO}(\boldsymbol{x}^I)$$
$$\wedge \ \dot{y}^{f_{hip}}(\boldsymbol{x}^I) > 0\},$$

recalling that the functions g_{LO}, g_{TD} are required to vanish on the hybrid periodic orbit's guard intersection.

We first concentrate on $T_{\mathrm{F,D}}^I \Big|_{\Sigma^I(\tilde{\bar{\boldsymbol{x}}}^I)}$. The flow through mode F given by $\phi_{\mathrm{F}}^t \circ \Sigma^I(\tilde{\bar{\boldsymbol{x}}}^I)$ intersects the guard $G_{\mathrm{F,D}}^I$ when:

$$y^{r_{hip}}\Big|_{\phi_{\mathrm{F}}^t \circ \Sigma^I(\tilde{\bar{\boldsymbol{x}}}^I)} = l_0 + g_{TD}\Big|_{\phi_{\mathrm{F}}^t \circ \Sigma^I(\tilde{\bar{\boldsymbol{x}}}^I)} \ \wedge \ \dot{y}^{r_{hip}}\Big|_{\phi_{\mathrm{F}}^t \circ \Sigma^I(\tilde{\bar{\boldsymbol{x}}}^I)} < 0.$$
$$(88)$$

The terms in (88) evaluated at time $\bar{T}_{\mathrm{F,D}}$ are:

$$g_{TD}\Big|_{\phi_{\mathrm{F}}^{\bar{T}_{\mathrm{F,D}}} \circ \Sigma^I(\tilde{\bar{\boldsymbol{x}}}^I)} = 0,$$

$$y^{r_{hip}}\Big|_{\phi_{\mathrm{F}}^{\bar{T}_{\mathrm{F,D}}} \circ \Sigma^I(\tilde{\bar{\boldsymbol{x}}}^I)} = y^{r_{hip}}\left(\begin{pmatrix} l_0 - \frac{a^{-1}u_y(g-u_y)}{4(2u_y-g)}\bar{T}_{\mathrm{F,D}}^2 \\ -\frac{a^{-1}u_y(g-u_y)}{2d(2u_y-g)}\bar{T}_{\mathrm{F,D}}^2 \\ -\frac{g-u_y}{2}\bar{T}_{\mathrm{F,D}} \\ \frac{a^{-1}u_y}{d}\bar{T}_{\mathrm{F,D}} \\ \bar{T}_{\mathrm{F,D}} \end{pmatrix} \right),$$

$$= l_0,$$

$$\dot{y}^{r_{hip}}\Big|_{\phi_{\mathrm{F}}^{\bar{T}_{\mathrm{F,D}}} \circ \Sigma^I(\tilde{\bar{\boldsymbol{x}}}^I)} = \dot{y}^{r_{hip}}\left(\begin{pmatrix} l_0 - \frac{a^{-1}u_y(g-u_y)}{4(2u_y-g)}\bar{T}_{\mathrm{F,D}}^2 \\ -\frac{a^{-1}u_y(g-u_y)}{2d(2u_y-g)}\bar{T}_{\mathrm{F,D}}^2 \\ -\frac{g-u_y}{2}\bar{T}_{\mathrm{F,D}} \\ \frac{a^{-1}u_y}{d}\bar{T}_{\mathrm{F,D}} \\ \bar{T}_{\mathrm{F,D}} \end{pmatrix} \right)$$

$$= -\frac{\bar{T}_{\mathrm{F,D}}}{2}\left(g + (a^{-1} - 1)u_y \right) < 0,$$

and so the predicates of (88) are satisfied and $\phi_{\mathrm{F}}^{\bar{T}_{\mathrm{F,D}}} \circ \Sigma^I(\tilde{\bar{\boldsymbol{x}}}^I) \in G_{\mathrm{F,D}}^I$.

We still must show that $\bar{T}_{\mathrm{F,D}}$ is the *minimum* positive value of time t at which this predicate is satisfied. It is helpful to note that the rear hip has constant negative-acceleration dynamics, and thus $y^{r_{hip}} \circ \phi_{\mathrm{F}}^t \circ \Sigma^I(\tilde{\bar{\boldsymbol{x}}}^I)$ has the graph of a downwards-facing parabola. At both times $t = 0$ and $t = \bar{T}_{\mathrm{F,D}}$, we have that $y^{r_{hip}} \circ \phi_{\mathrm{F}}^t \circ \Sigma^I(\tilde{\bar{\boldsymbol{x}}}^I) = l_0$, and so (because a parabola can intersect a line no more than two times) at no other time may the predicate $y^{r_{hip}} \circ \phi_{\mathrm{F}}^t \big|_{\Sigma^I(\tilde{\bar{\boldsymbol{x}}}^I)} = l_0$ be true. The parabola is downwards-facing, hence on the time interval $(0, \bar{T}_{\mathrm{F,D}})$ the rear hip height is greater than l_0 in value. Since we require that the lie derivative of g_{TD} along the vector field not be decreasing (27), we have – on the time interval $(0, \bar{T}_{\mathrm{F,D}})$ – that $g_{TD}\big|_{\phi_{\mathrm{F}}^t \circ \Sigma^I(\tilde{\bar{\boldsymbol{x}}}^I)} \leq 0$. Then:

$$y^{r_{hip}}\Big|_{\phi_{\mathrm{F}}^t \circ \Sigma^I(\tilde{\bar{\boldsymbol{x}}}^I)} > l_0 + g_{TD}\Big|_{\phi_{\mathrm{F}}^t \circ \Sigma^I(\tilde{\bar{\boldsymbol{x}}}^I)}, \quad t \in (0, \bar{T}_{\mathrm{F,D}}), \quad (89)$$

and so $\phi_F^t \circ \Sigma^I(\widetilde{\boldsymbol{x}}^I) \notin G_{F,D}^I$ for $t \in (0, \bar{T}_{F,D})$. Thus $T_{D,R}^I$ is indeed the minimum positive time at which the guard predicate is satisfied, allowing us to conclude that:

$$\bar{T}_{F,D} = T_{F,D}^I \Big|_{\Sigma^I(\widetilde{\boldsymbol{x}}^I)}.$$

By similar reasoning (omitted for brevity) one can show that:

$$\bar{T}_{D,R} = T_{D,R}^I \Big|_{\Phi_{F,D}^I \circ \Sigma^I(\widetilde{\boldsymbol{x}}^I)},$$

allowing us to conclude that: $\widetilde{\boldsymbol{x}}^I = H^I(\widetilde{\boldsymbol{x}}^I)$ and $\bar{T}_{D,R}$ is the time-duration spent in mode D of the hybrid execution from $\bar{\boldsymbol{x}}^I$. Additionally, $\widetilde{\boldsymbol{x}}^I$ is a fixed point of S^I since $S^I = H^I \circ H^I$. $\qquad\square$

Proof of Proposition 1, part 2

Proof. We wish to solve for the fixed point of H, parametrized by its velocity component $\dot{\bar{x}}$ as well as the model's physical parameters and the in-place model's fixed point parametrization. Recall that H (46) has the form:

$$H = \Pi \circ b \circ \Phi_{D,R} \circ \Phi_{F,D} \circ \Sigma, \qquad (90)$$

where Π, b, and Σ are simple linear maps (43), (40), (32), while the mode maps $\Phi_{D,R}$ and $\Phi_{F,D}$ are given by (37). In the form of the mode maps, the horizontal flows are given by (35) and the horizontal resets are given by (31), recalling that the otherwise unspecified control functions $r_{F,D}, r_{D,R}$ in the resets are required to vanish on the hybrid periodic orbit's guard intersections.

The map H has the structure:

$$H(\widetilde{\boldsymbol{x}}) = \begin{pmatrix} H^I(\widetilde{\boldsymbol{x}}^I) \\ H^H(\widetilde{\boldsymbol{x}}^I, \widetilde{\boldsymbol{x}}^H) \end{pmatrix}, \quad \widetilde{\boldsymbol{x}} = \begin{pmatrix} \widetilde{\boldsymbol{x}}^I \\ \widetilde{\boldsymbol{x}}^H \end{pmatrix},$$

where, by the previous proof, H^I has the fixed point $\widetilde{\boldsymbol{x}}^I$ (48). It remains to find a fixed point $\widetilde{\boldsymbol{x}}^H = (\dot{\bar{x}}, \Delta\bar{x}^r, \Delta\bar{x}^f)^T$ such that:

$$\widetilde{\boldsymbol{x}}^H = H^H(\widetilde{\boldsymbol{x}}^I, \widetilde{\boldsymbol{x}}^H) = H^H\big|_{\widetilde{\boldsymbol{x}}^I}(\widetilde{\boldsymbol{x}}^H),$$

where:

$$H^H\big|_{\widetilde{\boldsymbol{x}}^I} = \Pi^H \circ b^H \circ R_{D,R}^H \circ \hat{\phi}_D^{\bar{T}_{D,R}} \circ R_{F,D}^H \circ \hat{\phi}_F^{\bar{T}_{F,D}} \circ \Sigma.$$

Finally, to aid in our search, we assume that the forward speed at the fixed point $\dot{\bar{x}}$ returns to the same value after application of each mode map.

Consider:

$$\hat{\phi}^{\bar{T}_{F,D}} \circ \Sigma^H(\widetilde{\boldsymbol{x}}^H)$$

$$= \begin{pmatrix} e^{C_F \bar{T}_{F,D}} \begin{pmatrix} 0 \\ \dot{\bar{x}} \end{pmatrix} + \left(e^{C_F \bar{T}_{F,D}} - I\right) \begin{pmatrix} \Delta x^{\text{Avg}} - \Delta\bar{x}^f \\ 0 \end{pmatrix} \\ \Delta\bar{x}^r \\ \Delta\bar{x}^f \end{pmatrix}$$

$$= \begin{pmatrix} x_F \\ \dot{\bar{x}} \\ \Delta\bar{x}^r \\ \Delta\bar{x}^f \end{pmatrix},$$

where x_F is the distance traveled horizontally by the mass center in mode F. The system of equations given by the first two rows simplify to:

$$\left(e^{C_F \bar{T}_{F,D}} - I\right) \begin{pmatrix} \Delta x^{\text{Avg}} - \Delta\bar{x}^f \\ \dot{\bar{x}} \end{pmatrix} = \begin{pmatrix} x_F \\ 0 \end{pmatrix},$$

allowing us to solve for x_F and $\Delta\bar{x}^f$:

$$x_F = \begin{pmatrix} 1 & 0 \end{pmatrix} \left(e^{C_F \bar{T}_{F,D}} - I\right) \begin{pmatrix} \Delta x^{\text{Avg}} - \Delta\bar{x}^f \\ \dot{\bar{x}} \end{pmatrix},$$

$$\Delta\bar{x}^f = \frac{\begin{pmatrix} 0 & 1 \end{pmatrix} \left(e^{C_F \bar{T}_{F,D}} - I\right) \begin{pmatrix} \Delta x^{\text{Avg}} \\ \dot{\bar{x}} \end{pmatrix}}{\begin{pmatrix} 0 & 1 \end{pmatrix} \left(e^{C_F \bar{T}_{F,D}} - I\right) \begin{pmatrix} 1 \\ 0 \end{pmatrix}}.$$

Letting x_D denote the distance traveled horizontally by the mass center at the end of mode D, we have that (successively adding on terms):

$$R_F^H \circ \hat{\phi}^{\bar{T}_{F,D}} \circ \Sigma^H(\widetilde{\boldsymbol{x}}^H) = (x_F, \ \dot{\bar{x}}, \ x_F + \Delta\bar{x}^r, \ \Delta\bar{x}^f)^T,$$

$$\hat{\phi}^{\bar{T}_{D,R}} \circ R_F^H \circ \hat{\phi}^{\bar{T}_{F,D}} \circ \Sigma^H(\widetilde{\boldsymbol{x}}^H) = (x_D, \ \dot{\bar{x}}, \ x_F + \Delta\bar{x}^r, \ \Delta\bar{x}^f)^T,$$

$$R_D^H \circ \hat{\phi}^{\bar{T}_{D,R}} \circ R_F^H \circ \hat{\phi}^{\bar{T}_{F,D}} \circ \Sigma^H(\widetilde{\boldsymbol{x}}^H) = (x_D, \ \dot{\bar{x}}, \ x_F + \Delta\bar{x}^r, \ \Delta x^{\text{Nom}})^T,$$

$$b^H \circ R_D^H \circ \hat{\phi}^{\bar{T}_{D,R}} \circ R_F^H \circ \hat{\phi}^{\bar{T}_{F,D}} \circ \Sigma^H(\widetilde{\boldsymbol{x}}^H) = (x_D, \ \dot{\bar{x}}, \ \Delta x^{\text{Nom}} - 2\Delta x^{\text{Avg}}, \ x_F + \Delta\bar{x}^r + 2\Delta x^{\text{Avg}})^T,$$

$$\Pi^H \circ b^H \circ R_D^H \circ \hat{\phi}^{\bar{T}_{D,R}} \circ R_F^H \circ \hat{\phi}^{\bar{T}_{F,D}} \circ \Sigma^H(\widetilde{\boldsymbol{x}}^H) = (\dot{\bar{x}}, \ \Delta x^{\text{Nom}} - 2\Delta x^{\text{Avg}}, \ x_F + \Delta\bar{x}^r + 2\Delta x^{\text{Avg}} - x_D)^T,$$

and so:

$$H^H \begin{pmatrix} \dot{\bar{x}} \\ \Delta\bar{x}^r \\ \Delta\bar{x}^f \end{pmatrix} = \begin{pmatrix} \dot{\bar{x}} \\ \Delta x^{\text{Nom}} - 2\Delta x^{\text{Avg}} \\ x_F + \Delta\bar{x}^r + 2\Delta x^{\text{Avg}} - x_D \end{pmatrix},$$

giving us $\Delta x^{\text{Nom}} = \Delta\bar{x}^r + 2\Delta x^{\text{Avg}}$ and $\Delta\bar{x}^r = \Delta\bar{x}^f - 2\Delta x^{\text{Avg}} + (x_D - x_F)$. As we already have the form of x_F and $\Delta\bar{x}^f$, all that remains is to calculate the form of x_D so as to obtain $\Delta\bar{x}^r$.

The first two rows of:

$$\hat{\phi}^{\bar{T}_{D,R}} \circ R_F^H \circ \hat{\phi}^{\bar{T}_{F,D}} \circ \Sigma^H(\widetilde{\boldsymbol{x}}^H) = (x_D, \ \dot{\bar{x}}, \ x_F + \Delta\bar{x}^r, \ \Delta\bar{x}^f)^T$$

give us:

$$\begin{pmatrix} x_D \\ \dot{\bar{x}} \end{pmatrix} = e^{C_D \bar{T}_{D,R}} \begin{pmatrix} x_F \\ \dot{\bar{x}} \end{pmatrix} + \left(e^{C_D \bar{T}_{D,R}} - I\right) \begin{pmatrix} -\frac{1}{2}(x_F + \Delta\bar{x}^r + \Delta\bar{x}^f) \\ 0 \end{pmatrix}.$$

Solving for x_D gives:

$$x_\mathrm{D} = 2(1,0)\left(e^{C_\mathrm{D}\bar{T}_\mathrm{D,R}} + I\right)^{-1}$$
$$\left[e^{C_\mathrm{D}\bar{T}_\mathrm{D,R}}\begin{pmatrix} x_\mathrm{F} \\ 0 \end{pmatrix} + \left(e^{C_\mathrm{D}\bar{T}_\mathrm{D,R}} - I\right)\begin{pmatrix} \Delta x^{\mathrm{Avg}} - \Delta \bar{x}^f \\ \dot{\bar{x}} \end{pmatrix}\right].$$

Plugging the values of x_D and x_F into $\Delta \bar{x}^r = \Delta \bar{x}^f - 2\Delta x^{\mathrm{Avg}} + (x_\mathrm{D} - x_\mathrm{F})$ yields:

$$\Delta \bar{x}^r = \Delta \bar{x}^f - 2\Delta x^{\mathrm{Avg}} + \begin{pmatrix} 1 & 0 \end{pmatrix}\left(e^{C_\mathrm{D}\bar{T}_\mathrm{D,R}} + I\right)^{-1}$$
$$\left(e^{C_\mathrm{D}\bar{T}_\mathrm{D,R}} - I\right)\left(e^{C_\mathrm{F}\bar{T}_\mathrm{F,D}} + I\right)\begin{pmatrix} \Delta x^{\mathrm{Avg}} - \Delta \bar{x}^f \\ \dot{\bar{x}} \end{pmatrix},$$

completing the proof.

Note that x_F and x_D simplify (in terms of $\Delta \bar{x}^r$ and $\Delta \bar{x}^r$ just derived) to:

$$x_\mathrm{F} = 2(\Delta \bar{x}^f - \Delta x^{\mathrm{Avg}}),$$
$$x_\mathrm{D} = \Delta \bar{x}^f + \Delta \bar{x}^r.$$

This allows us to conclude that on the periodic orbit at the end of D before the reset is applied, the front and rear leg splays (used in (62)) are:

$$\Delta \bar{x}^r{}_\mathrm{D} = \Delta \bar{x}^r - (x_\mathrm{D} - x_\mathrm{F}) = \Delta \bar{x}^f - 2\Delta x^{\mathrm{Avg}}, \quad (91)$$
$$\Delta \bar{x}^f{}_\mathrm{D} = \Delta \bar{x}^f - x_\mathrm{D} = -\Delta \bar{x}^r.$$

□

APPENDIX D
PROOF OF LEMMA 1

Proof. For brevity we only show the calculation of $\left.\frac{\partial T^I_{\mathrm{F,D}}}{\partial \widetilde{\boldsymbol{x}}^I}\right|_{\tau=0}$, as the calculation of $\left.\frac{\partial T^I_{\mathrm{D,R}}}{\partial \widetilde{\boldsymbol{x}}^I}\right|_{\tau=0}$ is nearly identical.

According to the definition of $T^I_{i,j}$ (39) and $G^I_{\mathrm{F,D}}$ (85), we have that:

$$T^I_{\mathrm{F,D}}(\boldsymbol{x}^I) = \min\{t \in \mathbb{R}^+ | \phi^t_\mathrm{F}(\boldsymbol{x}^I) \in G^I_{\mathrm{F,D}}\}$$
$$= \min\{t \in \mathbb{R}^+ | y^{r hip} \circ \phi^t_\mathrm{F}(\boldsymbol{x}^I) = l_0 + g_{TD} \circ \phi^t_\mathrm{F}(\boldsymbol{x}^I)$$
$$\wedge\ \dot{y}^{r hip} \circ \phi^t_\mathrm{F}(\boldsymbol{x}^I) < 0\}.$$

Differentiating the predicate's equality term yields:

$$Dy^{r hip}\Big|_{\phi^{T^I_{\mathrm{F,D}}(\boldsymbol{x}^I)}_\mathrm{F}(\boldsymbol{x}^I)} \cdot \left\{\frac{\partial \phi^t_\mathrm{F}(\boldsymbol{x}^I)}{\partial \boldsymbol{x}^I} + \frac{\partial \phi^t_\mathrm{F}(\boldsymbol{x}^I)}{\partial t}\frac{\partial T^I_{\mathrm{F,D}}}{\partial \boldsymbol{x}^I}\right\}\Big|_{\boldsymbol{x}^I, T^I_{\mathrm{F,D}}(\boldsymbol{x}^I)}$$
$$=$$
$$Dg_{TD}\Big|_{\phi^{T^I_{\mathrm{F,D}}(\boldsymbol{x}^I)}_\mathrm{F}(\boldsymbol{x}^I)} \cdot \left\{\frac{\partial \phi^t_\mathrm{F}(\boldsymbol{x}^I)}{\partial \boldsymbol{x}^I} + \frac{\partial \phi^t_\mathrm{F}(\boldsymbol{x}^I)}{\partial t}\frac{\partial T^I_{\mathrm{F,D}}}{\partial \boldsymbol{x}^I}\right\}\Big|_{\boldsymbol{x}^I, T^I_{\mathrm{F,D}}(\boldsymbol{x}^I)},$$

and so:

$$\frac{\partial T^I_{\mathrm{F,D}}}{\partial \boldsymbol{x}^I} = -\frac{1}{s_\mathrm{F}}\{Dy^{r hip} - Dg_{TD}\}\Big|_{\phi^{T^I_{\mathrm{F,D}}(\boldsymbol{x}^I)}_\mathrm{F}(\boldsymbol{x}^I)}$$
$$\left.\frac{\partial \phi^t_\mathrm{F}(\boldsymbol{x}^I)}{\partial \boldsymbol{x}^I}\right|_{\boldsymbol{x}^I, T^I_{\mathrm{F,D}}(\boldsymbol{x}^I)},$$
$$s_\mathrm{F} = \{Dy^{r hip} - Dg_{TD}\}\Big|_{\phi^{T^I_{\mathrm{F,D}}(\boldsymbol{x}^I)}_\mathrm{F}(\boldsymbol{x}^I)}$$
$$\left.\frac{\partial \phi^t_\mathrm{F}(\boldsymbol{x}^I)}{\partial t}\right|_{\boldsymbol{x}^I, T^I_{\mathrm{F,D}}(\boldsymbol{x}^I)}.$$

Then:

$$\frac{\partial T^I_{\mathrm{F,D}}}{\partial \widetilde{\boldsymbol{x}}^I} = -\frac{1}{s_\mathrm{F}}\{Dy^{r hip} - Dg_{TD}\}\Big|_{\phi^{T^I_{\mathrm{F,D}}(\boldsymbol{x}^I)}_\mathrm{F}(\boldsymbol{x}^I)} \quad (92)$$
$$\left.\frac{\partial \phi^t_\mathrm{F}(\boldsymbol{x}^I)}{\partial \widetilde{\boldsymbol{x}}^I}\right|_{\boldsymbol{x}^I, T^I_{\mathrm{F,D}}(\boldsymbol{x}^I)},$$
$$s_\mathrm{F} = \{Dy^{r hip} - Dg_{TD}\}\Big|_{\phi^{T^I_{\mathrm{F,D}}(\boldsymbol{x}^I)}_\mathrm{F}(\boldsymbol{x}^I)}$$
$$\left.\frac{\partial \phi^t_\mathrm{F}(\boldsymbol{x}^I)}{\partial t}\right|_{\boldsymbol{x}^I, T^I_{\mathrm{F,D}}(\boldsymbol{x}^I)}.$$

The rest of the proof is concerned with evaluating each of the terms in (92) at $\tau = 0$.

As $y^{r hip} : \boldsymbol{x}^I \mapsto y - \frac{d}{2}\varphi$ (28), we have that:

$$Dy^{r hip} = \begin{pmatrix} 1, & -\frac{d}{2}, & 0, & 0, & 0 \end{pmatrix},$$

and (recalling the structure of the flow (34)):

$$\left.\frac{\partial \phi^t_\mathrm{F}(\boldsymbol{x}^I)}{\partial \widetilde{\boldsymbol{x}}^I}\right|_{\boldsymbol{x}^I, T^I_{\mathrm{F,D}}(\boldsymbol{x}^I)} = \begin{pmatrix} I & T^I_{\mathrm{F,D}}(\boldsymbol{x}^I)I \\ 0 & I \\ 0 & 0 \end{pmatrix},$$
$$\left.\frac{\partial \phi^t_\mathrm{F}(\boldsymbol{x}^I)}{\partial t}\right|_{\boldsymbol{x}^I, T^I_{\mathrm{F,D}}(\boldsymbol{x}^I)} = \begin{pmatrix} \dot{\boldsymbol{q}}^I + \boldsymbol{c}_\mathrm{F}T^I_{\mathrm{F,D}}(\boldsymbol{x}^I) \\ \boldsymbol{c}_\mathrm{F} \\ 1 \end{pmatrix}.$$

The only remaining term in (92) is the quantity $Dg_{TD}\Big|_{\phi^{T^I_{\mathrm{F,D}}(\boldsymbol{x}^I)}_\mathrm{F}(\boldsymbol{x}^I)}$. Recall that g_{TD} (57) is given by:

$$g_{TD}(\boldsymbol{x}^I) = {\boldsymbol{k}^I_\mathrm{F}}^T \begin{pmatrix} y^{r hip}{}_{\mathrm{F0}}(\boldsymbol{x}^I) - y^{r hip}(\bar{\boldsymbol{x}}^I_{\mathrm{F0,D}}) \\ y^{f hip}{}_{\mathrm{F0}}(\boldsymbol{x}^I) - y^{f hip}(\bar{\boldsymbol{x}}^I_{\mathrm{F0,D}}) \\ \tau - \bar{T}_{\mathrm{F,D}} \end{pmatrix},$$

where $\bar{\boldsymbol{x}}^I_{\mathrm{F0,D}}$ and $\bar{T}_{\mathrm{F,D}}$ are constants, and the maps $y^{r hip}{}_{\mathrm{F0}}, y^{f hip}{}_{\mathrm{F0}}$ (58) are:

$$y^{r hip}{}_{\mathrm{F0}}(\boldsymbol{x}^I) = y^{r hip} \circ \phi^{-\tau}_\mathrm{F}(\boldsymbol{x}^I),$$
$$y^{f hip}{}_{\mathrm{F0}}(\boldsymbol{x}^I) = y^{f hip} \circ \phi^{-\tau}_\mathrm{F}(\boldsymbol{x}^I).$$

For clarity we introduce the following:

$$\phi^{-\tau}_i(\boldsymbol{x}^I) \equiv \widetilde{\phi}_i(\boldsymbol{x}^I),$$

Then:

$$Dg_{TD}\Big|_{\phi^{T^I_{\mathrm{F,D}}(\boldsymbol{x}^I)}_\mathrm{F}(\boldsymbol{x}^I)} = \left(k^I_{\mathrm{F}1}Dy^{r hip} + k^I_{\mathrm{F}2}Dy^{f hip}\right),$$
$$\left.\frac{\partial \widetilde{\phi}_\mathrm{F}}{\partial \boldsymbol{x}^I}\right|_{\phi^{T^I_{\mathrm{F,D}}(\boldsymbol{x}^I)}_\mathrm{F}(\boldsymbol{x}^I)} + k^I_{\mathrm{F}3}\frac{\partial \tau}{\partial \boldsymbol{x}^I},$$

where:

$$Dy^{r hip} = \begin{pmatrix} 1, & -\frac{d}{2}, & 0, & 0, & 0 \end{pmatrix},$$
$$Dy^{f hip} = \begin{pmatrix} 1, & \frac{d}{2}, & 0, & 0, & 0 \end{pmatrix},$$
$$\frac{\partial \widetilde{\phi}_\mathrm{F}}{\partial \boldsymbol{x}^I} = \begin{pmatrix} I & -\tau I & \left(-\dot{\boldsymbol{q}}^I + \boldsymbol{c}_\mathrm{F}\tau\right) \\ 0 & I & -\boldsymbol{c}_\mathrm{F} \\ 0 & 0 & 0 \end{pmatrix},$$

and so (simplifying terms):

$$
\frac{\partial \widetilde{\phi}_{\mathrm{F}}}{\partial \boldsymbol{x}^I}\bigg|_{\phi_{\mathrm{F}}^{T_{\mathrm{F,D}}^I(\boldsymbol{x}^I)}(\boldsymbol{x}^I)}
$$

$$
= \begin{pmatrix} I & \big(-(T_{\mathrm{F,D}}^I(\boldsymbol{x}^I)+\tau)I\big) & \big(-\dot{\boldsymbol{q}}^I + \boldsymbol{c}_{\mathrm{F}}\tau\big) \\ 0 & I & -\boldsymbol{c}_{\mathrm{F}} \\ 0 & 0 & 0 \end{pmatrix}.
$$

We have the form of all terms in (92), multiplying them together gives:

$$
\frac{\partial T_{\mathrm{F,D}}}{\partial \widetilde{\boldsymbol{x}}^I}\bigg|_{\tau=0} = -\frac{1}{s_{\mathrm{F}}} \begin{pmatrix} 1 - k_{\mathrm{F},1}^I - k_{\mathrm{F},2}^I \\ (-1 + k_{\mathrm{F},1}^I - k_{\mathrm{F},2}^I)\frac{d}{2} \\ \bar{T}_{\mathrm{F,D}} \\ -\frac{d}{2}\bar{T}_{\mathrm{F,D}} \end{pmatrix}^T,
$$

$$
s_{\mathrm{F}} = \dot{y} - \frac{d}{2}\dot{\varphi} + \big((1 - a^{-1})u_y - g\big)\bar{T}_{\mathrm{F,D}} - k_{\mathrm{F},3}^I.
$$

$\square$

APPENDIX E
PROOF OF LEMMA 2

Proof. We aim to choose $\widetilde{\boldsymbol{k}}_{\mathrm{F}}^I$, $\widetilde{\boldsymbol{k}}_{\mathrm{D}}^I$ to make $DH^I\big|_{\widetilde{\boldsymbol{x}}^I}$ nilpotent.

Recall that $DH^I\big|_{\widetilde{\boldsymbol{x}}^I} = D\widetilde{b}^I \cdot D\widetilde{\Phi}_{\mathrm{D,R}}^I\big|_{\Phi_{\mathrm{F,D}}^I(\bar{\boldsymbol{x}}^I)} \cdot D\widetilde{\Phi}_{\mathrm{F,D}}^I\big|_{\bar{\boldsymbol{x}}^I}$
(71), where $D\widetilde{b}^I$ is a simple linear map (72) and:

$$
D\widetilde{\Phi}_{\mathrm{D,R}}^I\big|_{\Phi_{\mathrm{F,D}}^I(\bar{\boldsymbol{x}}^I)} = \begin{pmatrix} I & \bar{T}_{\mathrm{D,R}}I \\ 0 & I \end{pmatrix} + \begin{pmatrix} \dot{y} \\ -\dot{\varphi} \\ 2u_y - g \\ 0 \end{pmatrix} \widetilde{\boldsymbol{k}}_{\mathrm{D}}^{I^T} M_{\mathrm{D}}^I,
$$

$$
D\widetilde{\Phi}_{\mathrm{F,D}}^I\big|_{\bar{\boldsymbol{x}}^I} = \begin{pmatrix} I & \bar{T}_{\mathrm{F,D}}I \\ 0 & I \end{pmatrix} + \begin{pmatrix} -\dot{y} \\ -\dot{\varphi} \\ u_y - g \\ -\frac{2u_y}{da} \end{pmatrix} \widetilde{\boldsymbol{k}}_{\mathrm{F}}^{I^T} M_{\mathrm{F}}^I.
$$

A necessary requirement for nilpotency of $DH^I\big|_{\widetilde{\boldsymbol{x}}^I}$ is that its determinant is zero, and so one of its factors must have a zero determinant. We find it algebraically convenient to zero the determinant of $D\widetilde{\Phi}_{\mathrm{D,R}}^I\big|_{\Phi_{\mathrm{F,D}}^I(\bar{\boldsymbol{x}}^I)}$:

$$
\det D\widetilde{\Phi}_{\mathrm{D,R}}^I\big|_{\Phi_{\mathrm{F,D}}^I(\bar{\boldsymbol{x}}^I)}
$$

$$
= \det\left(\begin{pmatrix} I & \bar{T}_{\mathrm{D,R}}I \\ 0 & I \end{pmatrix} + \begin{pmatrix} \dot{y} \\ -\dot{\varphi} \\ 2u_y - g \\ 0 \end{pmatrix} \widetilde{\boldsymbol{k}}_{\mathrm{D}}^{I^T} M_{\mathrm{D}}^I \right)
$$

$$
\stackrel{[52,\, \mathrm{Lem.}\, 1.1]}{=} \det \begin{pmatrix} I & \bar{T}_{\mathrm{D,R}}I \\ 0 & I \end{pmatrix}.
$$

$$
\left(1 + \widetilde{\boldsymbol{k}}_{\mathrm{D}}^{I^T} M_{\mathrm{D}}^I \begin{pmatrix} I & -\bar{T}_{\mathrm{D,R}}I \\ 0 & I \end{pmatrix} \begin{pmatrix} \dot{y} \\ -\dot{\varphi} \\ 2u_y - g \\ 0 \end{pmatrix} \right)
$$

$$
= 1 + \widetilde{\boldsymbol{k}}_{\mathrm{D}}^{I^T} M_{\mathrm{D}}^I \begin{pmatrix} I & -\bar{T}_{\mathrm{D,R}}I \\ 0 & I \end{pmatrix} \begin{pmatrix} \dot{y} \\ -\dot{\varphi} \\ 2u_y - g \\ 0 \end{pmatrix}
$$

$$
= 1 + \widetilde{\boldsymbol{k}}_{\mathrm{D}}^{I^T} M_{\mathrm{D}}^I \begin{pmatrix} -\dot{y} \\ -\dot{\varphi} \\ 2u_y - g \\ 0 \end{pmatrix}
$$

$$
= 1 + \widetilde{\boldsymbol{k}}_{\mathrm{D}}^{I^T} \begin{pmatrix} -\dot{y} \\ -\dot{\varphi} \\ 2u_y - g \end{pmatrix}
$$

$$
= 0 \iff \widetilde{\boldsymbol{k}}_{\mathrm{D}}^{I^T} \begin{pmatrix} -\dot{y} \\ -\dot{\varphi} \\ 2u_y - g \end{pmatrix} = -1. \tag{93}
$$

The choice of $\widetilde{\boldsymbol{k}}_{\mathrm{D}}^I$ according to (93) results in the Jordan decomposition $D\widetilde{\Phi}_{\mathrm{D,R}}^I\big|_{\Phi_{\mathrm{F,D}}^I(\bar{\boldsymbol{x}}^I)} = V^I \Lambda^I V^{I-1}$, where:

$$
V^I = \begin{pmatrix} -\dot{y} & \dot{y} + \widetilde{k}^{I-1}_{\mathrm{D},1} & -\frac{\widetilde{k}_{\mathrm{D},2}^I}{\widetilde{k}_{\mathrm{D},1}^I} & -\frac{\widetilde{k}_{\mathrm{D},3}^I(\widetilde{k}_{\mathrm{D},2}^I - \frac{d}{2}\widetilde{k}_{\mathrm{D},1}^I)}{\widetilde{k}^{I2}_{\mathrm{D},1}\bar{T}_{\mathrm{D,R}}} \\ -\dot{\varphi} & -\dot{\varphi} & 1 & 0 \\ 2u_y - g & 2u_y - g & 0 & -\frac{\widetilde{k}_{\mathrm{D},2}^I}{\widetilde{k}_{\mathrm{D},1}^I \bar{T}_{\mathrm{D,R}}} \\ 0 & 0 & 0 & \bar{T}_{\mathrm{D,R}}^{-1} \end{pmatrix},
$$
$$\tag{94}$$

$$
\Lambda^I = \begin{pmatrix} 0 & 0 & 0 & 0 \\ 0 & 1 + \widetilde{k}_{\mathrm{D},1}^I \bar{T}_{\mathrm{D,R}}(2u_y - g) & 0 & 0 \\ 0 & 0 & 1 & 1 \\ 0 & 0 & 0 & 1 \end{pmatrix}.
$$

We have that $\det V^I = \frac{2u_y - g}{\widetilde{k}_{\mathrm{D},1}^I \bar{T}_{\mathrm{D,R}}}(1 + 2\dot{y}\widetilde{k}_{\mathrm{D},1}^I)$, and so we will require that:

$$
\widetilde{k}_{\mathrm{D},1}^I \neq -\frac{1}{2\dot{y}}, \quad \widetilde{k}_{\mathrm{D},1}^I \neq 0. \tag{95}
$$

Nilpotency of a real matrix product is equivalent to nilpotency of the product of any cyclic permutation of its factors[12], thus achieving our goal of a nilpotent:

$$
DH^I\big|_{\widetilde{\boldsymbol{x}}^I} = D\widetilde{b}^I \cdot D\widetilde{\Phi}_{\mathrm{D,R}}^I\big|_{\Phi_{\mathrm{F,D}}^I(\bar{\boldsymbol{x}}^I)} \cdot D\widetilde{\Phi}_{\mathrm{F,D}}^I\big|_{\bar{\boldsymbol{x}}^I}
$$

$$
= D\widetilde{b}^I \cdot V^I \cdot \Lambda^I \cdot V^{I-1} \cdot D\widetilde{\Phi}_{\mathrm{F,D}}^I\big|_{\bar{\boldsymbol{x}}^I},
$$

is equivalent to nilpotency of the cyclic permutation:

$$
\Lambda^I \cdot V^{I-1} \cdot D\widetilde{\Phi}_{\mathrm{F,D}}^I\big|_{\bar{\boldsymbol{x}}^I} \cdot D\widetilde{b}^I \cdot V^I.
$$

The block structure of the leading factor Λ^I guarantees both a zero eigenvalue and that the remaining three eigenvalues of the product can only be affected by the lower three-by-three block matrix of the product. This lower three-by-three block – which we represent by the matrix N – is given by:

$$
N = T^I \cdot \Lambda^I \cdot V^{I-1} \cdot D\widetilde{\Phi}_{\mathrm{F,D}}^I\big|_{\bar{\boldsymbol{x}}^I} \cdot D\widetilde{b}^I \cdot V^I \cdot T^{I^T},
$$

$$
T^I = \begin{pmatrix} 0 & 1 & 0 & 0 \\ 0 & 0 & 1 & 0 \\ 0 & 0 & 0 & 1 \end{pmatrix}.
$$

---

[12]Proof: Let $M \in \mathbb{R}^{n \times n}, A \in \mathbb{R}^{n \times m}, B \in \mathbb{R}^{m \times n}$, $M = AB$. Assume there exists a $k \in \mathbb{N}$ such that $M^k = 0$ (M is nilpotent). Then $(AB)^k = 0$ and so $(BA)^{k+1} = B(AB)^k A = B(0)A = 0$. Then the cyclic permutation BA is nilpotent. Similarly, assume there exists a $k \in \mathbb{N}$ such that $(BA)^k = 0$ (the cyclic permutation BA is nilpotent). Then $M^{k+1} = (AB)^{k+1} = A(BA)^k B = A(0)B = 0$. Then M is nilpotent.

Expanding $D\widetilde{\Phi}^I_{\mathrm{F},\mathrm{D}}\big|_{\bar{x}^I}$ results in:

$$N = A^I + \boldsymbol{d}^I \widetilde{\boldsymbol{k}}_{\mathrm{F}}^{I\,T} M^I_{\mathrm{F}} D\widetilde{b}^I V^I T^{I\,T},$$

$$A^I = T^I \Lambda^I V^{I-1} \begin{pmatrix} I & I\bar{T}_{\mathrm{F},\mathrm{D}} \\ 0 & I \end{pmatrix} D\widetilde{b}^I V^I T^{I\,T},$$

$$\boldsymbol{d}^I = T^I \Lambda^I V^{I-1} \begin{pmatrix} -\dot{\bar{y}} \\ -\dot{\bar{\varphi}} \\ u_y - g \\ -\frac{2u_y}{da} \end{pmatrix}.$$

We place the eigenvalues of N at the origin using the standard Ackermann's formula [53, p. 611] via:

$$\widetilde{\boldsymbol{k}}_{\mathrm{F}}^{I\,T} M^I_{\mathrm{F}} D\widetilde{b}^I V^I T^{I\,T} = -\begin{pmatrix} 0 & 0 & 1 \end{pmatrix} R^{I-1} A^{I3},$$

where:

$$R^I = \begin{pmatrix} \boldsymbol{d}^I & A^I \boldsymbol{d}^I & A^{I2} \boldsymbol{d}^I \end{pmatrix}. \tag{96}$$

Equivalently:

$$\widetilde{\boldsymbol{k}}_{\mathrm{F}}^{I\,T} = -\begin{pmatrix} 0 & 0 & 1 \end{pmatrix} R^{I-1} A^{I3} \left(M^I_{\mathrm{F}} D\widetilde{b}^I V^I T^{I\,T} \right)^{-1},$$

where:

$$\det\left(M^I_{\mathrm{F}} D\widetilde{b}^I V^I T^{I\,T} \right) =$$

$$\frac{\widetilde{k}^I_{\mathrm{D},2} - \frac{d}{2}\widetilde{k}^I_{\mathrm{D},1}}{\widetilde{k}^{I2}_{\mathrm{D},1} \bar{T}_{\mathrm{D},\mathrm{R}}} \left(1 + \dot{\bar{y}}\widetilde{k}^I_{\mathrm{D},1} - \dot{\bar{\varphi}}\widetilde{k}^I_{\mathrm{D},2} + (2u_y - g)\widetilde{k}^I_{\mathrm{D},3} \right),$$

introducing the requirements that:

$$\widetilde{k}^I_{\mathrm{D},1} \neq 0, \tag{97}$$

$$\widetilde{k}^I_{\mathrm{D},2} \neq \frac{d}{2}\widetilde{k}^I_{\mathrm{D},1},$$

$$\dot{\bar{y}}\widetilde{k}^I_{\mathrm{D},1} - \dot{\bar{\varphi}}\widetilde{k}^I_{\mathrm{D},2} + (2u_y - g)\widetilde{k}^I_{\mathrm{D},3} \neq -1.$$

The determinant of R^I is exceedingly complicated and so we leave as a conjecture that R^I is generically invertible. We verified invertibility numerically using the values from Table III. $\qquad\square$

APPENDIX F
PROOF OF LEMMA 3

Proof. We desire a value of $\boldsymbol{k}^H = (k^H_{\mathrm{F}}, k^H_{\mathrm{D},1}, k^H_{\mathrm{D},2})^T$ that makes $D_{\widetilde{\boldsymbol{x}}^H} H^H\big|_{\widetilde{\bar{\boldsymbol{x}}}^I}$ (70) nilpotent. Recall that $D_{\widetilde{\boldsymbol{x}}^H} H^H\big|_{\widetilde{\bar{\boldsymbol{x}}}^I}$ has the form:

$$D_{\widetilde{\boldsymbol{x}}^H} H^H\big|_{\widetilde{\bar{\boldsymbol{x}}}^I} = D\Pi^H \cdot Db^H \cdot D_{\boldsymbol{x}^H} R^H_{\mathrm{D},\mathrm{R}} \cdot D_{\boldsymbol{x}^H} \hat{\phi}^{\bar{T}_{\mathrm{D},\mathrm{R}}}_{\mathrm{D}} \cdot$$
$$D_{\boldsymbol{x}^H} R^H_{\mathrm{F},\mathrm{D}} \cdot D_{\boldsymbol{x}^H} \hat{\phi}^{\bar{T}_{\mathrm{F},\mathrm{D}}}_{\mathrm{F}} \cdot D\Sigma^H,$$

where:

$$D\Pi^H = \begin{pmatrix} 0 & 1 & 0 & 0 \\ 0 & 0 & 1 & 0 \\ -1 & 0 & 0 & 1 \end{pmatrix}, \quad Db^H = \begin{pmatrix} 1 & 0 & 0 & 0 \\ 0 & 1 & 0 & 0 \\ 0 & 0 & 0 & 1 \\ 0 & 0 & 1 & 0 \end{pmatrix},$$

$$D\Sigma^H = \begin{pmatrix} 0 & 0 & 0 \\ 1 & 0 & 0 \\ 0 & 1 & 0 \\ 0 & 0 & 1 \end{pmatrix},$$

and:

$$D_{\boldsymbol{x}^H} \hat{\phi}^{\bar{T}_{\mathrm{F},\mathrm{D}}}_{\mathrm{F}} = \begin{pmatrix} e^{C_{\mathrm{F}} \bar{T}_{\mathrm{F},\mathrm{D}}} & (e^{C_{\mathrm{F}} \bar{T}_{\mathrm{F},\mathrm{D}}} - I) \begin{pmatrix} 0 & -1 \\ 0 & 0 \end{pmatrix} \\ 0 & I \end{pmatrix},$$

$$C_{\mathrm{F}} = \begin{pmatrix} 0 & 1 \\ \frac{u_y}{\bar{y}} & 0 \end{pmatrix},$$

$$D_{\boldsymbol{x}^H} \hat{\phi}^{\bar{T}_{\mathrm{D},\mathrm{R}}}_{\mathrm{D}} = \begin{pmatrix} e^{C_{\mathrm{D}} \bar{T}_{\mathrm{D},\mathrm{R}}} & \frac{1}{2}(e^{C_{\mathrm{D}} \bar{T}_{\mathrm{D},\mathrm{R}}} - I) \begin{pmatrix} -1 & -1 \\ 0 & 0 \end{pmatrix} \\ 0 & I \end{pmatrix},$$

$$C_{\mathrm{D}} = \begin{pmatrix} 0 & 1 \\ \frac{2u_y}{\bar{y}} & 0 \end{pmatrix},$$

$$D_{\boldsymbol{x}^H} R^H_{\mathrm{F},\mathrm{D}} = \begin{pmatrix} I & 0 \\ \begin{pmatrix} 1 & k^H_{\mathrm{F}} \\ 0 & 0 \end{pmatrix} & I \end{pmatrix},$$

$$D_{\boldsymbol{x}^H} R^H_{\mathrm{D},\mathrm{R}} = \begin{pmatrix} I & 0 \\ \begin{pmatrix} 0 & 0 \\ -(k^H_{\mathrm{D},1} + k^H_{\mathrm{D},2}) & 0 \end{pmatrix} & \begin{pmatrix} 1 & 0 \\ k^H_{\mathrm{D},1} & k^H_{\mathrm{D},2} \end{pmatrix} \end{pmatrix}.$$

Nilpotency of $D_{\widetilde{\boldsymbol{x}}^H} H^H\big|_{\widetilde{\bar{\boldsymbol{x}}}^I}$ is equivalent to nilpotency of the product of any cyclic permutation of the factors of $D_{\widetilde{\boldsymbol{x}}^H} H^H\big|_{\widetilde{\bar{\boldsymbol{x}}}^I}$. Consider the cyclic permutation:

$$D\Sigma^H \cdot D\Pi^H \cdot Db^H \cdot D_{\boldsymbol{x}^H} R^H_{\mathrm{D},\mathrm{R}} \cdot D_{\boldsymbol{x}^H} \hat{\phi}^{\bar{T}_{\mathrm{D},\mathrm{R}}}_{\mathrm{D}} \cdot D_{\boldsymbol{x}^H} R^H_{\mathrm{F},\mathrm{D}} \cdot D_{\boldsymbol{x}^H} \hat{\phi}^{\bar{T}_{\mathrm{F},\mathrm{D}}}_{\mathrm{F}}.$$

The product of the final four factors is equal to:

$$D_{\boldsymbol{x}^H} \hat{R}^H_{\mathrm{D},\mathrm{R}} := D\Sigma^H \cdot D\Pi^H \cdot Db^H \cdot D_{\boldsymbol{x}^H} R^H_{\mathrm{D},\mathrm{R}}$$
$$= \begin{pmatrix} 0 & 0 & 0 & 0 \\ 0 & 1 & 0 & 0 \\ -(k^H_{\mathrm{D},1} + k^H_{\mathrm{D},2}) & 0 & k^H_{\mathrm{D},1} & k^H_{\mathrm{D},2} \\ -1 & 0 & 1 & 0 \end{pmatrix},$$

which by inspection is generically rank three but drops to rank two when $k^H_{\mathrm{D},2} = 0$.

Let $k^H_{\mathrm{D},2} = 0$. Then:

$$D_{\boldsymbol{x}^H} \hat{R}^H_{\mathrm{D},\mathrm{R}} = \begin{pmatrix} 0 & 0 & 0 & 0 \\ 0 & 1 & 0 & 0 \\ -k^H_{\mathrm{D},1} & 0 & k^H_{\mathrm{D},1} & 0 \\ -1 & 0 & 1 & 0 \end{pmatrix} = V\Lambda V^{-1},$$

$$V = \begin{pmatrix} 0 & 1 & 0 & 0 \\ 0 & 0 & 1 & 0 \\ 0 & 1 & 0 & k^H_{\mathrm{D},1} \\ 1 & 0 & 0 & 1 \end{pmatrix}, \quad \Lambda = \mathrm{diag}\{0, 0, 1, k^H_{\mathrm{D},1}\}$$

$$\text{s.t. } \Lambda V^{-1} = \begin{pmatrix} 0 & 0 & 0 & 0 \\ 0 & 0 & 0 & 0 \\ 0 & 1 & 0 & 0 \\ -1 & 0 & 1 & 0 \end{pmatrix}.$$

We use these terms to simplify the previous cyclic permutation of $D_{\widetilde{\boldsymbol{x}}^H} H^H\big|_{\widetilde{\bar{\boldsymbol{x}}}^I}$:

$$D\Sigma^H \cdot D\Pi^H \cdot Db^H \cdot D_{\boldsymbol{x}^H} R^H_{\mathrm{D},\mathrm{R}} \cdot$$
$$D_{\boldsymbol{x}^H} \hat{\phi}^{\bar{T}_{\mathrm{D},\mathrm{R}}}_{\mathrm{D}} \cdot D_{\boldsymbol{x}^H} R^H_{\mathrm{F},\mathrm{D}} \cdot D_{\boldsymbol{x}^H} \hat{\phi}^{\bar{T}_{\mathrm{F},\mathrm{D}}}_{\mathrm{F}}$$
$$= D_{\boldsymbol{x}^H} \hat{R}^H_{\mathrm{D},\mathrm{R}} \cdot \left(D_{\boldsymbol{x}^H} \hat{\phi}^{\bar{T}_{\mathrm{D},\mathrm{R}}}_{\mathrm{D}} \cdot D_{\boldsymbol{x}^H} R^H_{\mathrm{F},\mathrm{D}} \cdot D_{\boldsymbol{x}^H} \hat{\phi}^{\bar{T}_{\mathrm{F},\mathrm{D}}}_{\mathrm{F}} \right)$$
$$= V \cdot \Lambda \cdot V^{-1} \cdot \left(D_{\boldsymbol{x}^H} \hat{\phi}^{\bar{T}_{\mathrm{D},\mathrm{R}}}_{\mathrm{D}} \cdot D_{\boldsymbol{x}^H} R^H_{\mathrm{F},\mathrm{D}} \cdot D_{\boldsymbol{x}^H} \hat{\phi}^{\bar{T}_{\mathrm{F},\mathrm{D}}}_{\mathrm{F}} \right),$$

and again cyclically permute it to:

$$\Lambda \cdot V^{-1} \cdot D_{\boldsymbol{x}^H}\hat{\phi}_{\mathrm{D}}^{\bar{T}_{\mathrm{D,R}}} \cdot D_{\boldsymbol{x}^H} R_{\mathrm{F,D}}^{H} \cdot D_{\boldsymbol{x}^H}\hat{\phi}_{\mathrm{F}}^{\bar{T}_{\mathrm{F,D}}} \cdot V,$$

which is four-by-four and, by virtue of Λ, has a block lower-triangular form with zeros in the upper-left two-by-two block. Then only the lower right two-by-two block can affect the remaining (possibly) non-zero eigenvalues, reducing our consideration to nilpotency of the two-by-two:

$$D_{\widetilde{\boldsymbol{x}}^H}\widetilde{H}^H\big|_{\widetilde{\boldsymbol{x}}^I} := \begin{pmatrix} 0 & I \end{pmatrix} \cdot \Lambda \cdot V^{-1} \cdot D_{\boldsymbol{x}^H}\hat{\phi}_{\mathrm{D}}^{\bar{T}_{\mathrm{D,R}}} \cdot$$
$$D_{\boldsymbol{x}^H} R_{\mathrm{F,D}}^{H} \cdot D_{\boldsymbol{x}^H}\hat{\phi}_{\mathrm{F}}^{\bar{T}_{\mathrm{F,D}}} \cdot V \cdot \begin{pmatrix} 0 \\ I \end{pmatrix}.$$

Expanding out $D_{\widetilde{\boldsymbol{x}}^H}\widetilde{H}^H\big|_{\widetilde{\boldsymbol{x}}^I}$ and simplifying results in:

$$D_{\widetilde{\boldsymbol{x}}^H}\widetilde{H}^H\big|_{\widetilde{\boldsymbol{x}}^I} =$$
$$\begin{pmatrix} 0 & 1 \\ -1 & 0 \end{pmatrix} e^{C_{\mathrm{D}}\bar{T}_{\mathrm{D,R}}} \left[e^{C_{\mathrm{F}}\bar{T}_{\mathrm{F,D}}} \begin{pmatrix} 0 & -1 \\ 1 & 0 \end{pmatrix} + \begin{pmatrix} 0 & 1 \\ 0 & 0 \end{pmatrix} \right] +$$
$$\frac{1}{2}\left[\begin{pmatrix} 0 & 1 \\ -1 & 0 \end{pmatrix} e^{C_{\mathrm{D}}\bar{T}_{\mathrm{D,R}}} \begin{pmatrix} -1 & -1 \\ 0 & 0 \end{pmatrix} + \begin{pmatrix} 0 & 0 \\ 1 & -1 \end{pmatrix} \right] \cdot$$
$$\begin{pmatrix} \tilde{k}_{\mathrm{F}}^H & \tilde{k}_{\mathrm{D},L}^H \\ 0 & 1 \end{pmatrix},$$

where:

$$\begin{pmatrix} k_{\mathrm{F}}^H \\ k_{\mathrm{D},1}^H \end{pmatrix} = \begin{pmatrix} \cosh\left(\bar{T}_{\mathrm{F,D}}\sqrt{\frac{u_y}{\bar{y}}}\right) & 0 \\ -\sqrt{\frac{u_y}{\bar{y}}}\sinh\left(\bar{T}_{\mathrm{F,D}}\sqrt{\frac{u_y}{\bar{y}}}\right) & 1 \end{pmatrix}^{-1}$$
$$\left\{ \begin{pmatrix} \tilde{k}_{\mathrm{F}}^H \\ \tilde{k}_{\mathrm{D},1}^H \end{pmatrix} - \begin{pmatrix} \sqrt{\frac{\bar{y}}{u_y}}\sinh\left(\bar{T}_{\mathrm{F,D}}\sqrt{\frac{u_y}{\bar{y}}}\right) \\ 1 - \cosh\left(\bar{T}_{\mathrm{F,D}}\sqrt{\frac{u_y}{\bar{y}}}\right) \end{pmatrix} \right\},$$

and:

$$\det\begin{pmatrix} \cosh\left(\bar{T}_{\mathrm{F,D}}\sqrt{\frac{u_y}{\bar{y}}}\right) & 0 \\ -\sqrt{\frac{u_y}{\bar{y}}}\sinh\left(\bar{T}_{\mathrm{F,D}}\sqrt{\frac{u_y}{\bar{y}}}\right) & 1 \end{pmatrix} = \cosh\left(\bar{T}_{\mathrm{F,D}}\sqrt{\frac{u_y}{\bar{y}}}\right),$$

which never equals zero by virtue of $\bar{T}_{\mathrm{F,D}}, u_y \neq 0$.

Then $D_{\widetilde{\boldsymbol{x}}^H}\widetilde{H}^H\big|_{\widetilde{\boldsymbol{x}}^I}$ simplifies to:

$$D_{\widetilde{\boldsymbol{x}}^H}\widetilde{H}^H\big|_{\widetilde{\boldsymbol{x}}^I} = A^H + \boldsymbol{d}^H \begin{pmatrix} \tilde{k}_{\mathrm{F}}^H \\ \tilde{k}_{\mathrm{D},1}^H \end{pmatrix}^T,$$

where:

$$A^H = \begin{pmatrix} 0 & 1 \\ -1 & 0 \end{pmatrix} e^{C_{\mathrm{D}}\bar{T}_{\mathrm{D,R}}} \left(e^{C_{\mathrm{F}}\bar{T}_{\mathrm{F,D}}} \begin{pmatrix} 0 & -1 \\ 1 & 0 \end{pmatrix} + \begin{pmatrix} 0 & \frac{1}{2} \\ 0 & 0 \end{pmatrix} \right)$$
$$- \begin{pmatrix} 0 & 0 \\ 0 & \frac{1}{2} \end{pmatrix},$$
$$\boldsymbol{d}^H = \begin{pmatrix} 0 & 1 \\ -1 & 0 \end{pmatrix} e^{C_{\mathrm{D}}\bar{T}_{\mathrm{D,R}}} \begin{pmatrix} -\frac{1}{2} \\ 0 \end{pmatrix} + \begin{pmatrix} 0 \\ \frac{1}{2} \end{pmatrix}.$$

We place the eigenvalues of $D_{\widetilde{\boldsymbol{x}}^H}\widetilde{H}^H\big|_{\widetilde{\boldsymbol{x}}^I}$ at the origin using the standard Ackermann's formula [53, p. 611] via:

$$\begin{pmatrix} \tilde{k}_{\mathrm{F}}^H \\ \tilde{k}_{\mathrm{D},1}^H \end{pmatrix} = -\left(R^{H^{-1}} A^{H^2} \right)^T \begin{pmatrix} 0 \\ 1 \end{pmatrix},$$

where:

$$R^H = \begin{pmatrix} \boldsymbol{d}^H & A^H \boldsymbol{d}^H \end{pmatrix},$$

and:

$$\det R^H = \frac{1}{8}\sqrt{\frac{u_y}{\bar{y}}} e^{-\sqrt{\frac{u_y}{\bar{y}}}(\bar{T}_{\mathrm{F,D}} + \bar{T}_{\mathrm{D,R}})} \left(1 + e^{\sqrt{\frac{u_y}{\bar{y}}}\bar{T}_{\mathrm{D,R}}} \right)^2$$
$$\left(-1 + e^{2\sqrt{\frac{u_y}{\bar{y}}}(\bar{T}_{\mathrm{F,D}} + \bar{T}_{\mathrm{D,R}})} \right),$$

thus R^H is invertible, as $u_y \neq 0$ and $2\sqrt{\frac{u_y}{\bar{y}}}(\bar{T}_{\mathrm{F,D}} + \bar{T}_{\mathrm{D,R}}) \neq 0$. $\qquad \square$

REFERENCES

[1] J. Duperret and D. E. Koditschek, "Simple sagittal running: Stability of a quadrupedal bound," *IEEE Transactions on Robotics*, 2019, submitted.

[2] D. J. Hyun, S. Seok, J. Lee, and S. Kim, "High speed trot-running: Implementation of a hierarchical controller using proprioceptive impedance control on the mit cheetah," *International Journal of Robotics Research*, vol. 33, no. 11, pp. 1417–1445, 2014.

[3] "Boston dynamics," http://www.bostondynamics.com.

[4] H.-W. Park, P. M. Wensing, S. Kim *et al.*, "Online planning for autonomous running jumps over obstacles in high-speed quadrupeds," in *Proceedings of the Robotics: Science and System (RSS)*, Rome, Italy, July 2015, doi: 10.15607/RSS.2015.XI.047.

[5] T. T. Topping, V. Vasilopoulos, A. De, and E. Koditschek, Daniel, "Composition of templates for transitional pedipulation behaviors," in *International Symposium on Robotics Research (ISRR)*, 2019, (in press).

[6] S. Kuindersma, R. Deits, M. Fallon, A. Valenzuela, H. Dai, F. Permenter, T. Koolen, P. Marion, and R. Tedrake, "Optimization-based locomotion planning, estimation, and control design for the atlas humanoid robot," *Autonomous Robots*, vol. 40, no. 3, pp. 429–455, 2016.

[7] X. Da and J. Grizzle, "Combining trajectory optimization, supervised machine learning, and model structure for mitigating the curse of dimensionality in the control of bipedal robots," *International Journal of Robotics Research*, vol. 38, no. 9, pp. 1063–1097, 2019.

[8] J. Hwangbo, J. Lee, A. Dosovitskiy, D. Bellicoso, V. Tsounis, V. Koltun, and M. Hutter, "Learning agile and dynamic motor skills for legged robots," *Science Robotics*, vol. 4, no. 26, 2019. [Online]. Available: https://robotics.sciencemag.org/content/4/26/eaau5872

[9] A. De and D. E. Koditschek, "Parallel composition of templates for tail-energized planar hopping," in *Proceedings - IEEE International Conference on Robotics and Automation*, 2015, pp. 4562–4569.

[10] R. Altendorfer, D. Koditschek, and P. Holmes, "Stability analysis of a clock-driven rigid-body slip model for rhex," *International Journal of Robotics Research*, vol. 23, no. 10–11, p. 1001–1012, 2004.

[11] C. Chevallereau, E. R. Westervelt, and J. W. Grizzle, "Asymptotically stable running for a five-link, four-actuator, planar bipedal robot," *International Journal of Robotics Research*, vol. 24, no. 6, pp. 431–464, 2005.

[12] J. M. Duperret, B. Kramer, and D. E. Koditschek, "Core actuation promotes self-manipulability on a direct-drive quadrupedal robot," in *2016 International Symposium on Experimental Robotics (ISER)*, Tokyo, Japan, Oct. 2016, pp. 147–159.

[13] M. H. Raibert, *Legged Robots That Balance*. Cambridge: MIT Press, 1986.

[14] H. . Park, P. M. Wensing, and S. Kim, "High-speed bounding with the mit cheetah 2: Control design and experiments," *International Journal of Robotics Research*, vol. 36, no. 2, pp. 167–192, 2017.

[15] R. Altendorfer, N. Moore, H. Komsuoglu, M. Buehler, H. B. Brown Jr., D. Mcmordie, U. Saranli, R. Full, and D. E. Koditschek, "Rhex: A biologically inspired hexapod runner," *Autonomous Robots*, vol. 11, no. 3, pp. 207–213, 2001.

[16] E. R. Westervelt, J. W. Grizzle, and D. E. Koditschek, "Hybrid zero dynamics of planar biped walkers," *IEEE Transactions on Automatic Control*, vol. 48, no. 1, pp. 42–56, 2003.

[17] I. Poulakakis and J. W. Grizzle, "The spring loaded inverted pendulum as the hybrid zero dynamics of an asymmetric hopper," *IEEE Transactions on Automatic Control*, vol. 54, no. 8, pp. 1779–1793, 2009.

[18] K. Sreenath, H. . Park, I. Poulakakis, and J. W. Grizzle, "A compliant hybrid zero dynamics controller for stable, efficient and fast bipedal walking on mabel," *International Journal of Robotics Research*, vol. 30, no. 9, pp. 1170–1193, 2011.

[19] A. De and D. E. Koditschek, "Vertical hopper compositions for preflex-ive and feedback-stabilized quadrupedal bounding, pacing, pronking, and trotting," *International Journal of Robotics Research*, vol. 37, no. 7, pp. 743–778, 2018.

[20] A. De, "Modular hopping and running via parallel composition," Ph.D. dissertation, The University of Pennsylvania, 2017.

[21] A. De, S. A. Burden, and D. E. Koditschek, "A hybrid dynamical extension of averaging and its application to the analysis of legged gait stability," *The International Journal of Robotics Research*, vol. 37, no. 2–3, p. 266–286, 2018.

[22] E. D. Sontag, "Further facts about input to state stabilization," *IEEE Transactions on Automatic Control*, vol. 35, no. 4, pp. 473–476, 1990.

[23] M. Vidyasagar, "Decomposition techniques for large-scale systems with nonadditive interactions: Stability and stabilizability," *IEEE Transactions on Automatic Control*, vol. 25, no. 4, pp. 773–779, 1980.

[24] D. S. Laila and D. Nešić, "Changing supply rates for input-output to state stable discrete-time nonlinear systems with applications," *Automatica*, vol. 39, no. 5, pp. 821–835, 2003.

[25] T. Boaventura, G. A. Medrano-Cerda, C. Semini, J. Buchli, and D. G. Caldwell, "Stability and performance of the compliance controller of the quadruped robot hyq," in *IEEE International Conference on Intelligent Robots and Systems*, 2013, pp. 1458–1464.

[26] C. K. Jones, "Geometric singular perturbation theory," in *Dynamical systems*, ser. Lecture Notes in Mathematics. Springer, 1995, vol. 1609, pp. 44–118.

[27] J. Eldering, M. Kvalheim, and S. Revzen, "Global linearization and fiber bundle structure of invariant manifolds," *Nonlinearity*, vol. 31, no. 9, pp. 4202–4245, 2018.

[28] J. Schmitt, "A simple stabilizing control for sagittal plane locomotion," *Journal of Computational and Nonlinear Dynamics*, vol. 1, no. 4, pp. 348–357, 2006.

[29] A. Seyfarth, H. Geyer, and H. Herr, "Swing-leg retraction: A simple control model for stable running," *Journal of Experimental Biology*, vol. 206, no. 15, pp. 2547–2555, 2003.

[30] D. G. E. Hobbelen and M. Wisse, "Swing-leg retraction for limit cycle walkers improves disturbance rejection," *IEEE Transactions on Robotics*, vol. 24, no. 2, pp. 377–389, 2008.

[31] J. G. D. Karssen, M. Haberland, M. Wisse, and S. Kim, "The optimal swing-leg retraction rate for running," in *Proceedings - IEEE International Conference on Robotics and Automation*, 2011, pp. 4000–4006.

[32] A. Seyfarth, H. Geyer, M. Günther, and R. Blickhan, "A movement criterion for running," *Journal of biomechanics*, vol. 35, no. 5, p. 649–655, 2002.

[33] R. M. Ghigliazza, R. Altendorfer, P. Holmes, and D. Koditschek, "A simply stabilized running model," *SIAM review*, vol. 47, no. 3, pp. 519–549, 2005.

[34] S. G. Carver, N. J. Cowan, and J. M. Guckenheimer, "Lateral stability of the spring-mass hopper suggests a two-step control strategy for running," *Chaos*, vol. 19, no. 2, 2009.

[35] A. Wu and H. Geyer, "The 3-d spring-mass model reveals a time-based deadbeat control for highly robust running and steering in uncertain environments," *IEEE Transactions on Robotics*, vol. 29, no. 5, pp. 1114–1124, 2013.

[36] G. Council, S. Yang, and S. Revzen, "Deadbeat control with (almost) no sensing in a hybrid model of legged locomotion," in *International Conference on Advanced Mechatronic Systems, ICAMechS*, 2014, pp. 475–480.

[37] Y. Blum, S. W. Lipfert, J. Rummel, and A. Seyfarth, "Swing leg control in human running," *Bioinspiration and Biomimetics*, vol. 5, no. 2, p. 026006, 2010.

[38] M. A. Daley and A. A. Biewener, "Running over rough terrain reveals limb control for intrinsic stability," *Proceedings of the National Academy of Sciences of the United States of America*, vol. 103, no. 42, pp. 15 681–15 686, 2006.

[39] M. A. Daley, J. R. Usherwood, G. Felix, and A. A. Biewener, "Running over rough terrain: Guinea fowl maintain dynamic stability despite a large unexpected change in substrate height," *Journal of Experimental Biology*, vol. 209, no. 1, pp. 171–187, 2006.

[40] A. V. Birn-Jeffery and M. A. Daley, "Birds achieve high robustness in uneven terrain through active control of landing conditions," *Journal of Experimental Biology*, vol. 215, no. 12, pp. 2117–2127, 2012.

[41] W. C. Martin, A. Wu, and H. Geyer, "Experimental evaluation of deadbeat running on the atrias biped," *IEEE Robotics and Automation Letters*, vol. 2, no. 2, pp. 1085–1092, 2017.

[42] J. K. Yim and R. S. Fearing, "Precision jumping limits from flight-phase control in salto-1p," in *IEEE International Conference on Intelligent Robots and Systems*, 2018, pp. 2229–2236.

[43] S. Grimmer, M. Ernst, M. Günther, and R. Blickhan, "Running on uneven ground: Leg adjustment to vertical steps and self-stability," *Journal of Experimental Biology*, vol. 211, no. 18, pp. 2989–3000, 2008.

[44] R. Müller and R. Blickhan, "Running on uneven ground: Leg adjust-ments to altered ground level," *Human Movement Science*, vol. 29, no. 4, pp. 578–589, 2010.

[45] A. M. Johnson, S. A. Burden, and D. E. Koditschek, "A hybrid systems model for simple manipulation and self-manipulation systems," *International Journal of Robotics Research*, vol. 35, no. 11, pp. 1289–1327, 2016.

[46] C. T. Farley, J. Glasheen, and T. A. McMahon, "Running springs: speed and animal size," *Journal of Experimental Biology*, vol. 185, no. 1, pp. 71–86, 1993.

[47] J. Koechling and M. Raibert, "How fast can a legged robot run," in *American Society of Mechanical Engineers, Dynamic Systems and Control Division (Publication) DSC*, vol. 11, 1988, pp. 241–249.

[48] S. Seok, A. Wang, M. Y. Chuah, D. J. Hyun, J. Lee, D. M. Otten, J. H. Lang, and S. Kim, "Design principles for energy-efficient legged locomotion and implementation on the mit cheetah robot," *IEEE/ASME Transactions on Mechatronics*, vol. 20, no. 3, pp. 1117–1129, 2014.

[49] G. Kenneally, A. De, and D. E. Koditschek, "Design principles for a fam-ily of direct-drive legged robots," *IEEE Robotics and Automation Letters*, vol. 1, no. 2, p. 900–907, Jul 2016, doi: 10.1109/LRA.2016.2528294.

[50] C. Conley, "The gradient structure of a flow: I," *Ergodic Theory and Dynamical Systems*, vol. 8, no. 8, pp. 11–26, 1988.

[51] R. J. Full and D. E. Koditschek, "Templates and anchors: Neuromechan-ical hypotheses of legged locomotion on land," *Journal of Experimental Biology*, vol. 202, no. 23, pp. 3325–3332, 1999.

[52] J. Ding and A. Zhou, "Eigenvalues of rank-one updated matrices with some applications," *Applied Mathematics Letters*, vol. 20, no. 12, pp. 1223–1226, 2007.

[53] S. M. Shinners, *Modern control system theory and design*, 2nd ed. John Wiley & Sons, 1998.